Pre-Cenozoic geologic history of the central and northern Tibetan Plateau and the role of Wilson cycles in constructing the Tethyan orogenic system

Chen Wu[1,*], An Yin[1,2,*], Andrew V. Zuza[2,*], Jinyu Zhang[3,*], Wencan Liu[1,*], and Lin Ding[4,*]

[1]STRUCTURAL GEOLOGY GROUP, CHINA UNIVERSITY OF GEOSCIENCES (BEIJING), BEIJING 100083, CHINA
[2]DEPARTMENT OF EARTH, PLANETARY, AND SPACE SCIENCES, UNIVERSITY OF CALIFORNIA, LOS ANGELES, CALIFORNIA 90095-1567, USA
[3]INSTITUTE OF GEOLOGY, CHINA EARTHQUAKE ADMINISTRATION, BEIJING 100029, CHINA
[4]INSTITUTE OF TIBETAN PLATEAU RESEARCH, CHINESE ACADEMY OF SCIENCES, P.O. BOX 9825, BEIJING 100085, CHINA

ABSTRACT

In order to better constrain the evolution of the Tethyan orogenic system, we conducted an integrated investigation involving U-Pb dating of igneous and detrital zircon, geochemical analysis of igneous rocks, compositional analysis of sedimentary strata, and a synthesis of existing work across the Qilian Shan, Qaidam Basin, and the Eastern Kunlun Range of central and northern Tibet. This effort reveals five stages of arc magmatism at 1005–910 Ma, 790–720 Ma, 580–500 Ma, 490–375 Ma, and 290–195 Ma, respectively. Arc activities were interrupted by repeated continent-continent collision followed by ocean opening along the older suture zones first created in the Neoproterozoic. This suggests that Wilson cycles have played a controlling role in constructing the southern Asian continent. The magmatic history and regional geologic constraints allow us to construct a coherent tectonic model that has the following key features. (1) The linked South Qilian suture in the west and North Qinling suture in the east formed the northern boundary of the coherent Kunlun–Qaidam–North Qinling Terrane in the early Paleozoic. (2) The Songpan-Ganzi Terrane has been the western part of the Yangtze craton since the Neoproterozoic. (3) Development of the wide (>700 km) Permian–Triassic arc across the Kunlun-Qaidam Terrane was induced by flat subduction and rapid slab rollback, which also caused extreme extension of the Songpan-Ganzi Terrane. (4) The formation of the Anymaqen-Kunlun-Muztagh Ocean (= the Neo–Kunlun Ocean in this study) was created within Laurasia rather than being a preexisting ocean between Gondwana and Laurasia as postulated by most early studies.

INTRODUCTION

The Tethyan orogenic system in southern Eurasia is bounded by two belts of interconnected Precambrian cratons in the north and south (Fig. 1A; e.g., Şengör, 1984; Şengör and Natal'in, 1996; Heubeck, 2001). As one of the major Phanerozoic orogenic belts on Earth (Şengör, 1984), understanding its tectonic evolution has several important implications. First, its history can provide better constraints on the assembling processes of Pangea—arguably the best understood supercontinent in Earth's history (e.g., Şengör, 1984; Şengör et al., 1988; Stampfli et al., 2013). Second, establishing its tectonic evolution will help to determine the formation history of Asia, the youngest and largest continental landmass on Earth (e.g., Şengör and Natal'in, 1996; Yin and Nie, 1996; Badarch et al., 2002; Sone and Metcalfe, 2008; Yin, 2010; Gehrels et al., 2011). Third, the timing and processes of Tethyan ocean closure may have drastically impacted global climate change and mass extinction (e.g., Şengör et al., 2008; Osen et al., 2013). Finally, determining the opening and closure history of the Neo-Tethys, the youngest ocean in the long-evolving Tethyan system, has important implications for understanding the tectonic history of the Himalayan-Alpine collisional zone (e.g., Hsü et al., 1995; Yin and Nie, 1996; Yin and Harrison, 2000; Yin, 2006, 2010; Yin et al., 2007a; Dai et al., 2008, 2013a; Dupont-Nivet et al., 2010; van Hinsbergen et al., 2011;

Webb et al., 2011, 2013), which in turn has impacted the Cenozoic climate history of Asia (e.g., Harrison et al., 1992; Molnar et al., 1993).

The evolution of the Tethyan orogen has been generally regarded as a result of tectonic interactions between the supercontinents of Laurasia and Gondwana (Şengör, 1984; Şengör and Natal'in, 1996). In this context, the following issues remain unresolved (Şengör, 1984; Şengör et al., 1988; Hsü et al., 1995; Yin and Harrison, 2000; Stampfli and Borel, 2002): (1) What were the provenances and transport processes of continental fragments, arcs, and oceanic assemblages within the Tethyan orogenic realm between Laurasia in the north and Gondwana in the south? (2) Were the elongated continental strips in the amalgamated orogenic system continuous along strike from the continental-drift stage to the continental-collision stage? (3) Did opening and closure of backarc basins play an important role in the evolution of the Tethyan orogenic system?

The above issues are manifested in the diverse views on the tectonic development of the eastern Tethyan orogenic system in the Qilian Shan and Eastern Kunlun Range of central and northern Tibet, where series of east-trending suture zones and arcs are exposed (Fig. 1B; Yin and Harrison, 2000). The end-member models include (Fig. 2): (1) the single-arc model of Şengör (1992), which requires a long-evolving arc above a north-dipping subduction zone since the Neoproterozoic in northern Tibet (Fig. 2A), (2) the backarc-basin model of Hsü et al. (1995), which emphasizes the role of backarc extension and the development of a large accretionary wedge along the southern rim of the Kunlun-Qaidam Terrane (Fig. 2B), (3) a two-phase arc model that requires the southern margin of the Kunlun-Qaidam Terrane to have evolved through an active-passive-active margin
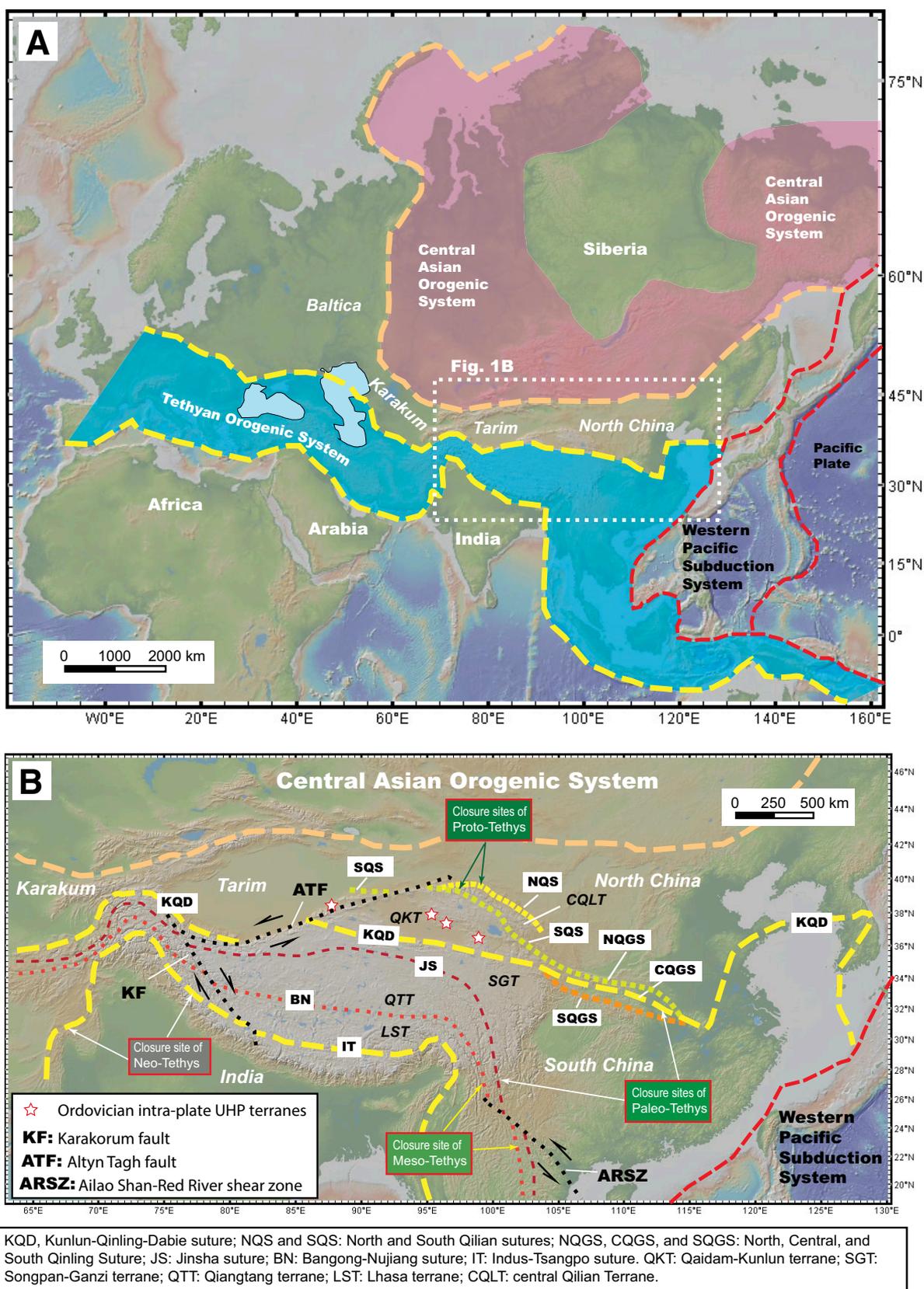
Figure 1. (A) Tectonic map of the Tethyan orogenic system and its bounding terranes across Eurasia. Location of B is also indicated on the map. (B) Tectonic division of the Tethyan orogenic system across the Tibetan Plateau modified after Yin and Nie (1996) and Yin and Harrison (2000).

KQD, Kunlun-Qinling-Dabie suture; NQS and SQS: North and South Qilian sutures; NQGS, CQGS, and SQGS: North, Central, and South Qinling Suture; JS: Jinsha suture; BN: Bangong-Nujiang suture; IT: Indus-Tsangpo suture. QKT: Qaidam-Kunlun terrane; SGT: Songpan-Ganzi terrane; QTT: Qiangtang terrane; LST: Lhasa terrane; CQLT: central Qilian Terrane.
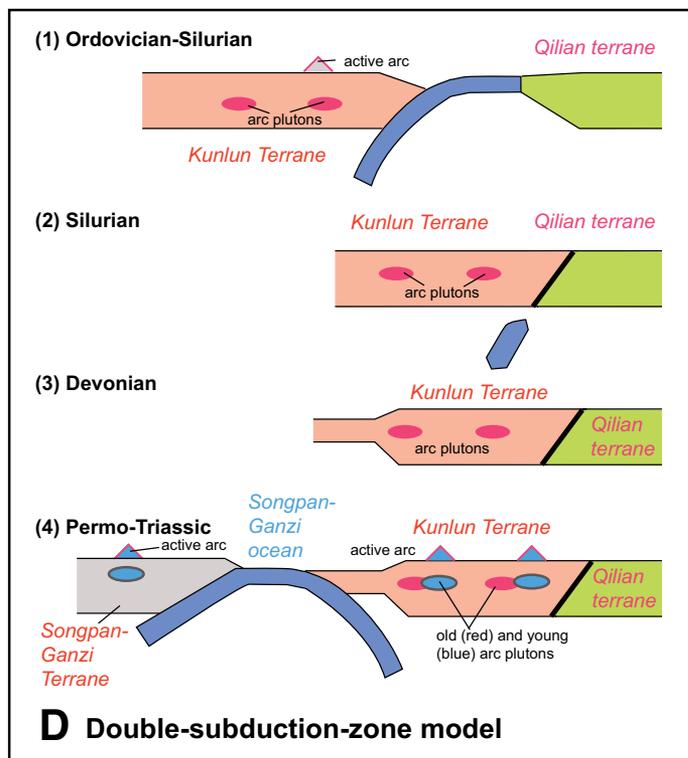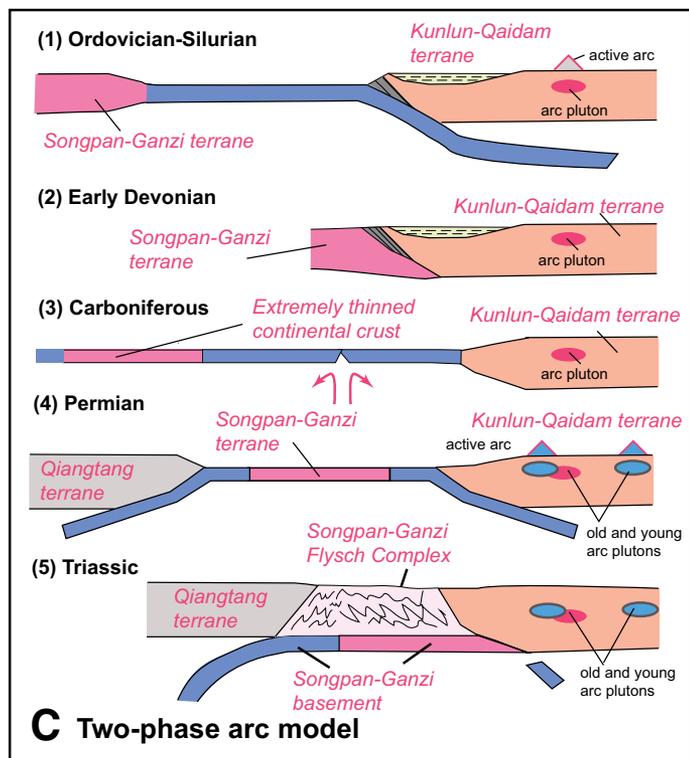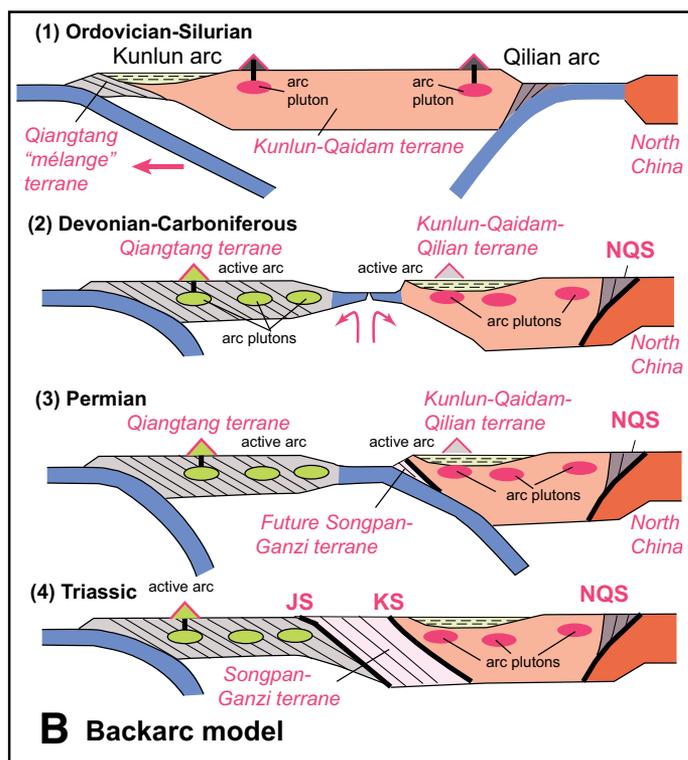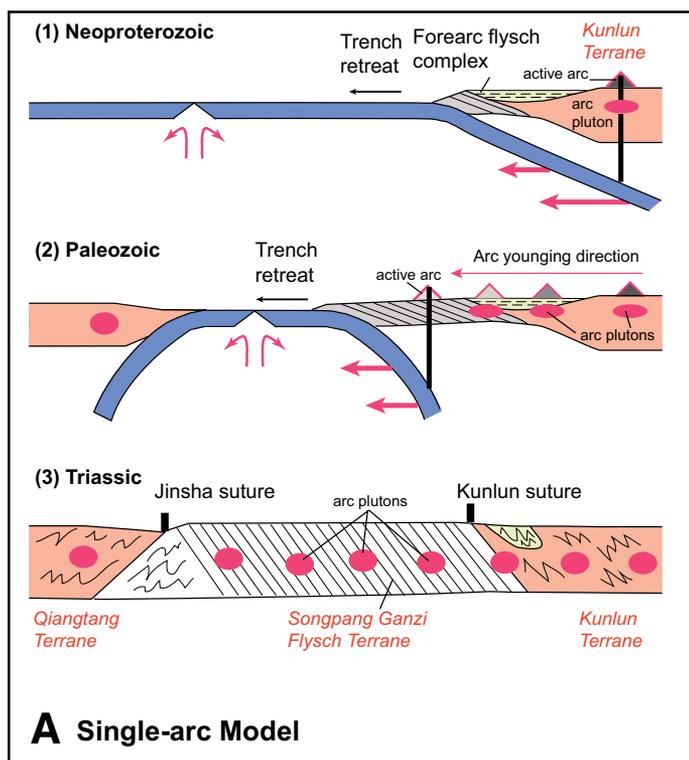
Figure 2. Major tectonic models for the evolution of the Tethyan orogenic system in the Eastern Kunlun Range of central and northern Tibet. See text for details. JS—Jinsha Suture; NQS—North Qilian suture, KS—Kunlun Suture. (*Continued on following page.*)

(1) Neoproterozoic-Early Paleozoic

(2) Devonian

(3) Early Carboniferous

(4) End of Early Carboniferous

(5) End of Carboniferous

(6) Permian

(7) Triassic

E **Multiple-collision model**
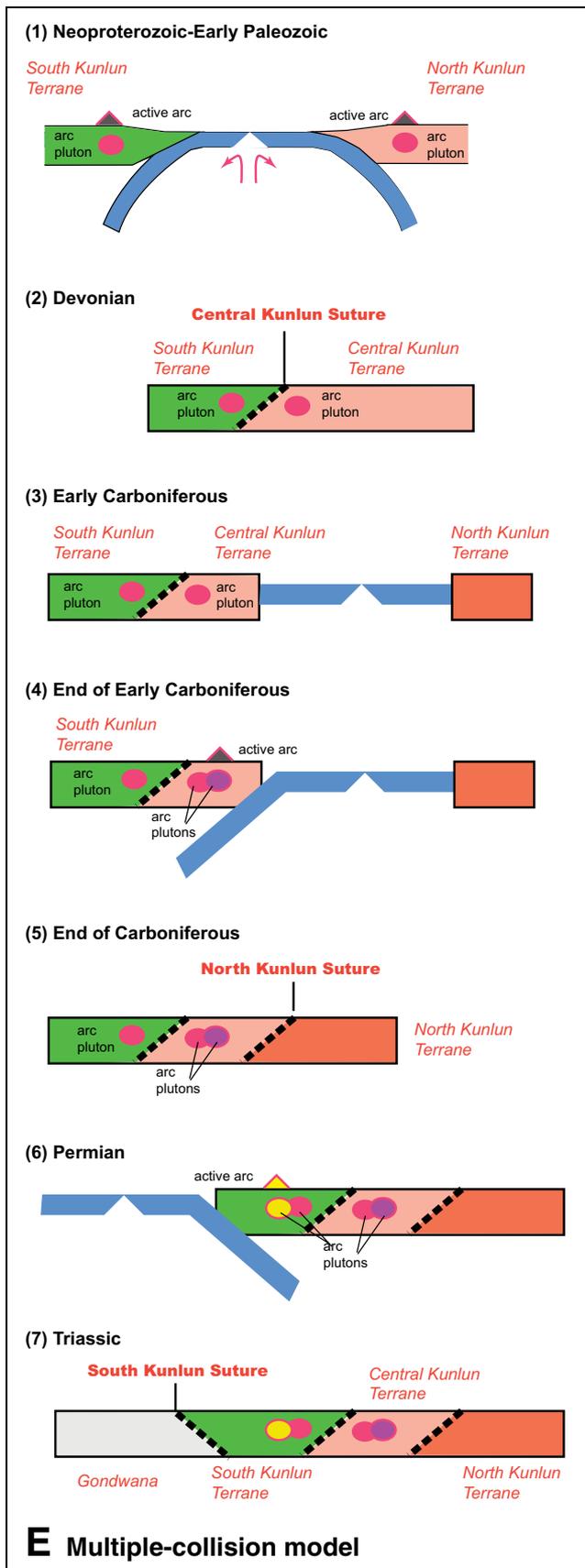
Figure 2 (*continued*).

cycle (Fig. 2C; Yin and Harrison, 2000), and (4) a double-subduction-zone model that predicts the southern margin of the Kunlun-Qaidam Terrane and the northern margin of the Songpan-Ganzi Terrane were subducted by the Songpan-Ganzi oceanic plate in the Permian–Triassic (Fig. 2D; Stampfli and Borel, 2002). In contrast to the single-suture zone models in Figures 2A–2D, Jiang et al. (1992), Yang et al. (1996), and Meng et al. (2013a, 2015) have suggested that the closure of the Tethyan ocean in the Kunlun region of central Tibet occurred along two or even three suture zones as a result of sequential accretion of continental fragments (Fig. 2E; cf. Mo et al., 2007).

In this study, we test these models using the history of arc magmatism and sediment dispersal across central and northern Tibet using both existing and our own new data. Our results suggest that the southern margin of the Kunlun-Qaidam Terrane had experienced two major phases of Phanerozoic arc activity: one from the latest Cambrian to the Devonian (490–375 Ma), and the other from the Early Permian to the Late Triassic (290–225 Ma). All Phanerozoic geologic times follow those defined in Gradstein et al. (2012), whereas Proterozoic ages and period divisions are based on the updated geologic timescale of the Chinese Geological Survey (2014), which is commonly referenced in the Chinese literature. As the two Phanerozoic arcs were built on top of a Neoproterozoic (940–820 Ma) continental arc, the southern margin of the Kunlun-Qaidam Terrane must have been the site of multiple continental collision and separation events in the style of Wilson cycles over a period of ~700 m.y. The cyclic nature of Tethyan development in central Tibet contrasts sharply with the classic view that the formation of the Tethyan orogenic system was accomplished by a sequential and unidirectional accretion of continental strips of Gondwana onto the southern margin of Laurasia (see Stampfli et al., 2013, and references therein).

REGIONAL GEOLOGY

Qilian Orogen

The early Paleozoic Qilian orogen is located across the northern margin of the Tibetan Plateau (Fig. 3). The development of this orogen is not well understood, with the current debates centered on (1) the polarities of ocean subduction and ocean closure, (2) the number of sutures and their lateral extent, and (3) the timing of the onset and termination of the orogenic processes (e.g., Yang et al., 2001; Sobel and Arnaud, 1999; Yin and Harrison, 2000; Gehrels et al., 2003a, 2003b; Yin et al., 2007a; Xiao et al., 2009; Xu et al., 2010a, 2010b; Song et al., 2013). Most researchers agree that: (1) the Qilian ocean(s) existed prior to 530 Ma (e.g., Smith, 2006; Tseng et al., 2007; Song et al., 2013), (2) oceanic subduction occurred during 490–445 Ma, expressed by arc magmatism (Gehrels et al., 2003a; Zhang et al., 2007), and (3) the Qilian arcs were constructed on top of continental crust (Bian et al., 2001; Tseng et al., 2009a, 2009b; Xu et al., 2010a, 2010b).

The Qilian orogen involves three tectonic units bounded by the North and South Qilian suture zones (Fig. 1): (1) the southern margin of the North China craton, consisting of 1.8 Ga basement and a Mesoproterozoic cover sequence intruded locally by postorogenic early Paleozoic granitoids, (2) the Central Qilian Terrane, consisting of Precambrian basement with characteristic 900–1100 Ma plutonic rocks, and (3) the northern margin of the Kunlun-Qaidam Terrane, which is dominated by an early Paleozoic arc belt constructed on top of Precambrian continental basement (Figs. 3 and 4A–4C; e.g., Yin and Harrison, 2000; Gehrels et al., 2003a, 2003b; Yin et al., 2007a; Song et al., 2013). The southern margin of North China consists of a high-grade Paleoproterozoic metamorphic complex (the Beidahe Group), a low-grade Mesoproterozoic stromatolite-bearing metasedimentary sequence deposited in the shelf setting of a stable craton (the Zhulongguan Group), and a Mesoproterozoic high-grade gneissic

Figure 3. An index geologic map of Tibet after Yin and Harrison (2000) that shows the locations of the study areas. Also shown are sample sites of Ding et al. (2013) discussed in the text. Note that the Songpan-Ganzi Terrane is divided into the Bayan Har (BYH), Hoh Xil (HOX), Tianshuihai (TSH), and Karakul-Mazar (KMZ) sectors from east to west. Major lithologic and tectonic units are defined as: N-Q—Neogene-Quaternary sedimentary strata; Ts—Tertiary sedimentary rocks; Tv(lz)—Early Tertiary (60–40 Ma) Linzizong volcanic rocks in the Lhasa Terrane; gnAm—Amdo gneiss; THS—Tethyan Himalayan sequences (Proterozoic to Late Cretaceous passive continental margin strata); HHM—High Himalayan metamorphic rocks; LHS—Lesser Himalayan metasedimentary series. Major plutonic rocks: Czgr—Cenozoic granites in eastern Tibet and northern Karakorum Mountains; gr(NH)—North Himalayan granites; gr(HH)—High Himalayan leucogranites; K-Tgr—plutonic rocks belonging to the Gangdese batholith, Ladakh batholith, and Kohistan arc; gr(Q)—Mesozoic plutonic rocks in the Qiangtang Terrane; gr(SGH)—Mesozoic plutonic rocks in the Songpan-Ganzi-Hoh Xil Terrane; gr(KQ)—Paleozoic and Mesozoic plutonic rocks in the Kunlun and Qilian Terranes. Major sutures: ITS—Indus-Tsangpo suture; BNS—Bangong-Nujiang suture; JS—Jinsha suture; KQD—Kunlun-Qinling-Dabie suture; SQS—south Qilian suture; NQS—North Qilian suture; KS—Kudi suture. Major Cenozoic structures: PGES—Purang-Gurla Mandhata extensional system; STDS—South Tibet detachment system; MCT—Main Central thrust; MBT—Main Boundary thrust; SGA—Shiquanhe-Gaize-Amdo thrust system. GHC—Greater Himalayan Sequence and age equivalents in the Shilong Plateau; Oph—ophiolite; gr(SP)—Songpan-Ganzi granite; gr(NC)—North China Craton granite; gr(QN)—Qilian Shan-Nan Shan granite; gr(YD)—Yidu arc granite; MKT—Main Karakorum Thrust.

(A) Southern Margin of North China

Arc activity started ~480 Ma
Submarine arc sequence (rhyolite, andesite) overlain by limestone, cherty slate, and conglomerate[3].

Dahuangshan Group: Dominantly fine-grained sandstone intruded by Ordovician-Silurian granitoids.

Contact not exposed

Rifting started ~750 Ma
Hannu Shan Group[2,3]: Limestone, diamictite (interpreted as glacial deposits), phyllite, and basalt.

Conformable

Dunzigou Group[2,3]: Cherty limestone containing stromatolite and interbedded with minor phyllite, slate, siltstone, and conglomerate.

Unconformity

Mobile belt rocks
Longshou Shan Group[1,2]: Marble, schist, gneiss, leucogranites, meta-volcanics. K-Ar muscovite ages of 1786-1319 Ma. Orthogneisses have upper and lower intersection ages of 1914-2015 Ma and 758-452 Ma. DZ ages > ~1725 Ma.

Contact not exposed

Stable craton rocks
Zhulongguan Group[3]: Stromatolite-bearing limestone interlayered with basalt, andesite, quartz arenite, banded iron formation, and phyllite.

Contact not exposed

Beidahe Group[3]: Schist, marble, gneiss, metabasite. Protolith may be a turbidite sequence.

~2 Ga

Ordovician / Cambrian / Neoproterozoic / Mesoproterozoic / Paleoproterozoic

(B) Central Qilian Terrane

Arc activity started ~480 Ma
Maojiagou Fm: Dominantly fine-grained sandstone intruded by Ordovician-Silurian granitoids.

Contact not exposed

Rifting started ~750 Ma
Huangzhong/Baiyanggou Groups[3]: Quartz arenite, slate, and diamictite (interpreted as glacial deposits).

Unconformity

Mobile belt rocks
Tuolai Shan Group[3,4,5]: A shallow marine sequence. **Gaolan and Huangyuan Groups[3]:** High-grade gneiss, marble, and schist, containing 930-775 Ma orthogneiss.

930-775 Ma

Contact not exposed

Craton rocks
Zhulongguan Group[3]: Stromatolite-bearing limestone interlayered with basalt and andesite.

Contact not exposed

Tuolai Group[3]: Schist, marble, gneiss, metabasite. Protolith may be a turbidite sequence.

Ordovician / Cambrian / Neoproterozoic / Mesoproterozoic / Paleoproterozoic

(C) N. Kunlun-Qaidam Terrane

Arc activity started ~480 Ma
A turbidite sequence overlain by an arc volcanic sequence.

Middle member[2]: Pelitic limestone, slate, conglomerate.
Middle member[2]: Cherty limestone, dolostone, and limestone.
Lower member[2]: Dolostone and sandstone.

Contact not exposed

Rifting started ~740 Ma
Quanji Group[3]: Tillite, limestone, quartz arenite, and ca. 738 Ma basalt.

Contact not exposed

Mobile-belt rocks
Wandonggou Group[3]: Stromatolite-bearing and cherty limestone and marble, phyllite, schist. Minor metamorphosed mafic volcanics.

Stable craton rocks

Contact not exposed

Dakendaban Group/Delingha Complex[3,6]: Schist, marble, gneiss, 2.2-2.3 Ga meta-volcanic rocks, and 1.8 Ga and 2.2-2.4 Ga metagranites.

2.3-2.4 Ga

Ordovician / Cambrian / Neoproterozoic / Mesoproterozoic / Paleoproterozoic

Figure 4 (*on this and following page*).

Figure 4. Tectono-stratigraphic sections of the (A) southern margin of North China, (B) Central Qilian Terrane, (C) northern Kunlun-Qaidam Terrane, (D) southern Kunlun-Qaidam Terrane, (E) eastern Songpan-Ganzi Terrane, and (F) western Songpan-Ganzi Terrane. Key references used for constructing these sections include: 1—Tung et al. (2007a), 2—Zhang (1992), 3—Wang et al. (2013), 4—Tseng et al. (2006), 5—Tung et al. (2007b), 6—Lu (2002), 7—Chen et al. (2011), 8—N.S. Chen et al. (2006a), 9—N.S. Chen et al. (2006b), 10—Tan et al. (2004), 11—Ma et al. (2013), 12—Meng et al. (2013b), 13—Ren et al. (2010), 14—Bian et al. (2006), 15—Zhou et al. (2002a), 16—Zhou et al. (2006), 17—Yan et al. (2006), 18—Ji et al. (2011), 19—Robinson et al. (2012). DZ—detrital zircon.

and leucogranite complex most likely representing a mobile belt (the Longshou Shan Group; Fig. 4A). The Longshou Shan Group experienced multiple phases of metamorphism, with youngest ages at 758 Ma and 452 Ma, as expressed by a phase of zircon rim growth around older zircon grain cores (Tung et al., 2007a; Wang et al., 2013). This sequence is overlain by a Neoproterozoic continental-shelf sequence (the Dunzigou and Hanmu Shan Groups) composed of glacial deposits (Tung et al., 2007a; Wang et al., 2013) and is interpreted to have been deposited in a passive continental margin during continental separation (Fig. 4A; Zhang, 1992). The Longshou Shan Group has been assigned a general age of 850–680 Ma, deposited in the middle Qingbaikou to middle Nanhua (Chinese Geological Survey, 2014), which is the same as the middle Tonian to middle Cryogenian (Gradstein et al., 2012). Cambrian (541–485 Ma) strata with unknown contact relationships to the older strata consist of siliciclastic rocks and are intruded by Ordovician (485–444 Ma) and Silurian (444–419 Ma) granitoids along the southern margin of North China (Wang et al., 2013). Locally, an Ordovician arc sequence (Fig. 4A; Wang et al., 2013), overlain by a Silurian turbidite sequence/flysch strata (Yang et al., 2009; Xu et al., 2010a, 2010b; Yang et al., 2012a, 2012b) and Devonian molasse deposits (Xu et al., 2010b), is also exposed along the southern margin of North China. Deposition of the Lower Silurian turbidite sequence is interpreted to have occurred in a foreland basin during the collision of the Central Qilian Terrane with North China (e.g., Yang et al., 2012b). Based on the regional stratigraphic relationships shown in Figure 4A, the passive margin along the southern margin of North China formed after 758 Ma but before 680 Ma.

The Central Qilian Terrane may be divided into western and eastern sectors. In the western sector, Mesoproterozoic cratonal and/or passive-margin strata are intruded by 930–920 Ma plutons (Fig. 4B; Gehrels et al., 2003a, 2003b) and lie structurally below an early Paleozoic eclogite-bearing metamorphic complex (Tseng et al., 2006). The metamorphic complex consists of 930–775 Ma Neoproterozoic orthogneiss (Tseng et al., 2006; Tung et al., 2007b) and paragneiss with detrital-zircon ages older than 880 Ma (Tung et al., 2007b). Arc activity at 520–440 Ma in the western Qilian orogen was followed by 435–345 Ma postorogenic magmatism (e.g., Gehrels et al., 2003a; Wu et al., 2004a, 2006, 2010; M. Liu et al., 2006; He et al., 2007; Tseng et al., 2009a, 2009b; Xiong et al., 2012; Song et al., 2013). In the eastern sector, Paleoproterozoic crystalline rocks are intruded by 1190–750 Ma plutons and overlain by a Neoproterozoic shelf sequence; the latter are intruded by early Paleozoic arc assemblages (e.g., Tung et al., 2012) and, locally, 245–218 Ma Mesozoic plutons (Chen et al., 2008; Yong et al., 2008; Guo et al., 2012).

The early Paleozoic Qilian orogeny is manifested by the development of an arc belt and the intra-arc North Qaidam ultrahigh-pressure (UHP) metamorphic belt (Fig. 3; Yin and Harrison, 2000; Yin et al., 2007a; Menold et al., 2009). The North Qaidam UHP belt is regarded by some as a relic of an early Paleozoic suture zone (e.g., Yang et al., 2001). However, the coeval development and spatial overlapping of UHP metamorphism and arc magmatism and the lack of collision-induced thrust belts in the region rule out this interpretation (see discussion in Yin et al., 2007a). The protolith of the early Paleozoic (480–430 Ma) UHP metamorphic rocks in northern Qaidam Basin consists of ca. 785 Ma and 930–920 Ma meta-granites (Gehrels et al., 2003a; Xiong et al., 2012). The original extent and trend of the North Qaidam UHP Terrane are unclear, as its exposure is strongly controlled by the occurrence of west-northwest–striking Cenozoic thrusts that bound the northern margin of Qaidam Basin (Yin et al., 2008a, 2008b).

The basement of the northern Kunlun-Qaidam Terrane consists of the high-grade Delingha metamorphic complex, the medium- to low-grade Dakendaban Group, and the low-grade Wandonggou Group, from older

to younger based on their protolith ages (Fig. 4C; Wang et al., 2013). The Delingha complex is dominated by 2.4–2.2 Ga meta-granites that contain ca. 2.4 Ga mafic enclaves (Lu, 2002; Gong et al., 2012). The Dakendaban Group consists of 2.32–2.20 Ga metavolcanic and metasedimentary strata and a 2.20–1.96 Ga metapelite assemblage (e.g., Lu, 2002; N.S. Chen et al., 2012). Both the Delingha and Dakendaban metamorphic complexes experienced protracted metamorphism from 1.95 Ga to 1.83 Ga (Zhang et al., 2011; Chen et al., 2013a) and were intruded by 1.80–1.77 Ga rapakivi granites (Lu et al., 2006; N.S. Chen et al., 2012, 2013b) and 1.83 Ga mafic dikes (Liao et al., 2014). The Wandonggou Group is composed mainly of metasedimentary rocks with minor metavolcanics deposited after the emplacement of 1.80 Ga rapakivi granites but before a ca. 1.0 Ga low-grade metamorphic event (Lu et al., 2006, 2008; Wang et al., 2013). The diamictite-bearing Quanji Shan Group is the oldest sedimentary cover sequence on top of the Precambrian basement of the northern Kunlun-Qaidam Terrane (Fig. 4C; Wang et al., 2013), which was deposited during the Ediacaran, postdating the Gaskiers glaciation (Shen et al., 2010). Cambrian shallow-marine strata rest on top of the Quanji Shan strata, which in turn are overlain by an Ordovician–Silurian arc sequence (Wang et al., 2013).

Southern Margin of the Kunlun-Qaidam Terrane

The geology of the southern margin of the Kunlun-Qaidam Terrane is best exposed in the Eastern Kunlun Range, which is bounded by Qaidam Basin in the north and the active left-slip Kunlun fault in the south, which follows the Triassic Anymaqen-Kunlun-Muztagh suture zone (Fig. 3; Yin and Harrison, 2000). A zone of mafic-ultramafic intrusive rocks and ophiolitic fragments occurs as tectonic lenses within an eclogite-bearing high-grade metamorphic complex north of the Kunlun fault (Xiao et al., 1986; Yang et al., 1996; Meng et al., 2013a, 2015). Some researchers regard the mafic-ultramafic belt and the occurrence of eclogite-bearing metamorphic rocks as indicating the presence of an early Paleozoic suture in the Eastern Kunlun Range (e.g., Xiao et al., 1986; Yang et al., 1996; Meng et al., 2013a, 2015). In contrast, others regard the belt as a closure site of a small backarc basin (Mo et al., 2007). We note that although the high-grade metamorphism occurred at ca. 428 Ma, the protolith age of the eclogite-bearing metamorphic belt is ca. 930 Ma (Meng et al., 2013a), similar to the basement plutonic ages of the Eastern Kunlun Range (Fig. 4D). This implies that the high-grade metamorphism in the Eastern Kunlun Range may represent intracontinental and/or backarc processes, similar to that documented by Gilotti and McClelland (2007) in Greenland, rather than a suturing process between two continents. Alternatively, the colliding terrane south of the inferred suture must have a similar basement to that of the Eastern Kunlun Range, for which there is no evidence.

The oldest Precambrian basement rocks exposed in the Eastern Kunlun Range consist of 1.93 Ga meta-basite, 1.85 Ga meta-granite, and 940–820 Ma meta-granites that are tectonically mingled with migmatite and metasedimentary rocks (Fig. 4D; Tan et al., 2004; N.S. Chen et al., 2006a, 2006b; Ma et al., 2013; Meng et al., 2013b; also see a summary and references in Zhang et al., 2012; Wang et al., 2013). U-Pb detrital-zircon dating suggests a maximum deposition age of 1683–1554 Ma for the metasedimentary rocks in this metamorphic assemblage (Chen et al., 2011). The metamorphic complex of the Kunlun basement is cut by 733 Ma mafic dikes (Ren et al., 2010). Ordovician, Devonian, and Triassic sedimentary and volcaniclastic rocks are also widely distributed across the Eastern Kunlun Range (e.g., Wang et al., 2013). Ordovician sedimentary strata include shallow- and deep-marine clastic rocks, carbonate, volcanic rocks, and volcaniclastic rocks (Wang et al., 2013), which may represent an arc sequence. The Lower Devonian strata are missing in the

Eastern Kunlun Range, whereas the Upper Devonian strata are composed of marine-continental facies clastic rocks, carbonates, and intermediate to felsic volcanic rocks of an arc origin (Wang et al., 2013). The Carboniferous sequence is dominated by shallow-marine limestone, whereas the Permian to Triassic strata consist mostly of clastic and volcanic rocks (e.g., Wang et al., 2013). Two episodes of arc magmatism have been identified across the Eastern Kunlun Range: one was dominantly in the Ordovician to Silurian but lasted until the Late Devonian, and the other was mostly in the Permian and Triassic (e.g., Cowgill et al., 2003; Gehrels et al., 2003a, 2003b; Mo et al., 2007; X.H. Chen et al., 2012; Liu et al., 2012; Li et al., 2013; Dai et al., 2013b).

The current knowledge of the basic structural framework of the Eastern Kunlun Range remains incomplete. For example, the subduction polarity of the northern Kunlun suture is unknown, and basic information regarding the fault-zone characteristics and kinematics is lacking. Additionally, the proposed early Paleozoic closure, rather than the commonly accepted Triassic closure, of the Anymaqen-Kunlun-Muztagh Ocean requires the presence of a forearc basin prior to and during the inferred 440–420 Ma collisional event (Meng et al., 2015). Both features have not been reported in the area. The present-day topography of the Eastern Kunlun Range was created mostly in the past 30–20 m.y. during the Cenozoic collision of India-Asia (W.M. Yuan et al., 2006; Yin et al., 2007b; Duvall et al., 2013; D.Y. Yuan et al., 2013; Dai et al., 2013b; cf. Clark et al., 2010).

Lateral Extent of the Qilian Orogen and the Kunlun-Qaidam Terrane

The North and South Qilian suture zones mark the closure of early Paleozoic oceans in the Devonian (Yin and Harrison, 2000) or earliest Silurian (e.g., Xu et al., 2010a). Along strike to the east, the Qinling orogen developed along the southern margin of North China, and it is divided into the North, Central, and South Qinling Terranes by the North and South Qinling suture zones (Fig. 1B). The North Qinling Ocean (= Erlangping backarc basin) was established before 540 Ma, which is interpreted by some as a branch of the Proto-Tethyan ocean (e.g., Dong and Santosh, 2015). This ocean was closed in the Early Devonian (ca. 400 Ma) as a result of collision along a south-dipping subduction zone between the North Qinling Terrane and North China. The Central Qinling Ocean was closed in the Devonian as a result of collision between the South and North Qinling Terranes (e.g., Ratschbacher et al., 2003; Dong and Santosh, 2015). The South Qinling Ocean may have started opening in the Early Devonian (Meng and Zhang, 1999; Dong and Santosh, 2015) and was closed diachronously from the late Early Permian in the east to the Late Triassic in the west during the collision between North and South China (Enkin et al., 1992; Yin and Nie, 1993, 1996; Hacker et al., 2000). Continuous convergence between North and South China in the Jurassic was expressed by shortening and strike-slip faulting within the Qinling orogen (e.g., Li et al., 2013) and along its southern margin in the Daba Shan area (Dong et al., 2013; Li et al., 2015). Finally, the South Qinling Ocean was closed in the Triassic by the collision between South China and North China with the South and North Qinling Terrane along the southern margin of the North China block (Meng and Zhang, 1999; Ratschbacher et al., 2003; Dong and Santosh, 2015). The closure of the Qinling oceans was accompanied by multiple episodes of high- to ultrahigh-pressure and high- to ultrahigh-temperature metamorphism (e.g., Bader et al., 2013).

The North Qilian suture zone is laterally limited (Yin and Harrison, 2000; Song et al., 2013) and may represent a backarc basin within North China (Fig. 3), whereas the South Qilian suture zone can be traced continuously to the east and links with the North Qinling suture zone (= Erlangping suture; Fig. 1B; Yin and Nie, 1996; Tseng et al., 2009a,

2009b). The Anymaqen-Kunlun-Muztagh suture zone, which bounds the southern margin of the Kunlun-Qaidam Terrane, correlates eastward with the Shangdan suture zone of Ratschbacher et al. (2003) and Dong and Santosh (2015) in the Qinling area (Fig. 1B). In the west, the North and South Qilian sutures are truncated by the active left-slip Altyn Tagh fault (Yin and Harrison, 2000), with the offset estimates ranging from ~1200 km (CSBS, 1992) to ~500 km (Cowgill, 2001). A 500 km offset of the Qilian suture zones would require the presence of two suture zones in central Tarim (Yin and Nie, 1996), which may have reactivated along a ca. 900 Ma Proterozoic orogenic belt (Guo et al., 2005). The lack of early Paleozoic sutures in southern Tian Shan requires that the two Qilian suture zones terminate in the Tarim Basin.

Songpan-Ganzi Terrane and South China

The Songpan-Ganzi flysch complex of Yin and Nie (1993) or the Songpan-Ganzi Terrane of Yin and Harrison (2000) has several local names, including the Bayan Har (BYH in Fig. 3), Hoh Xil (HXL in Fig. 3), Tianshuihai (TSH in Fig. 3), and Karakul-Mazar (KMZ in Fig. 3) Terranes from east to west. This terrane (also spelled as Songpan-Ganzê Terrane) is composed dominantly of Triassic submarine-fan turbidite deposits with diverse sources (Yin and Nie, 1993, 1996; Nie et al., 1994; Zhou and Graham, 1996; Weislogel et al., 2006, 2010; Enkelmann et al., 2007; Weislogel, 2008; Yin and Harrison, 2000; Zhang et al., 2014), and its basement rocks are exposed only at its eastern end, where Triassic sedimentary strata rest conformably and disconformably on top of Permian and Devonian strata, which comprise parts of an 8–9-km-thick Sinian-Cryogenian to Early Permian passive-margin sequence along the western margin of the South China craton (Fig. 4E; Wang et al., 2013). The crystalline basement of the westernmost South China craton below the aforementioned passive-margin sequence contains 825–750 Ma felsic arc rocks (Fig. 4E; Zhou et al., 2002a, 2002b, 2006; Yan et al., 2006). Farther west, the contact relationship between the Songpan-Ganzi Terrane and South China is obscured by the deposition of thick Triassic marine sediments.

The thick sequence of Triassic Songpan-Ganzi flysch deposits, locally exceeding 10 km (Nie et al., 1994), may have been induced by (1) the development of a mélange complex (Şengör, 1984, 1990; Schwab et al., 2004; Robinson et al., 2012; Robinson, 2015) during the consumption of the Paleo-Tethys Ocean, (2) sedimentary accumulation in a remnant ocean extending from the western South China craton (Yin and Nie, 1993; Nie et al., 1994; Zhou and Graham, 1996; Weislogel et al., 2006, 2010; Weislogel, 2008), or (3) deposition of a thick sedimentary sequence during extreme extension of the southern margin of the Kunlun-Qaidam Terrane related to slab rollback of the Paleo-Tethyan oceanic plate (Pullen et al., 2008; Zhang et al., 2014, 2015). Note that the remnant-ocean model of Yin and Nie (1993) does not require the existence of an oceanic basin on the west side of South China (i.e., the basement of the Songpan-Ganzi Terrane could either be highly thinned continental crust or oceanic crust). A key prediction of the remnant ocean model is that the basement of the Songpan-Ganzi Terrane should be the same as that of South China, which contrasts to the prediction of the model by Pullen et al. (2008), which requires the basement of the Songpan-Ganzi Terrane to be a thinned Kunlun-Qaidam Terrane.

Isolated Late Triassic plutons also occur across the Songpan-Ganzi Terrane (Wang et al., 2013). Their origin has been attributed to (1) arc magmatism during hidden subduction (Şengör, 1984, 1990), (2) slab rollback of the Paleo-Tethyan oceanic plate (Pullen et al.,, 2008; Zhang et al. 2014, 2015), (3) extensional cracking of the mantle lithosphere (Yuan et al., 2010), and (4) delamination of the mantle lithosphere (Roger et al., 2004). Among these models, the slab rollback model of Pullen et al. (2008) predicts southward and eastward migration of arc magmatism,

which appears to be inconsistent with the age distribution of Triassic plutons in the Songpan-Ganzi Terrane (see fig. 1 of Zhang et al., 2014).

The nature of the Songpan-Ganzi basement rocks in regions where only Triassic strata are exposed at the surface has been inferred from U-Pb zircon dating and Nd isotope analysis of the Triassic plutonic rocks. Roger et al. (2004) suggested that the Triassic plutons in the eastern Songpan-Ganzi Terrane (i.e., the Bayan Har area) originated from melting of Proterozoic basement rocks. This conclusion is consistent with the seismic work of Jiang et al. (2006), who showed that the low Vp/Vs and Vp values obtained from a wide-angle reflection experiment constrain a felsic composition for the whole crust in the same area. M. Liu et al. (2006) reached a similar conclusion that the basement of the Songpan-Ganzi Terrane consists of intermediate and felsic crust in the Bayan Har area. In the Hoh Xil area, Zhang et al. (2014) derived a Nd model age of 1.6–1.1 Ga for the source region of the Triassic plutons. In the same region, lower-crustal xenoliths carried up to the surface by Cenozoic volcanism are exclusively mafic in composition (Lai et al., 2003, 2007), which is consistent with the geochemistry of the source regions for the Cenozoic volcanic rocks in the Hoh Xil area (Wang et al., 2005).

In the Tianshuihai area, a Paleoproterozoic metavolcanic complex, consisting of basaltic andesite and rhyolite and located in the hanging wall of the late Cenozoic Kongur-Muztaghata detachment fault, is interpreted to be the basement of the Songpan-Ganzi Terrane in the westernmost part of Tibet south of the Western Kunlun Range (Fig. 4F; Ji et al., 2011). However, there is no direct contact between the Triassic strata and the inferred basement in the area (Wang et al., 2013). A volcanic sample in the metamorphic complex yielded a U-Pb laser-ablation inductively coupled plasma–mass spectrometry (LA-ICP-MS) zircon age of 2481 ± 14 Ma (Ji et al., 2011). Detrital-zircon dating of high-grade gneiss and schist in the footwall of the Kongur-Muztaghata detachment fault (Robinson et al., 2004, 2007) in the Tianshuihai sector of the Songpan-Ganzi Terrane reveals their protolith to be Triassic sedimentary rocks (Robinson et al., 2012; Robinson, 2015). The presence of early Paleozoic and Permian–Triassic detrital zircon suggests that the Triassic rocks in this area were mainly derived from the southern margin of the Kunlun-Qaidam Terrane (Robinson et al., 2012; Robinson, 2015).

SAMPLE DESCRIPTIONS

Our study areas are located at the eastern and western ends of the Eastern Kunlun Range (Fig. 3). Fourteen granitoid samples, two volcanic samples, and five sedimentary samples were collected in the autumn of 2010 and the summer of 2011. U-Pb zircon age dating and geochemical analysis were carried out for the igneous samples, whereas U-Pb detrital-zircon dating and sandstone composition analysis were performed on the sedimentary samples. Sample locations are listed in Table 1 and also shown in Figures 5 and 6. To place our samples in the context of regional geology, we constructed a composite lithostratigraphic column for the Eastern Kunlun Range (Fig. 7).

Igneous Samples

In total, 14 medium- to coarse-grained granitoid samples, consisting of plagioclase feldspar, potassium feldspar, quartz, biotite, and hornblende, were collected in this study. The accessory minerals of the granitoid samples include zircon, apatite, titanite, and magnetite. Two volcanic samples, which display a porphyritic texture and consist of subidiomorphic altered plagioclase, kaersutite, clinopyroxene, and olivine, were also collected in this study. Accessory minerals in the volcanic samples include zircon and titanite. The volcanic samples are locally altered, which is expressed

by the alteration of plagioclase to albite and in some cases to chlorite and partial alteration of hornblende to chlorite. The altered parts of the volcanic samples were not used in our chemical analysis.

Sedimentary Samples

Using the newly published regional geologic map of the Tibetan Plateau by Wang et al. (2013) as a guide, we collected medium-grained sandstone samples for detrital-zircon dating from (1) Proterozoic(?) (sample WC051411-10), (2) Proterozoic(?) (sample WC051411-6), (3) Triassic (sample WC100410-4A), (4) Lower Triassic (sample WC100410-3A), and (5) Cretaceous (sample WC051411-5) strata. Although sample WC051411-10 and WC051411-6 were collected from the Proterozoic unit of Wang et al. (2013), their detrital-zircon ages are as young as Devonian, which indicate an incorrect original age assignment. In light of this new geochronology data, we have reassigned this unit an undifferentiated Devonian-Permian age (Fig. 6).

ANALYTICAL METHODS

Mineral Separation

Mineral separation was conducted at the Institute of the Hebei Regional Geology and Mineral Survey in Langfang, China. The mineral separation procedures are as follows. Samples were crushed to pass a 60 mesh sieve and were then manually washed by water and alcohol. We used an electromagnetometer to remove magnetic minerals and a heavy liquids to concentrate heavy minerals. Zircon grains were then handpicked under a binocular microscope. Zircon grains from individual samples were randomly mounted in epoxy resin and polished close to one-third of individual grain diameters. Cathodoluminescence (CL) imaging was employed to investigate the internal texture of zircon, which in turn was used for selecting appropriate spots for U-Pb dating.

U-Pb Zircon Dating

U-Pb dating of zircon was conducted using an Agilent 7500a Q-ICP-MS with a 193 nm excimer ArF laser-ablation system at the Institute of Tibetan Plateau Research, Chinese Academy of Science. The first 15 s with the laser-off mode were used to collect the background values, and the following 40 s with the laser-on mode were employed to measure the peak intensities of the ablated material. Considering the size distribution of these magma zircon grains and signal stability, we adopted 25 μm ablation pits for all grains. The analytical procedure is similar to that in Xie et al. (2008), using Plesovice zircon and NIST SRM 612 as standards.

Geochemical Analyses of Igneous Rocks

Granitoid and volcanic samples were analyzed for major and trace elements at the Institute of Hebei Regional Geology and Mineral Survey in Langfang, China. Sample preparation began with the removal of weathered surfaces by chipping until a fresh, unweathered surface was exposed. Portions of samples were crushed and then powdered. Major-element measurements were carried out using an Axios Max X-ray fluorescence spectrometer. The accuracies of the analyses are estimated to be ~1% for SiO_2 and ~2% for other oxides. Trace-element measurements were carried out using a plasma mass spectrometer. Two multi-element standard solutions, one containing Li, Ba, V, Cr, Co, Ni, Cu, Zn, Ga, Rb, Sr, Cs, Ba, Pb, Th, U, Sc, Y, and fourteen rare earth elements (REEs) and another containing W, Mo, Nb, Ta, Zr, and Hf, were employed for external

TABLE 1. SUMMARY OF SAMPLE LOCATIONS AND THEIR CORRESPONDING SITE NUMBERS SHOWN IN FIGURES 3, 5 AND 6

Sample number	Description	Dating method	Latitude (°N)	Longitude (°E)	Sample sites	Data source	Age (Ma)
Samples of igneous rocks							
WC051411-4A	Granitoid		37.47	91.671	Site 11 in Fig. 6	This study	
WC051411-7	Granitoid	U-Pb zircon	37.25	91.908	Site 8 in Fig. 6	This study	416.5 ± 2.6
WC051511-1B	Granitoid		37.39	91.468	Site 10 in Fig. 6	This study	
WC051511-2B	Granitoid		37.567	91.757	Site 12 in Fig. 6	This study	
WC051511-3A	Granitoid		37.55	91.904	Site 13 in Fig. 6	This study	
WC100110-1A	Granitoid		35.8	98.11	Site1 in Fig. 5	This study	
WC100110-1B	Granitoid	U-Pb zircon	35.833	98.267	Site 2 in Fig. 5	This study	222.6 ± 1.2
WC100110-5A	Granitoid	U-Pb zircon	35.9	98.096	Site 3 in Fig. 5	This study	433.6 ± 3.8
WC100210-2B	Granitoid		35.602	97.946	Site 6 in Fig. 5	This study	
WC100210-2C	Granitoid	U-Pb zircon	35.642	98.446	Site 4 in Fig. 5	This study	253.6 ± 1.4
WC100210-2A	Granitoid		35.742	98.006	Site 7 in Fig. 5	This study	
WC1002010-4B	Granitoid	U-Pb zircon	35.433	98.55	Site 5 in Fig. 5	This study	251.4 ± 1.7
WC051411-11	Granitoid	U-Pb zircon	37.363	91.861	Site 9 in Fig. 6	This study	432.4 ± 4.1
WC051411-12	Basaltic andesite	U-Pb zircon	37.442	91.717	Site 14 in Fig. 6	This study	ca. 283
WC051511-2C	Basaltic andesite		37.567	91.857	Site 15 in Fig. 6	This study	
Sedimentary and metasedimentary samples							
WC051411-6	Sandstone	U-Pb zircon	37.3820	91.8310	Upper Devonian strata; site D in Fig. 6	This study	
WC051411-10	Schist	U-Pb zircon	37.2760	91.9420	Devonian strata; site C in Fig. 6	This study	
WC100410-4A	Sandstone	U-Pb zircon	35.2330	98.7260	Triassic strata; site A in Fig. 5	This study	
WC100410-3A	Sandstone	U-Pb zircon	35.0670	98.6360	Lower Triassic strata; site B in Fig. 5	This study	
2004T004	Sandstone	U-Pb zircon	35.4120	99.3500	Middle Triassic strata; site 1 in Fig. 3	Ding et al. (2013)	
2004T283	Sandstone	U-Pb zircon	35.9930	93.5835	Upper Triassic strata; site 2 in Fig. 3	Ding et al. (2013)	
2004T284	Sandstone	U-Pb zircon	35.9439	94.3625	Upper Triassic strata; site 3 in Fig. 3	Ding et al. (2013)	
WC051411-5	Sandstone	U-Pb zircon	37.4630	91.6690	Cretaceous strata; site E in Fig. 6	This study	
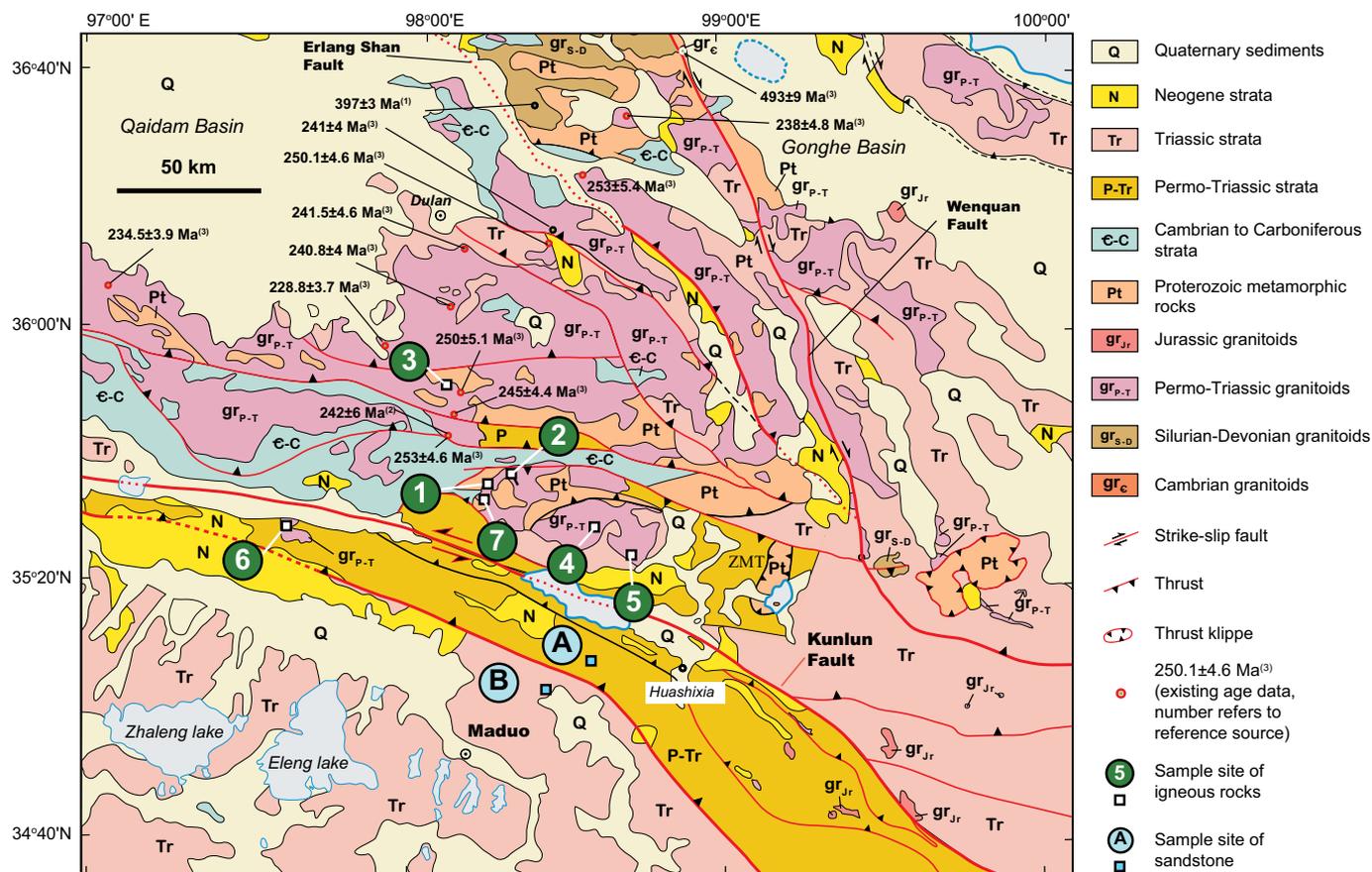
Data sources: (1) Wu et al. (2004a); (2) Liu et al. (2004); (3) Chen et al. (2012)

Figure 5. Simplified geologic map at the eastern end of the Eastern Kunlun Range, modified after Jiang et al. (2008) and X.H. Chen al. (2012). Shown in the map are locations of samples collected in this study. Sample locations of early studies by Wu et al. (2004a), Liu et al. (2004), and X.H. Chen et al. (2012) are also shown. ZMT—Zuimatan klippe.
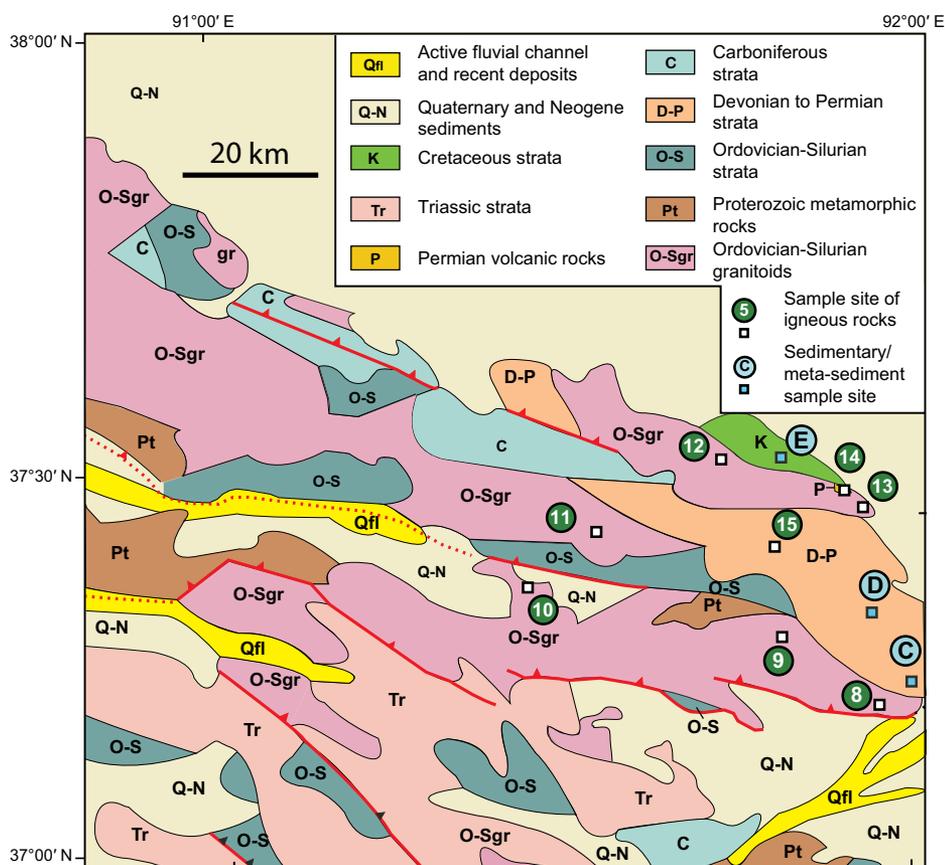
Figure 6. Geological map of the westernmost Eastern Kunlun Range, modified from Wang et al. (2013). The map shows the sample localities with circled numbers corresponding to those listed in Table 1.

calibration. Major-element data are reported in normalized percentage, and trace-element data are reported in parts per million (ppm). The reference standards are the same as those used for major-oxide analyses. The accuracies for most of the trace-element measurements are estimated to be better than 5%. All the geochemical data for major oxides and measured values of trace elements are summarized in Table 2.

Sandstone Composition

Modal compositions of sandstone samples were analyzed using the following procedure. At least 300 grains were counted using the Gazzi-Dickinson method on each thin section (Dickinson, 1970, 1985; Ingersoll et al., 1984,). The grain types were identified and tabulated following Ingersoll et al. (1984) and Dickinson (1985). As the purpose of this study was to determine the first-order trends, we only tabulated quartz (Q), feldspar (F), and lithic fragments (L) in our analysis. Potassium feldspar and plagioclase were differentiated optically.

RESULTS OF U-Pb ZIRCON DATING OF IGNEOUS ROCKS

U-Pb Zircon Ages of Granitoid Samples

The analytical data from U-Pb zircon dating of granitoid samples can be found in the GSA Data Repository.[1] Zircon grains chosen for this

study were euhedral and prismatic in shape and ~100–150 μm long. The length-to-width ratios of dated zircon grains were typically 2:1–3:1. Most of the dated zircon grains were transparent and colorless under the optical microscope, although some appeared brownish, possibly due to high U contents. Zircon grains display both concentric zoning and inherited cores with magmatic overgrowth rims (Fig. 8). In total, 180 zircons were analyzed, and the analytical data results are shown in Figure 9. Most analyses are concordant or nearly concordant, clustering as single age populations. To eliminate the effects of radiation damages (typically displayed by dark CL images indicating high contents), Pb loss, and error analyses, we used only the ages that clearly belonged the same Gaussian distribution for calculating the weighted mean ages of pluton emplacement (e.g., Dai et al., 2013b). Their weighted mean $^{206}Pb/^{238}U$ ages are interpreted to represent the crystallization age of the plutons from which the samples were collected. A few inherited zircons display discordant ages (Fig. 9).

Sample WC100110-5A

This sample was collected from a weakly foliated granitoid at the eastern end of the Eastern Kunlun Range (site 3 in Fig. 5). Zircon grains from the sample display oscillatory zonation. In total, 30 zircon grains were analyzed, each of which was sampled by one spot either at its rim or at the core (Fig. 8A). Among the measurements, 17 dates from zircon rims yielded a concordant $^{206}Pb/^{238}U$ age of 433.6 ± 3.8 Ma (mean square of weighted deviates [MSWD] = 0.9; Fig. 9A). The inherited cores of another six zircon grains were analyzed, which yielded older ages of ca. 460 Ma, ca. 499 Ma, ca. 503 Ma, ca. 820 Ma, ca. 827 Ma, ca. 975 Ma, and ca. 1251 Ma, respectively (see footnote 1; Fig. 8A). We interpret the younger age of 433.6 ± 3.8 Ma from the zircon rims as representing the

age of pluton crystallization, whereas the older core dates represent the wall rock or a remolten older crust.

Sample WC051411-11

This sample was collected from the western end of the Eastern Kunlun Range (site 9 in Fig. 6). In total, 30 zircon grains were analyzed, each of which was analyzed at one spot at the rim or the core (Fig. 8B). Among the 30 analyzed grains, 18 spots were collected from zircon rims, which yielded a concordant $^{206}Pb/^{238}U$ age of 432.4 ± 4.1 Ma (MSWD = 1.3; Fig. 9B). The rest of the grains were analyzed from the zircon cores, which yielded older ages of ca. 959 Ma, ca. 969 Ma, ca. 1249 Ma, ca. 1261 Ma, ca. 1645 Ma, ca. 2059 Ma, ca. 2412 Ma, ca. 2543 Ma, and ca. 3090 Ma, respectively. We interpret the younger date of 432.4 ± 4.1 Ma to represent the age of pluton crystallization and the older core ages to represent the ages of the assimilated wall rock or a remolten older crust.

Sample WC051411-7

This sample was collected from the western end of the Eastern Kunlun Range (site 8 in Fig. 6). In total, 30 zircon grains were analyzed from this sample. Each zircon grain was analyzed at one spot at the rim or the core (Fig. 8C). Among the 30 analyzed grains, 20 spots were collected from the zircon rims, which yielded a concordant $^{206}Pb/^{238}U$ age of 416.5 ± 2.6 Ma (MSWD = 2.1; Fig. 9C). The cores of the other grains yielded older ages of ca. 481 Ma, ca. 636 Ma, ca. 644 Ma, ca. 731 Ma, ca. 763 Ma, ca. 1241 Ma, and ca. 1313 Ma. We interpret the younger rim date of 416.5 ± 2.6 Ma to represent the age of pluton crystallization and the older core dates of 480–1313 Ma to represent the ages of inherited zircon, either from the wall rock or from a remolten crust. We note that the 481 Ma zircon age is similar to the oldest Paleozoic plutonic ages in the Eastern Kunlun Range area (Li et al., 2013), which implies remelting of older arc rocks generated by the same phase of subduction in the region.

Sample WC100210-2C

This sample was collected from the eastern end of the Eastern Kunlun Range (site 4 in Fig. 5). In total, 24 zircon grains were analyzed. Each grain was analyzed at one spot, and the beam was only focused on the grain rims for all cases (Fig. 8D). The 18 spots collected from the zircon rims yielded a concordant $^{206}Pb/^{238}U$ age of 253.6 ± 1.4 Ma (MSWD = 1.4; Fig. 9D), which we interpret to represent the crystallization age of the pluton.

Sample WC100210-4B

This sample was collected from the eastern end of the Eastern Kunlun Range (site 5 in Fig. 5). In total, 29 zircon grains were analyzed, with each grain analyzed at one spot. All 29 spots were collected from zircon rims (Fig. 8E), which yielded a concordant $^{206}Pb/^{238}U$ age of 251.4 ± 1.7 Ma (Fig. 9E). We interpret this age to represent the crystallization age of the pluton.

Sample WC100110-1B

This sample was collected from the eastern end of the Eastern Kunlun Range (site 2 in Fig. 5). In total, 29 zircon grains were analyzed, with each grain analyzed at one spot from the rim (Fig. 8F). The analyses from the zircon rims yielded a concordant $^{206}Pb/^{238}U$ age of 222.6 ± 1.2 Ma (Fig. 9F). We interpret this date to represent the crystallization age of the pluton.

U-Pb Zircon Ages of Volcanic Sample

We perform U-Pb zircon dating of a volcanic sample (sample WC051411-12 in Table 1) collected at the western end of the Eastern Kunlun Range (site 14 in Fig. 6). Zircon in this sample displays oscillatory
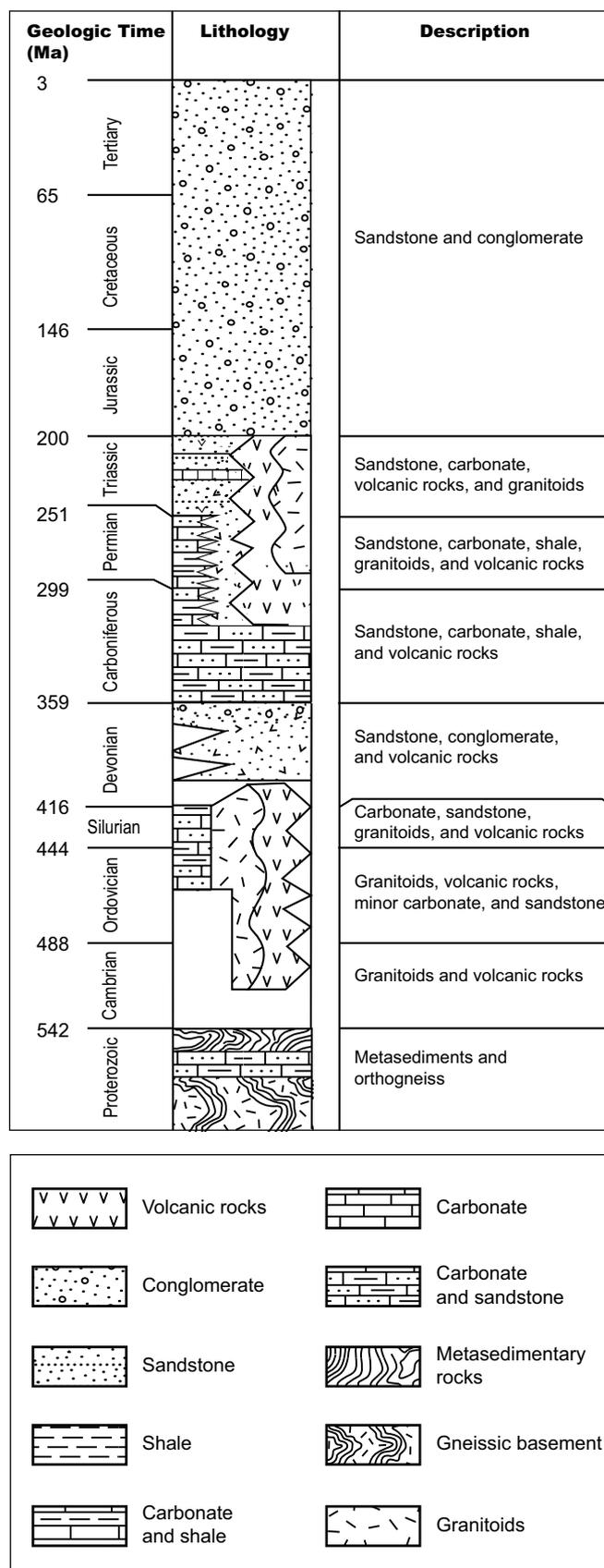
Figure 7. A simplified regional tectono-stratigraphic section of the Eastern Kunlun Range compiled from Wang et al. (2013).

TABLE 2. MAJOR AND TRACE ELEMENTS FOR THE GRANITOID AND VOLCANIC ROCK SAMPLES FROM THE EASTERN KUNLUN

Description:				Granitoid				
Samples:	WC051411-4A	WC051411-11	WC051411-7	WC051511-1B	WC051511-2B	WC051511-3A	WC100110-1A	WC1001010-1B
Major element (wt%)								
SiO_2	67.66	68.92	68.05	68.00	75.26	71.09	67.84	61.67
TiO_2	0.54	0.66	0.57	0.56	0.17	0.31	0.45	0.68
Al_2O_3	14.16	13.89	14.16	14.13	13.17	15.21	14.77	16.19
Fe_2O_3	1.27	0.25	1.34	1.08	0.11	0.46	1.25	1.66
MgO	2.19	1.31	1.79	1.67	0.29	0.64	1.50	2.82
CaO	1.92	2.04	3.53	3.71	1.43	2.58	3.55	5.08
MnO	0.08	0.07	0.09	0.07	0.03	0.03	0.09	0.08
FeO	3.09	3.54	3.28	3.21	0.77	1.27	2.66	3.54
Na_2O	2.66	2.81	2.26	2.21	3.64	4.44	3.43	3.34
K_2O	3.94	4.06	3.41	3.17	3.94	3.01	3.12	3.19
P_2O_5	0.10	0.13	0.09	0.09	0.05	0.09	0.10	0.16
A/CNK	1.16	1.09	1.02	1.02	1.02	1.00	0.95	0.89
A/NK	1.64	1.54	1.91	2.00	1.28	1.44	1.63	1.81
$Na_2O + K_2O$	6.61	6.87	5.67	5.38	7.58	7.45	6.56	6.53
H_2O^+	2.04	1.72	1.09	1.61	0.70	0.52	0.99	0.92
H_2O^-	0.11	0.21	0.11	0.16	0.16	0.20	0.24	0.16
Total	99.88	99.90	99.86	99.87	99.94	99.90	99.87	99.84
Trace element (ppm)								
Li	21.40	36.02	121.80	50.50	34.42	105.52	39.34	33.68
Be	3.21	2.89	5.53	2.95	6.44	6.18	2.03	2.45
Sc	18.26	19.63	13.41	17.00	3.49	5.91	13.02	16.36
V	61.26	71.33	66.09	65.39	9.47	24.95	80.12	114.20
Cr	37.52	39.71	35.29	38.00	8.46	9.29	13.19	29.58
Co	9.40	10.91	10.00	9.76	0.89	2.68	8.28	16.18
Ni	8.20	8.69	12.02	8.52	1.30	1.46	2.95	14.04
Cu	19.23	19.72	22.64	18.84	15.87	12.00	13.63	18.68
Zn	38.00	43.53	41.85	37.93	17.97	25.52	33.19	33.84
Ga	18.87	21.05	25.35	20.73	23.90	24.02	18.07	22.14
Rb	198.30	151.70	316.80	132.70	244.60	230.80	121.70	138.90
Sr	120.20	164.90	127.70	150.80	148.00	358.20	237.70	500.10
Y	36.85	33.27	75.40	28.53	25.22	30.72	25.35	23.56
Zr	188.63	257.91	175.40	170.00	65.35	113.26	140.44	191.89
Nb	15.73	16.72	29.99	15.78	12.82	29.41	11.62	15.56
Cs	3.56	10.26	21.23	7.12	11.81	18.68	7.14	7.79
Ba	829.30	699.00	614.90	944.40	311.60	459.20	902.10	951.20
La	38.58	28.32	72.92	26.72	24.00	22.67	30.38	22.39
Ce	79.88	61.43	183.75	55.73	47.65	45.03	58.89	52.74
Pr	10.05	7.84	19.84	7.13	6.07	5.76	7.08	7.72
Nd	34.05	27.55	67.46	24.67	19.90	19.77	22.96	27.90
Sm	6.93	5.98	14.79	5.19	4.69	4.25	4.52	5.80
Eu	1.11	1.14	1.20	1.16	0.57	0.81	1.00	1.17
Gd	5.91	5.02	12.18	4.47	3.73	3.75	3.91	4.52
Tb	1.13	1.01	2.36	0.88	0.78	0.76	0.75	0.83
Dy	6.61	6.04	13.37	5.21	4.42	4.57	4.42	4.39
Ho	1.38	1.26	2.70	1.09	0.85	0.99	0.91	0.87
Er	3.97	3.58	7.81	3.08	2.35	2.72	2.67	2.41
Tm	0.74	0.64	1.41	0.55	0.41	0.46	0.49	0.41
Yb	4.48	4.06	8.89	3.45	2.54	2.94	3.17	2.62
Lu	0.57	0.53	1.16	0.45	0.38	0.43	0.41	0.33
Hf	10.42	15.26	8.04	9.67	3.39	5.27	7.82	14.69
Ta	1.73	1.79	3.37	1.63	3.03	2.45	1.52	1.49
Pb	14.99	32.00	51.77	23.80	44.49	44.54	24.36	15.37
Th	19.42	18.41	68.82	14.28	18.98	13.83	16.22	10.28
U	3.97	1.84	7.57	1.22	3.46	7.30	1.63	1.14
Eu/Eu*	0.52	0.62	0.26	0.72	0.40	0.61	0.71	0.68
Sr/Y	3.26	4.96	1.69	5.29	5.87	11.66	9.38	21.23
(La/Yb)N	6.17	5.00	5.88	5.56	6.77	5.53	6.86	6.12

(continued)

TABLE 2. MAJOR AND TRACE ELEMENTS FOR THE GRANITOID AND VOLCANIC ROCK SAMPLES FROM THE EASTERN KUNLUN (*continued*)

Description:	Granitoid					Volcanic rock	
Samples:	WC10010-5A	WC1002010-2B	WC100210-2C	WC100210-2A	WC100210-4B	WC051511-2C	WC051411-12
Major element (wt%)							
SiO_2	74.99	73.67	69.34	65.09	65.84	50.58	50.31
TiO_2	0.14	0.35	0.42	0.58	0.56	16.54	15.48
Al_2O_3	13.32	13.27	14.45	15.03	15.52	1.32	1.07
Fe_2O_3	0.09	0.26	1.29	1.24	0.95	1.48	5.92
MgO	0.24	0.74	1.05	2.09	2.11	7.23	2.02
CaO	0.82	3.15	3.40	4.54	4.63	8.20	6.86
MnO	0.02	0.04	0.06	0.10	0.10	6.86	2.33
FeO	1.13	1.77	2.47	3.50	3.83	0.93	1.64
Na_2O	3.06	3.51	3.38	3.19	3.24	3.18	6.72
K_2O	5.45	1.44	2.85	2.59	1.14	0.17	0.10
P_2O_5	0.07	0.07	0.10	0.11	0.12	0.16	0.14
A/CNK	1.07	1.01	0.97	0.92	1.04	0.78	0.61
A/NK	1.22	1.81	1.67	1.86	2.37	2.65	1.21
$Na_2O + K_2O$	8.51	4.95	6.23	5.78	4.38	4.11	8.36
H_2O^+	0.57	1.04	0.77	1.41	1.65	2.97	2.10
H_2O^-	0.11	0.20	0.10	0.14	0.11	0.29	0.17
Total	99.95	99.90	99.87	99.87	99.92	99.88	99.95
Trace element (ppm)							
Li	15.21	8.58	6.05	8.15	17.76	49.27	21.39
Be	4.11	2.89	2.22	2.06	2.89	1.39	2.21
Sc	5.34	2.48	8.08	17.05	20.17	30.12	30.61
V	7.64	46.66	65.62	121.50	122.80	188.70	158.90
Cr	7.88	8.64	12.12	15.27	13.76	162.45	192.06
Co	2.70	4.95	7.25	12.02	11.85	39.70	18.72
Ni	1.40	1.44	2.31	3.94	4.29	70.44	69.47
Cu	13.33	12.01	14.23	14.60	19.14	22.35	17.30
Zn	17.89	19.33	33.52	39.03	37.62	63.66	59.13
Ga	22.55	16.69	19.95	18.93	21.41	19.89	23.84
Rb	320.40	37.31	102.10	86.79	57.98	50.04	121.20
Sr	69.36	321.90	270.90	289.10	288.50	285.90	124.30
Y	17.42	12.68	16.45	26.58	40.66	28.65	19.97
Zr	102.93	154.64	184.98	161.81	166.73	144.68	135.85
Nb	29.77	7.35	11.37	13.60	15.01	6.12	5.20
Cs	7.59	1.02	2.84	1.88	3.63	2.13	6.87
Ba	263.80	630.20	724.60	844.10	373.30	154.30	299.20
La	81.02	131.50	44.79	30.60	18.69	10.42	31.29
Ce	200.50	253.75	75.24	58.70	38.21	24.44	56.66
Pr	20.42	17.41	8.47	7.21	5.32	3.81	7.13
Nd	64.76	43.77	24.86	23.96	20.05	15.79	24.41
Sm	13.65	4.56	3.84	4.78	5.18	4.44	4.75
Eu	0.61	1.36	1.04	1.14	1.21	1.50	1.40
Gd	9.29	4.60	3.26	4.06	4.73	4.09	3.69
Tb	1.34	0.53	0.52	0.80	1.10	0.91	0.64
Dy	4.86	2.43	2.81	4.64	6.97	5.47	3.61
Ho	0.64	0.48	0.58	0.99	1.51	1.13	0.78
Er	1.39	1.41	1.72	2.90	4.37	3.17	2.44
Tm	0.16	0.25	0.33	0.54	0.85	0.55	0.45
Yb	0.92	1.56	2.12	3.46	5.52	3.36	2.95
Lu	0.27	0.21	0.30	0.44	0.67	0.56	0.48
Hf	4.31	7.37	8.95	10.47	11.21	4.67	4.52
Ta	3.79	0.99	1.82	1.64	2.08	0.60	0.56
Pb	45.17	16.73	28.37	27.33	22.25	6.46	20.06
Th	44.10	29.43	22.15	18.40	11.07	2.63	3.73
U	5.39	1.59	2.82	1.69	5.76	0.89	2.39
Eu/Eu*	0.16	0.90	0.87	0.77	0.73	1.06	0.98
Sr/Y	3.98	25.39	16.47	10.88	7.10	9.98	6.22
(La/Yb)N	6.33	6.03	15.18	6.35	2.43	2.22	7.61

Note: A/CNK—molecular $Al_2O_3/(CaO + Na_2O + K_2O)$; A/NK—molecular $Al_2O_3/(Na_2O + K_2O)$; Eu/Eu*—$Eu_N/(Sm_N + Gd_N)^{1/2}$, where N—chondrite-normalized value from Sun and McDonough (1989).
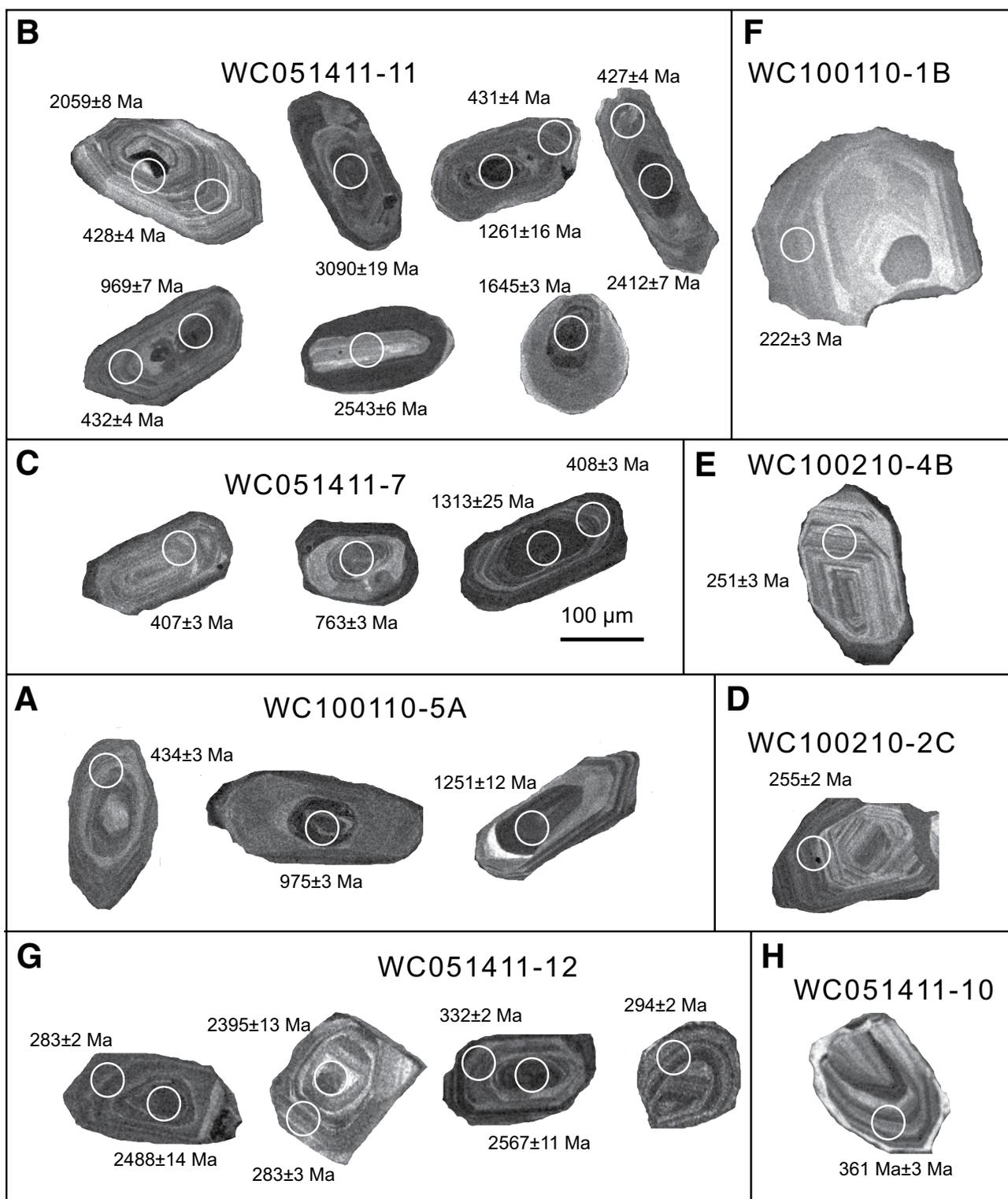
Figure 8. Representative cathodoluminescence (CL) images of zircon dated in this study. White circles are analyzed spots for U-Pb dating. Scale bar in C applies to all panels.
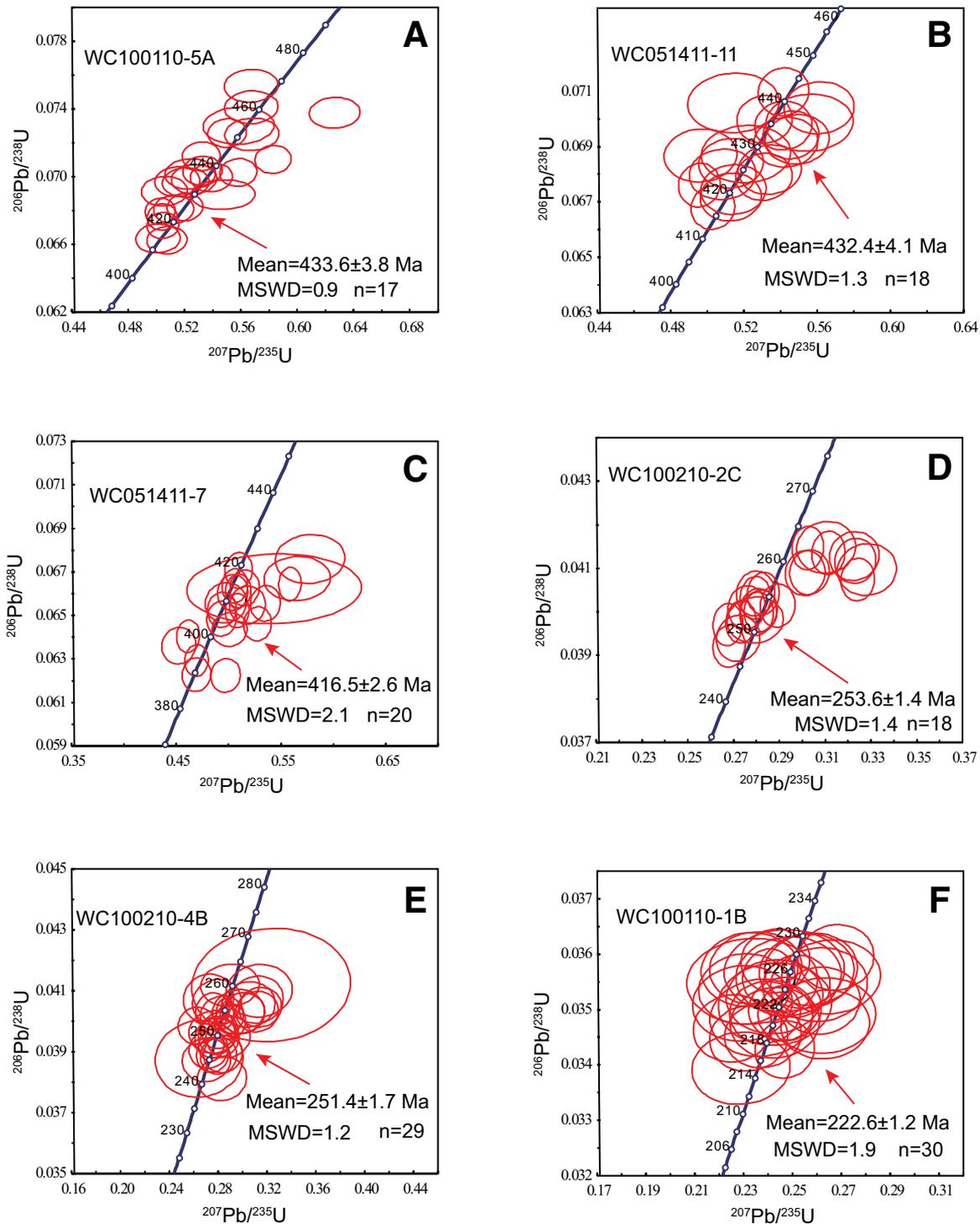
Figure 9. Zircon $^{207}Pb/^{235}U$-$^{206}Pb/^{238}U$ concordia diagrams of granitic samples collected from the Eastern Kunlun Range. MSWD—mean square of weighted deviates.

zonation (Fig. 8G). In total, 35 zircon grains were analyzed, with each grain sampled at one spot. Among the analyzed grains, 24 spots were collected from the zircon rims, which yielded two age peaks at ca. 283 Ma and ca. 330 Ma (Fig. 10). The cores of the rest of the nine grains yielded ages of ca. 2126 Ma, ca. 2338 Ma, ca. 2395 Ma, ca. 2423 Ma, ca. 2424 Ma, ca. 2462 Ma, ca. 2488 Ma, ca. 2519 Ma, and ca. 2567 Ma, respectively (Fig. 10). The wide range of zircon ages is likely a result of incorporation of older wall rock into the ascending magma from which the volcanic sample dated in this study was derived. Thus, we interpret the younger rim age of ca. 283 Ma to represent the emplacement age of the dated volcanic rock sample and the older core ages to represent the ages of inherited zircon from the basement of the arc. The analytical data for U-Pb zircon dating of the volcanic sample can be found in GSA Data Repository (see footnote 1).

RESULTS OF GEOCHEMICAL ANALYSIS OF IGNEOUS ROCKS

Major- and Trace-Element Compositions of the Granitoid Samples

In total, 13 granitoid samples were analyzed for major- and trace-element compositions. Oxide contents range from 75.2 to 77.7 wt% for SiO_2, 11.5 to 12.4 wt% for Al_2O_3, 0.24 to 2.19 wt% for MgO, 0.82 to 5.08 wt% for CaO, 2.21 to 4.44 wt% for Na_2O, 1.14 to 5.45 wt% for K_2O, 4.38 to 8.51 wt% for ($K_2O + Na_2O$), and 0.14 to 0.68 wt% for TiO_2 (Table 2). The samples ware peraluminous, as indicated by molar A/CNK = 0.89–1.16 and A/NK = 1.22–2.37 (Maniar and Piccoli, 1989). The analyzed samples are classified as granite, granodiorite, and tonalite on the ($K_2O + Na_2O$) versus SiO_2 plot (Fig. 11A; Middlemost, 1994). In the K_2O versus SiO_2 diagram (Le Maitre et al., 1989; Rickwood, 1989), most samples plot in the field of the high-potassium calc-alkaline series (Le Maitre et al., 1989; Rickwood, 1989), with the exception of samples WC051511-1B and WC051411-7, which fall in field of the calc-alkaline series (Fig. 11B).

Analytical results of trace-element measurements are summarized in Table 2. For the early Paleozoic granitoid samples, the multi-element diagram normalized by the primitive-mantle composition shows enrichment in large ion lithophile elements (LILEs) and depletion in high field strength elements (HFSEs; Fig. 11C). A similar multi-element concentration pattern was also obtained for the granitoid samples with Permian–Triassic ages (Fig. 11D).

The REE abundances normalized by chondrite values of Sun and McDonough (1989) vary from sample to sample. All samples displayed enriched light rare-earth element (LREE) and flat heavy rare-earth element (HREE) profiles without distinct Ce anomalies (Figs. 11E and 11F). The most prominent difference in the REE abundance plot between the early Paleozoic and Permian–Triassic samples is that the older samples display a stronger negative Eu anomaly relative to the younger samples (Figs. 11E and 11F). The negative Eu anomalies are commonly associated with removal of feldspar from felsic melts during crystal fractionation (e.g., Rollinson, 2014).

The early phase granitoids with early Paleozoic ages plotted in the field of A-type granites (Fig. 12A), which are generally associated with extension regardless of the origin of the magma source (e.g., Whalen et al., 1987; Eby, 1990, 1992; Turner et al., 1992). In contrast, the young phase granitoids with Permian–Triassic ages plotted in the field of I- and S-type of granites, which are commonly associated with arc magmatism and crustal anatexis (e.g., Whalen et al., 1987; Eby, 1990, 1992; Turner et al., 1992; Fig. 12B). Discrimination diagrams allow further refinement of the assigned tectonic environments of the two phases of granitoids from the Eastern Kunlun Range. In the Rb versus (Yb + Ta) diagram
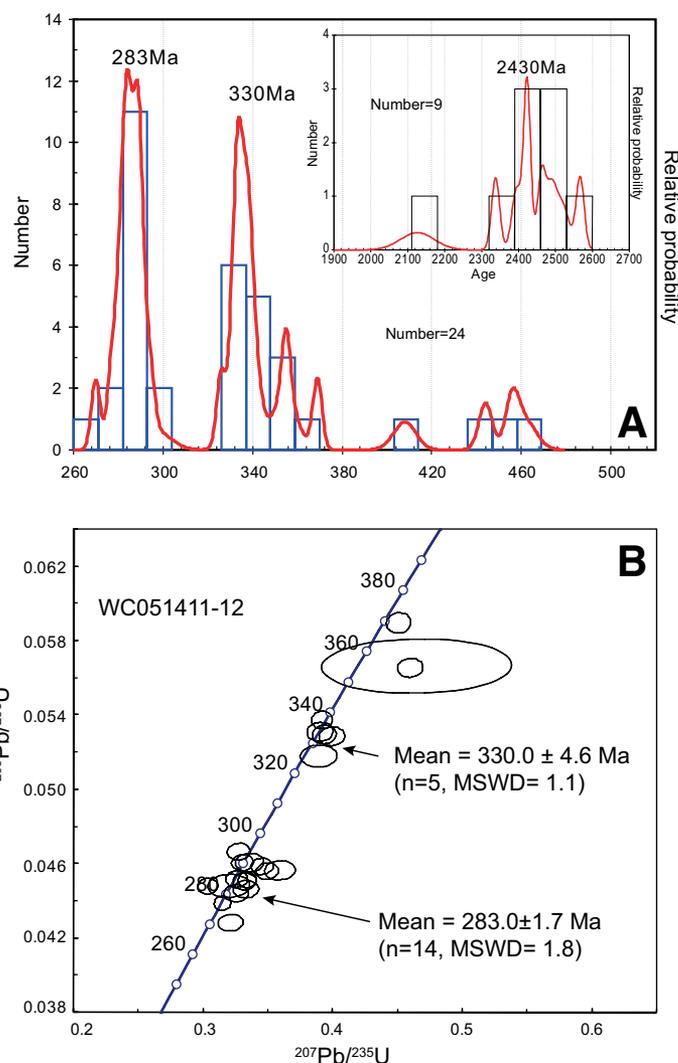
Figure 10. (A) U-Pb zircon age spectrum of a Permian volcanic sample (WC051411-12) obtained from this study. See site 14 in Figure 6 for sample location. (B) Zircon $^{207}Pb/^{235}U$-$^{206}Pb/^{238}U$ concordia diagrams of Permian volcanic sample (WC051411-12). MSWD—mean square of weighted deviates.

(Pearce et al., 1984; Pearce, 1996), the early phase granitoids with early Paleozoic ages plotted in the triple junction region of the volcanic-arc, collision-orogen, and within-plate fields, whereas the late-phase granitoids with Permian–Triassic ages mostly plotted in the volcanic-arc field (Figs. 12C and 12D). In the Nb versus Y diagram (Pearce et al., 1984; Pearce, 1996), the early Paleozoic granitoid samples fall in the transition region between the volcanic-arc/syncollisional field and the within-plate field, whereas the Permian–Triassic granitoids mostly belong to the volcanic-arc/syncollision fields (Figs. 12E and 12F).

Volcanic Samples

The SiO_2 contents of the volcanic samples, with one dated at ca. 283 Ma, range from 50.31 to 50.58 wt%, the MgO content from 2.33 to 6.86 wt%, the Al_2O_3 content from 15.48 to 16.54 wt%, the Fe* (Fe* = Fe_2O_3 + FeO) content from 7.94 to 8.71 wt%, the Na_2O content from 3.18 to 6.72 wt%, and the K_2O content from 0.93 to 1.64 wt% (Table 2). In the SiO_2 versus
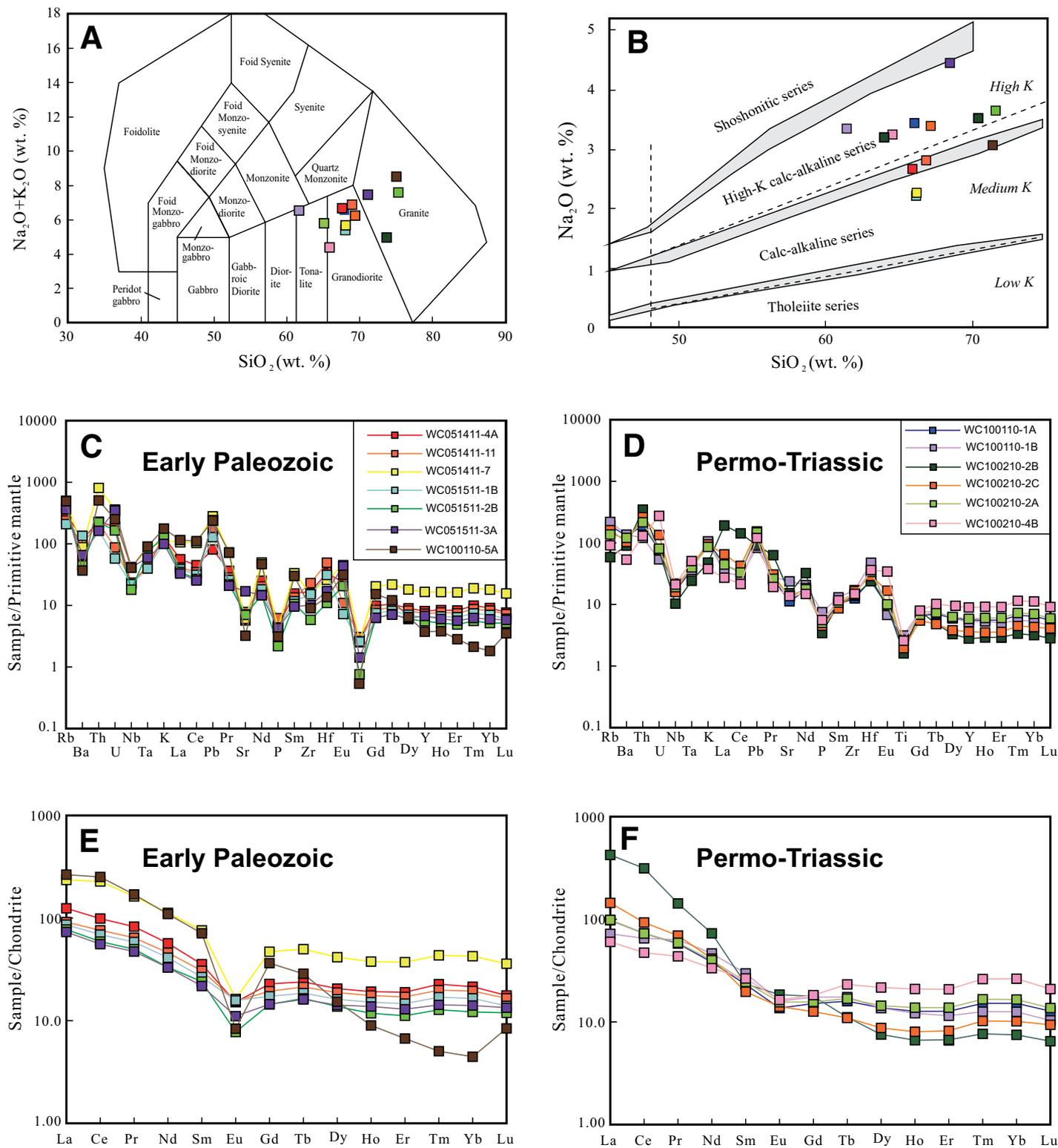
Figure 11. (A) SiO$_2$-(K$_2$O + Na$_2$O) (total alkali-silica [TAS]) diagram for intrusive rocks. Normalization values are from Middlemost (1994). (B) Na$_2$O vs. SiO$_2$ diagram for intrusive rocks. Normalization values are from Le Maitre et al. (1989) and Rickwood (1989), respectively. (C–D) Primitive mantle–normalized spider diagrams for early- and late-phase granitoid samples. Normalization values are from Sun and McDonough (1989). (E–F) Chondrite-normalized rare earth element (REE) diagrams for the early- and late-phase granitoid samples. Normalization values are from Boynton (1984).
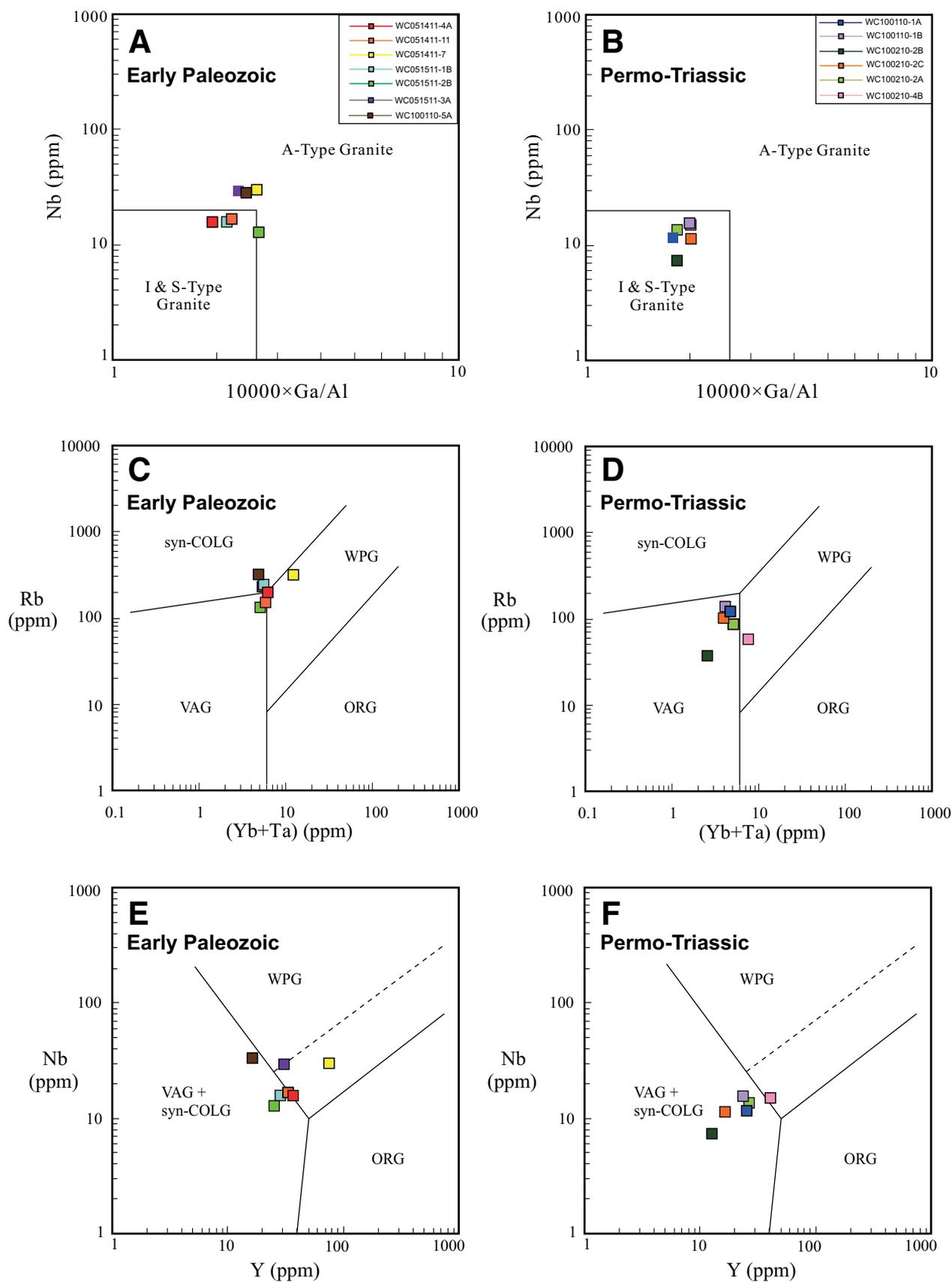
Figure 12. Discrimination diagrams based on Pearce et al. (1984) and Whalen et al. (1987) for plutonic samples. See text for details. Abbreviations: syn-COLG—syn-collisional granite; WPG—within-plate granite; ORG—orogenic granite; VAG—volcanic-arc granite.

($K_2O + Na_2O$) (total alkali-silica [TAS]) diagram (Le Maitre et al., 1989), our volcanic samples plot on the boundary between basalt and basaltic andesite (Fig. 13A). The volcanic samples can also be classified in the calc-alkaline series (Fig. 13B; Kuno, 1968; Irvine and Baragar, 1971; Le Maitre et al., 1989; Arculus, 2003). The LREEs are uniformly enriched, as seen in the chondrite-normalized REE and primitive mantle–normalized trace-element patterns (Figs. 13C and 13D). These geochemical analyses alone would indicate that the volcanic rocks were emplaced in an oceanic arc setting. However, we note that coeval granites also occur in the Eastern Kunlun Range area (Zhang et al., 2012). Thus, the emplacement of the basaltic flow and basaltic andesite most likely occurred in an Andean-type continental arc setting, possibly related to backarc extension and/or delamination of the eclogitized mafic arc root (e.g., Kay et al., 1994). Taken together, these geochemical characteristics suggest that the volcanic rocks were generated in a continental arc setting similar to the North American Cordillera (e.g., Christiansen et al., 1986) and the South America Andes (e.g., Hildreth and Moorbath, 1988; Kay et al., 1989, 2005).

All the volcanic samples can be inferred to have been derived from a fractionated magma, as indicated by the relatively low Mg# values (Mg# = 100 Mg/[Mg+Fe^{2+}]) of 48.69–53.56, high Ti/V ratios of 67.33–69.95, and higher Ti/V ratios than those of continental flood volcanic rocks (Table 2; Shervais, 1982; Rollinson, 12014). The Ti negative anomalies, relative to the neighboring elements of Eu and Y in the multi-element plot (Fig. 13D), are characteristic of continental crust (Rudnick and Gao, 2003). Negative Nb and Ta anomalies, as well as the high Ti/V ratios, also indicate the involvement of continental crust during magmatism (e.g., Rollinson, 2014). According to Fitton et al. (1997), mafic magma derived from plume exhibits ΔNb > 0, whereas magma derived from depleted mantle and crust shows ΔNb < 0, where ΔNb = 1.74 + log (Nb/Y) − 1.92 × log (Zr/Y) (also see Baksi, 2001). Our volcanic samples have ΔNb values ranging from −0.27 to −0.44 (Table 2), indicating they were sourced from a depleted mantle or a crust. All together, the geochemical data suggest that the volcanic rocks were generated in a continental arc setting.

DETRITAL ZIRCON DATING AND SANDSTONE COMPOSITION

U-Pb Dating of Detrital Zircon

The analytical data for U-Pb dating of detrital zircon can be found in the GSA Data Repository (see footnote 1). Reported uncertainties
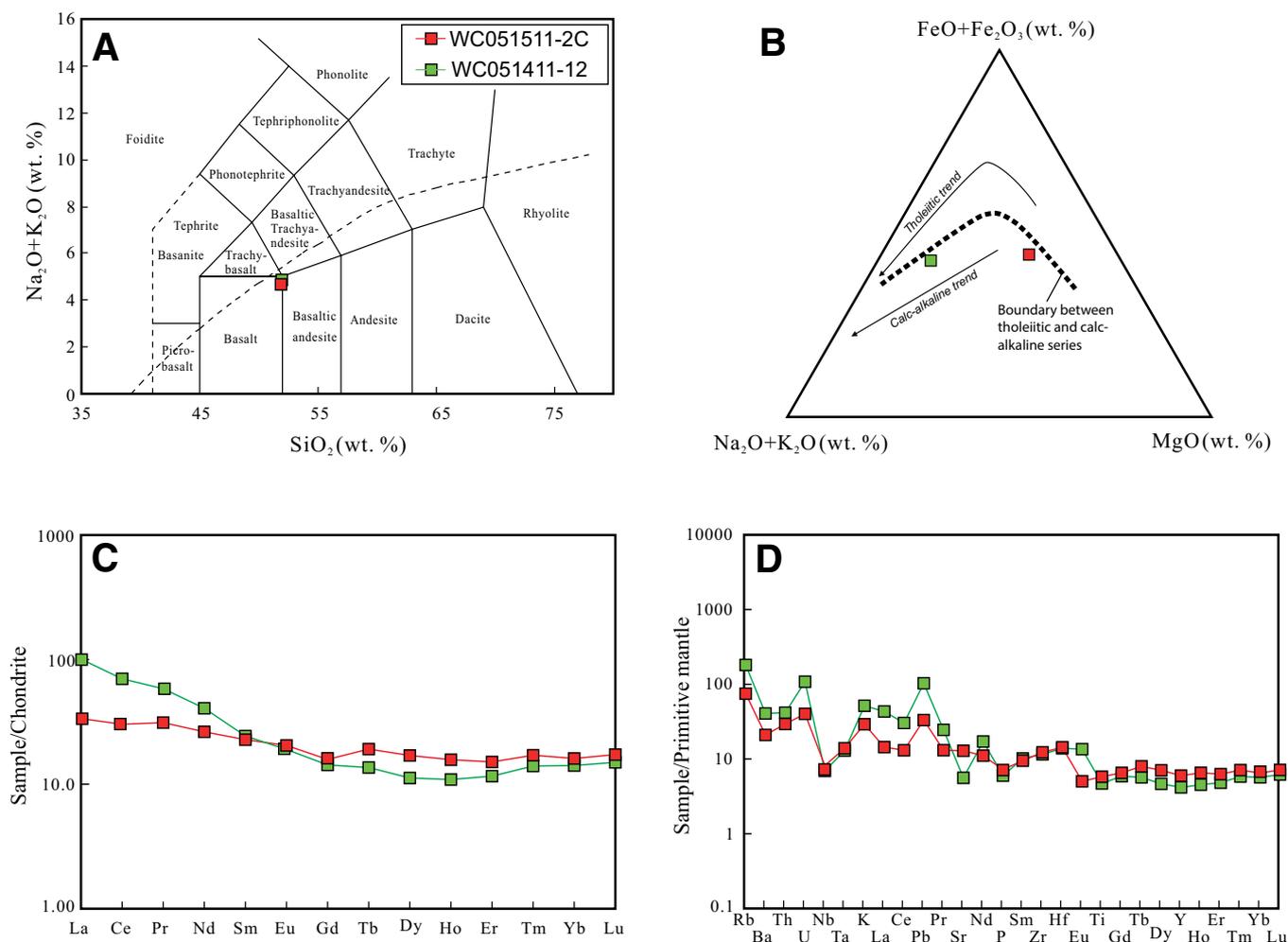
Figure 13. (A) SiO$_2$-(K$_2$O + Na$_2$O) (total alkali-silica [TAS]) diagram for volcanic rocks. (B) AFM ternary diagram after Irvine and Baragar (1971) for classification of the analyzed volcanic samples. (C) Chondrite-normalized rare earth element (REE) diagram for the two volcanic rocks from the Eastern Kunlun Range. Normalizing values are from Sun and McDonough (1989). (D) Primitive mantle–normalized spider diagram for the two volcanic rocks from the Eastern Kunlun Range. Normalizing values are from Sun and McDonough (1989).
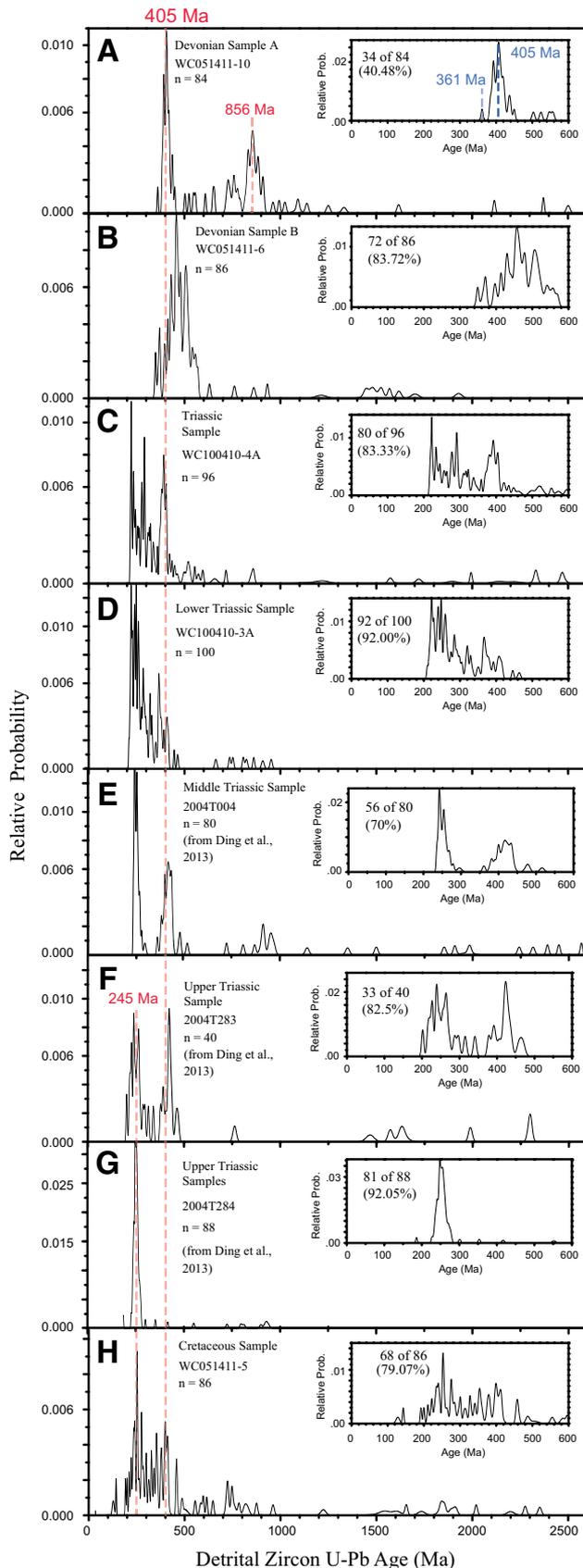
Figure 14. Relative probability plots of detrital zircon U-Pb ages from the Eastern Kunlun Range from this study and Ding et al. (2013).

are at the 1σ level. Analyses that were >30% discordant (by comparison of $^{206}Pb/^{238}U$ and $^{206}Pb/^{207}Pb$ ages) or >5% reverse discordant are not considered in this study. The interpreted ages of detrital zircon grains are shown on the relative age probability diagrams (Fig. 14). Results of three samples from Ding et al. (2013) are also used in the relative age–probability plot. Following Dickinson and Gehrels (2009), we used least three overlapping analyses to define the maximum depositional age of the collected sedimentary samples. A caveat of the Dickinson and Gehrels (2009) approach is that it could eliminate young age data with real geologic meaning. Kolmogorov-Smirnov (K-S) tests were also applied to the detrital zircon results (Fig. 15).

Devonian Sample A (WC051411-10)

This sample was collected from quartzofeldspathic schist (site C in Fig. 6) that is penetratively deformed by the development of spaced cleavage (see more detailed description in the following section). The schist is part of the herein reassigned undifferentiated Devonian to Permian strata shown in Figure 6. A single zircon grain with a U-Pb age of ca. 361 Ma was also obtained in this study. However, we are not certain about the geologic implication of this isolated age. As the rock sample experienced medium-grade metamorphism, which is expressed by the development of schistosity (see Fig. 16A), it is possible that Pb loss during metamorphism may have caused this young zircon age. In this case, the dominant age peak at 405 Ma may represent a maximum depositional age of the sample in the Lower Devonian, which is from 416 Ma to 398 Ma. Alternatively, if the single young zircon age of 361 Ma did not experience a Pb loss event, the maximum depositional age of the sample would be in the Upper Devonian, which is from 385 Ma to 359 Ma. We tested the two possibilities by examining a CL image of the zircon grain that yielded the 361 Ma age. As shown in Figure 8H, the zircon grain displays a zone typical of metamorphic growth (e.g., Vavra et al., 1996). Thus, the 361 Ma age may represent a metamorphic event associated with the development of schistosity in the Devonian strata. In addition to the 405 Ma age peak, another prominent age peak is centered at ca. 856 Ma (Fig. 14A). Zircon with ages younger than 600 Ma accounts for ~40% of the dated grains, and zircon with ages of 600–1000 Ma accounts for 48% of the dated grains.

Devonian Sample B (WC051411-6)

This sample was collected from a feldspathic sandstone layer in the same general unit of the undifferentiated section of Devonian to Permian strata (site D in Fig. 5). The age spectrum of this sample is significantly different from that for sample WC051411-10 in two aspects. First, most of the Paleozoic-age zircon ages are clustered between 420 Ma and 530 Ma (Fig. 14B). Second, the 856 Ma age peak from sample WC051411-10 (Fig. 14A) is not displayed in the age spectrum of this sample (Fig. 14B). U-Pb dating indicates that ~84% of the zircon from this sample is younger than 600 Ma, with a major age peak centered at ca. 460 Ma. Zircon ages in the range of 390–500 Ma account for ~50% of the total dated grains (Fig. 14B). We assign this unit an Upper Devonian age (Table 1).

Triassic Sample (WC100410-4A)

This sample was collected from medium-grained arkosic sandstone, which is part of an undifferentiated Permian–Triassic unit north of a major north-dipping thrust branching off from the Kunlun fault (site A in Fig. 5). U-Pb dating indicates that ~83% of the dated zircon grains are younger than 600 Ma, in which ages between 220 and 400 Ma account for ~65% of the total dated grains (Fig. 14C). The age spectrum from the sample displays a major age peak at ca. 221 Ma and two minor age peaks at ca. 292 Ma and ca. 390 Ma, respectively (Fig. 14C).
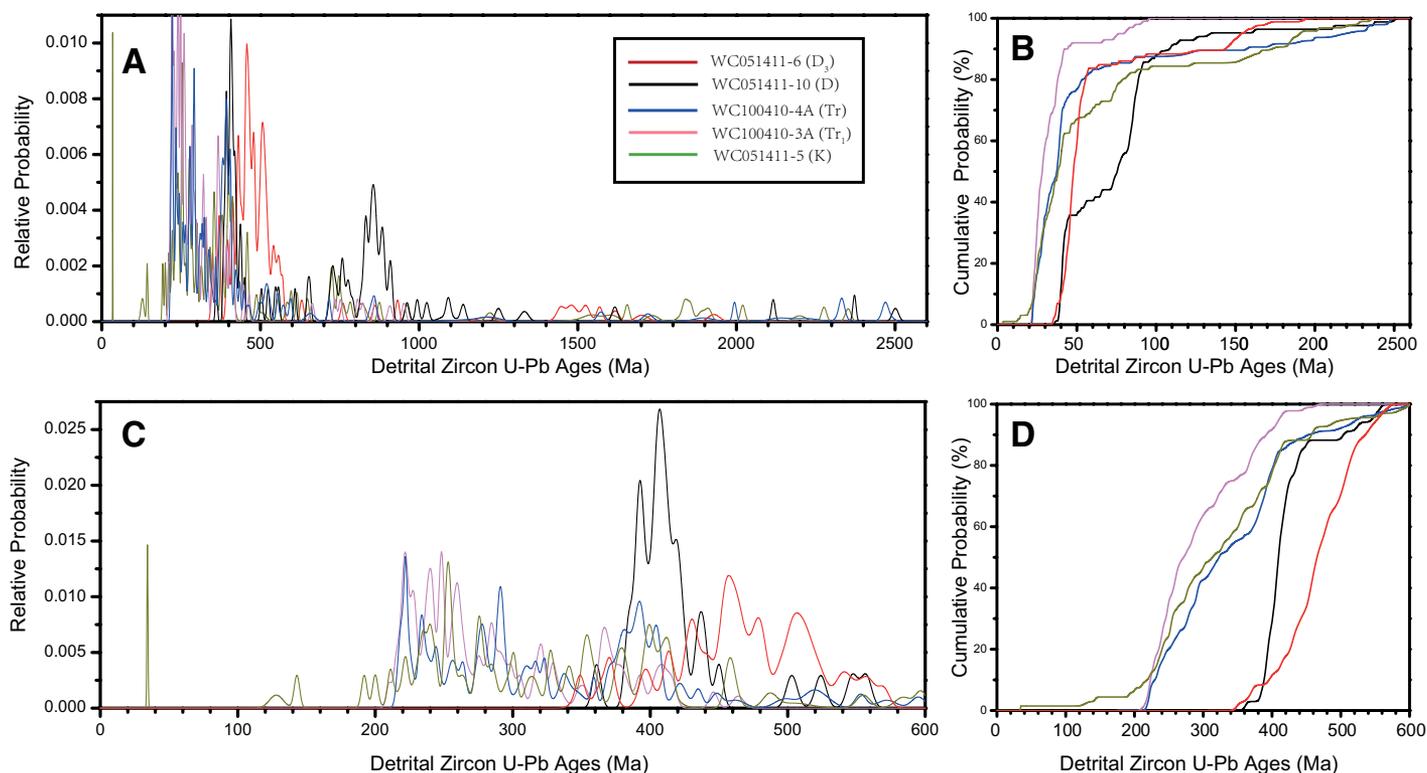
Figure 15. (A) Synthetic relative probability plots of U-Pb zircon ages in the range of 0–2600 Ma for the five detrital zircon samples from this study. **(B)** Cumulative probability plots of the detrital zircon samples in the age range of 0–2600 Ma. **(C)** Synthetic relative probability plot of U-Pb zircon ages in the range of 0–600 Ma for the five detrital zircon samples analyzed in this study. **(D)** Cumulative probability plot of the U-Pb zircon ages of the five detrital zircon samples in the age range of 0–600 Ma.

Lower Triassic Sample (WC100410-3A)

This sample was collected from medium-grained arkosic sandstone (site B in Fig. 5). U-Pb dating indicates that zircon ages younger than ca. 600 Ma account for ~92% of the total dated grains (Fig. 14D). These ages are mostly clustered between 221 Ma and 259 Ma, with a minor age peak at 370 Ma age. The rest of the zircon grains yielded ages from 600 Ma to 950 Ma without any obvious age clustering.

Middle Triassic Sample (2004T004)

This sample, reported in Ding et al. (2013), was collected from a sandstone unit that consists of plagioclase, quartz, muscovite, and lithic fragments of limestone and siltstone. The sample site was located in the southern margin of the Kunlun Range north of the Kunlun suture (site 1 in Fig. 3). U-Pb dating indicates that detrital zircon ages younger than 600 Ma are clustered at 270–228 Ma and 390–430 Ma, respectively (Fig. 14E).

Upper Triassic Samples (2004T283 and 2004T284)

These two samples were reported in Ding et al. (2013) as coarse-grained (2004T283) and medium-grained (2004T284) sandstone. The samples were collected from the southern margin of the Kunlun Range north of the Kunlun suture (site 2 in Fig. 3). They consist of monocrystalline quartz, plagioclase, muscovite, and epidote. Both samples yield detrital-zircon ages clustering between 270 Ma and 228 Ma (Figs. 14F and 14G). A significant difference between the two samples is sample 2004T283 displayed an age peak at ca. 410 Ma that is missing in the age spectrum for sample 2004T284. Note that the age spectrum from sample 2004T283 (Fig. 14F) is similar to that from sample 2004T004

(cf. Fig. 14E), whereas the age spectrum from Upper Triassic sample 2004T284 (Fig. 14G) is similar to the age spectra from our Triassic sample WC100410-4A (Fig. 14C) and Triassic sample WC100410-3A (Fig. 14C) characterized by the lack of the 410 Ma age peak.

Cretaceous Sample (WC051411-5)

This sample was collected from fine-grained arkosic arenite on the western end of the Eastern Kunlun Range (site E in Fig. 6). We interpret the Cretaceous unit, from which the sample was collected to have been deposited in a fluvial setting based on their sedimentary textures and structures observed in the field. U-Pb dating of detrital zircon indicates that ~79% of the dated grains are younger than 600 Ma, with a major age peak centered at ca. 254 Ma and two minor peaks centered at ca. 211 Ma and ca. 402 Ma, respectively. A minor but important age peak is centered at ca. 120 Ma (Fig. 14H), which provides a bound for the maximum deposition age of the sample.

Kolmogorov-Smirnov (K-S) Tests

The K-S statistical method is a nonparametric test for the equality of continuous one-dimensional probability distributions of two samples. The tested samples are typically displayed in cumulative probability diagrams (Fig. 15), and their largest vertical difference in the plot is defined as the D value (Table 3). Typically, a threshold value of $\alpha = 0.01$ or 0.05 is set. That is, if the D value is $> D_{critical}$ ($\alpha = 0.05$), the null hypothesis (H_0) that the two samples are drawn from the same population can be rejected. The critical value D can be calculated by
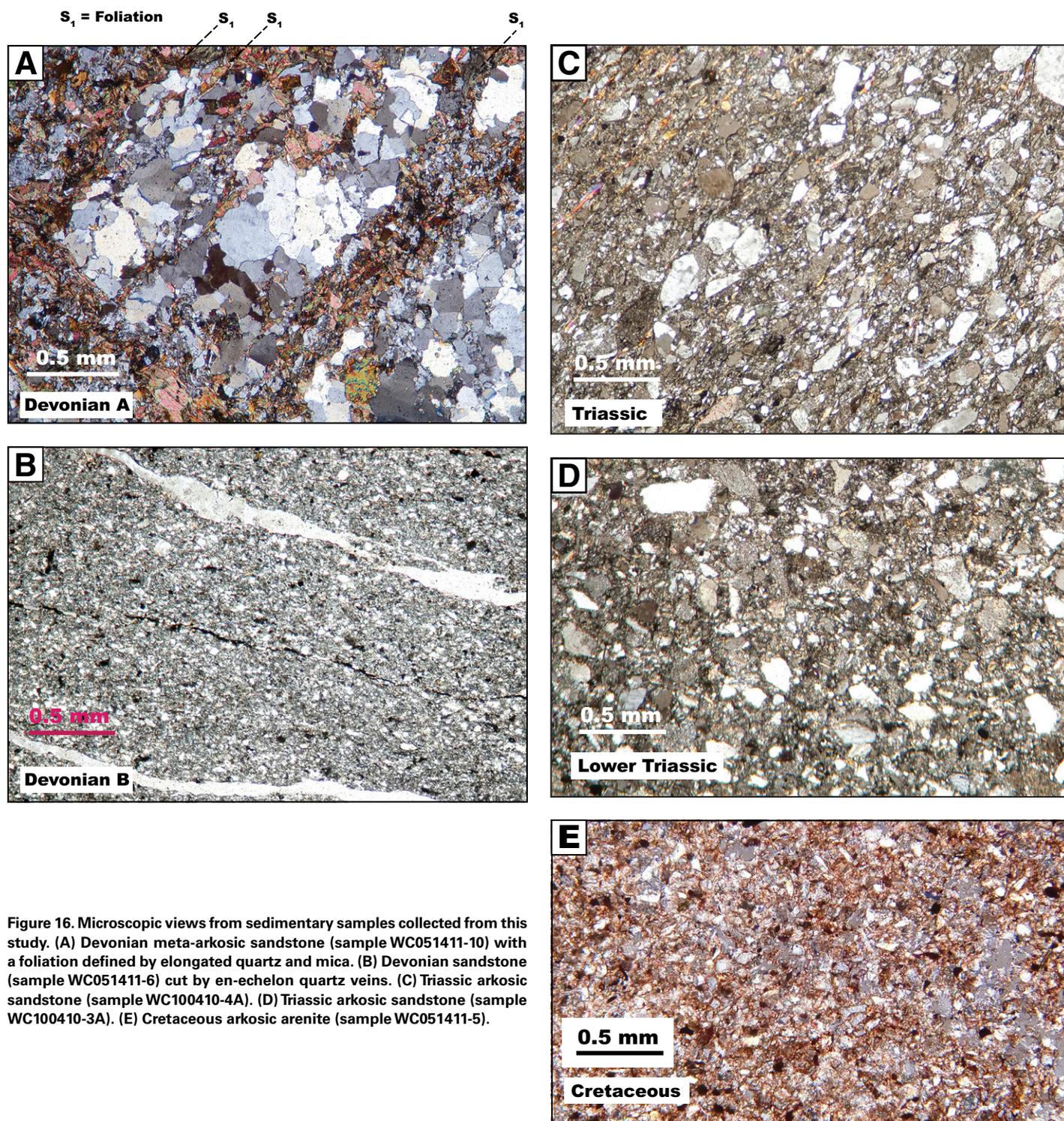
Figure 16. Microscopic views from sedimentary samples collected from this study. (A) Devonian meta-arkosic sandstone (sample WC051411-10) with a foliation defined by elongated quartz and mica. (B) Devonian sandstone (sample WC051411-6) cut by en-echelon quartz veins. (C) Triassic arkosic sandstone (sample WC100410-4A). (D) Triassic arkosic sandstone (sample WC100410-3A). (E) Cretaceous arkosic arenite (sample WC051411-5).

TABLE 3. TWO-SAMPLE KOLMOGOROV-SMIRNOV (K-S) TEST RESULTS

(A) *P* and *D* values used in two-sample K-S test (0–2600 Ma)

D-value / *P*-value	Tr₁ sample	Tr sample	K sample	D sample B	D sample A
Tr₁ sample	–	*0.276*	*0.306*	*0.759*	*0.791*
Tr sample	1.00E-03	–	*0.129*	*0.587*	*0.542*
K sample	0.00E+00	**4.03E-01**	–	*0.481*	*0.489*
D sample B	0.00E+00	0.00E+00	0.00E+00	–	*0.432*
D sample A	0.00E+00	0.00E+00	0.00E+00	0.00E+00	–

(B) *P* and *D* values used in two-sample K-S test (0–600 Ma)

D-value / *P*-value	Tr₁ sample	Tr sample	K sample	D sample B	D sample A
Tr₁ sample	–	*0.245*	*0.189*	*0.813*	*0.839*
Tr sample	1.20E-02	–	*0.093*	*0.710*	*0.610*
K sample	**1.23E-01**	**9.06E-01**	–	*0.705*	*0.670*
D sample B	0.00E+00	0.00E+00	0.00E+00	–	*0.552*
D sample A	0.00E+00	0.00E+00	0.00E+00	0.00E+00	–

(C) $D_{critical}$ values used in two-sample K-S test

	D sample A	Tr₁ sample	Tr sample	K sample	D sample B
D sample A	–	*0.201*	*0.203*	*0.209*	*0.209*
Tr₁ sample	0.201	–	*0.194*	*0.200*	*0.200*
Tr sample	0.203	0.194	–	*0.202*	*0.202*
K sample	0.209	0.200	0.202	–	*0.207*
D sample B	0.209	0.200	0.202	0.207	–

Note: Tr₁—Lower Triassic sample; Tr—Triassic sample; K—Cretaceous.

$$D_{critical} = 1.36 \sqrt{\frac{N_1 + N_2}{N_1 N_2}}$$

for α = 0.05, where N_1 and N_2 are the number of dated zircon grains from the two samples. In this study, we dated ~100 zircon grains for each sample (i.e., from 84 to 100; see Fig. 14), and the corresponding critical value of $D_{critical}$ is 0.192. The *P* value in K-S tests denotes the threshold of the significance level at which the null hypothesis (H_0) can be accepted. That is, the *P* value must be greater than 0.05 when two samples are considered to be derived from the same parent distribution at the 95% confidence level.

Table 3 and Figure 15 display a comparison of age spectra of all samples. We also isolated the age range of 0–600 Ma to highlight the presence and absence of detrital-zircon components from the Kunlun arc. The (*D*, *P*) values for the age range of 0–600 Ma between the age spectrum of the Cretaceous (K) sample and the Lower Triassic (Tr₁) sample are (0.189, 0.123) (Table 3). For the same age range, the (*D*, *P*) values between the age spectra of the Cretaceous (K) and the Triassic sample (Tr) are (0.093, 0.906) (Table 3). The large *P* values (i.e., >0.05) imply that the age spectra of the Lower Triassic (Tr₁) and Triassic (Tr) samples belong to the same population as the age spectrum of the Cretaceous (K) sample. The differences in the *D* values indicate that the age spectrum of the Cretaceous (K) sample is more similar to that of the Triassic sample, with a lower *D* value and a higher *P* value, than to that for the Triassic sample. The K-S tests suggest that the age spectra of the Lower Triassic (Tr₁) and Triassic (Tr) samples are significantly different. The (*D*, *P*) values are (0.245, 0.012), with a higher *D* value (i.e., >$D_{critical}$) and a lower *P* value (i.e., <0.05) than the (*D*, *P*) values for comparison between the Cretaceous sample age spectrum and the spectra of the Lower Triassic and Triassic samples. These results suggest that the Cretaceous sediments may have been largely derived from reworked Triassic strata. However, the source terranes for the Triassic and Lower Triassic sedimentary rocks

at the sample sites above and below a major thrust fault are quite different, which may reflect a change in the tectonic and/or paleogeographic settings at the two sites.

Sandstone Composition

In order to ascertain the tectonic settings of the sedimentary units from which our samples were collected, we performed sandstone composition analysis for two samples: one from Triassic strata and the other from Lower Triassic strata. The reason we did not conduct sandstone composition analysis on other samples was due to the effects of metamorphism and grain size. Specifically, the grain size of the Upper Devonian (i.e., Devonian Sample B) and Cretaceous samples is too fine (<0.0625 mm) to be appropriate for sandstone composition analysis (Dickinson, 1970, 1985). Devonian Sample A is a metamorphosed sandstone, with grain recrystallization and the development of cleavage schistosity. Sandstone composition is commonly plotted in a ternary QFL (i.e., quartz-feldspar-lithic fragment) plot (Dickinson, 1970, 1985), which can be used to distinguish tectonic settings among stable continental blocks, recycled orogens, and magmatic arcs. In the QFL diagram, the arc setting may be further divided into dissected, undissected, and transitional arcs (Dickinson, 1970, 1985).

Devonian Sample A (WC051411-10)

This quartzofeldspathic sandstone is penetratively deformed by the development of schistosity (Fig. 16A). The foliation is defined by a minor amount of elongated quartz grains bounded by foliation-parallel mica (Fig. 16A). The domains bounded by the foliation planes consist mostly of quartz and feldspar grains that display straight crystal edges and nearly 120° intersection angles as a result of recrystallization (Fig. 16A). Because of extensive recrystallization, we were unable to perform point counts on this sample.

Devonian Sample B (WC051411-6)

This feldspathic sandstone has feldspar grains with shapes ranging from highly angular to subrounded (Fig. 16B). En-echelon quartz veins cut at low angles across the bedding surfaces, suggesting that the sedimentary unit may have experienced bedding-subparallel shear. The matrix surrounding the feldspar grains consists of silt-sized grains, which are too small to be suitable for performing sandstone point counts.

Triassic Sample (WC100410-4A)

This medium-grained arkosic sandstone sample contains angular to subangular framework grains with sizes ranging from 0.4 mm to <0.1 mm (Fig. 16C). The framework grains in this sample include polycrystalline quartz, plagioclase, potassium feldspar, muscovite, epidote, lithic fragments of siltstone, and metamorphic rocks. Potassium feldspar is more abundant than the plagioclase in the sample. We performed point counting on this sample, and the result is shown in Figure 17. Granular quartz grains account for 42%, whereas feldspar grains account for 20% of the total tabulated grains. The rest (38%) are lithic fragments, dominantly metamorphic grains, indicating that the metamorphic basement was an important source of the sediments. In the QFL diagram, the sample composition is plotted in the recycled-orogen field next to the dissected-arc field (Fig. 17).

Lower Triassic Sample (WC100410-3A)

This sample was collected from medium-grained arkosic sandstone (site B in Fig. 6) with angular to subangular framework grains and grain sizes ranging from ~0.5 mm to <0.1 mm (Fig. 16D). The framework grains consist of quartz, plagioclase, potassium feldspar, epidote, and lithic fragments of siltstone and limestone. Point counting of the framework grains indicate that granular quartz grains account for 37% of the total counted points, whereas feldspar grains account for 14% of the total counted points. The rest of grains are lithic fragments that are dominantly metamorphic, with minor components of limestone and siltstone. In the QFL diagram, the composition of this sample, similar to Triassic sample WC100410-4A mentioned above, also plots in the recycled-orogen field

Figure 17. Modal composition of two sandstone samples analyzed in this study displayed in a QFL plot after Dickinson (1985). See text for details.

close to its boundary with the dissected-arc field (Fig. 17). A major difference between the two samples is that the Triassic sample contains a higher percentage of lithic fragments than that in the lower Triassic sample.

Cretaceous Sample (WC051411-5)

This sample was collected from fine-grained arkosic arenite (site E in Fig. 5). The framework grains have grain sizes of mostly <0.05 mm (Fig. 16E), too small to be suitable for conducting point counting. The most important distinction between the Cretaceous sample and the older samples is the lack of matrix material, suggesting that the sediments had been transported over a longer distance than those of the older samples through fluvial processes.

DISCUSSION

Ages, Geochemistry, and Tectonic Settings of the Paleozoic and Mesozoic Igneous Rocks in the Eastern Kunlun Range

U-Pb zircon ages of granitoid samples fall into two age groups, in the range of 434–417 Ma and 255–222 Ma, respectively (Fig. 9). The U-Pb zircon age spectrum of a single volcanic sample displays two prominent peaks at 283 Ma and 330 Ma (Fig. 10), with the younger peak interpreted to represent its emplacement age. Plutonic rocks examined in this study are granodiorite and granite (Fig. 11A), belonging to the high-K calc-alkaline series (Fig. 11B). The Permian volcanic sample with a basaltic composition also belongs to the calc-alkaline series (Figs. 13A and 13B). All the igneous samples display prominent negative Nb and Ta anomalies in the spider diagrams (Figs. 11C, 11D, and 13D), suggesting an arc setting and consistent with the conclusions of early studies in the Eastern Kunlun Range (e.g., Harris et al., 1988; Yin and Harrison, 2000; Mo et al., 2007). Discrimination diagrams show that the early Paleozoic plutons belong to A-, I-, and S-type granitoids, typically associated with syncollisional orogenesis, arc magmatism, and intraplate tectonism (Figs. 12A, 12C, and 12E). In contrast, the Permian–Triassic samples belong only to the I- and S-types of granitoids that occur typically in arc and/or syncollisional orogen settings (Figs. 12B, 12D, and 12F). The geochemical differences between early Paleozoic and Permian–Triassic samples are also indicated by the multi-element diagrams; a much stronger depletion in Eu for the early Paleozoic samples (Figs. 11E and 11F) may have been controlled by the partitioning melts and plagioclase as a function of temperature and oxygen fugacity (Weill and Drake, 1973; Drake and Weill, 1975).

The occurrence of A-type early Paleozoic granitoids requires a more detailed discussion. Loiselle and Wones (1979) attributed the formation of A-type granitoids to extensional tectonics. Subsequent studies also showed that the composition of extension-induced A-type granitoids is independent of the origin of magma sources (Whalen et al., 1987; Eby, 1990, 1992; Turner et al., 1992). A-type granitoids typically display the following characteristics: high Fe/(Fe + Mg) and K_2O/Na_2O ratios, high TiO_2/MgO ratios, high K_2O contents, and enrichment in incompatible elements such as REE (except Eu), Zr, Nb, and Ta (Whalen et al., 1987; Eby, 1990, 1992; Turner et al., 1992; Patiño Douce, 1997), which are recorded in some of the early Paleozoic granitoids that we examined. When combined with other geochemical data, we propose that the early Paleozoic granitoids were emplaced in an extensional intra-arc setting.

The results of our age dating of granitoid samples from the Eastern Kunlun Range are consistent with the early work that shows two stages of Phanerozoic arc magmatism in the region (e.g., Yin and Harrison, 2000; Cowgill et al., 2003; Gehrels et al., 2011; X.H. Chen et al., 2012; Ding et al., 2013; Dai et al., 2013b). The two phases of igneous activity not only affected the Kunlun Range area, as suggested in Cowgill et al. (2003), but also the Qilian Shan region in northern Tibet (Fig. 18). Because of this,
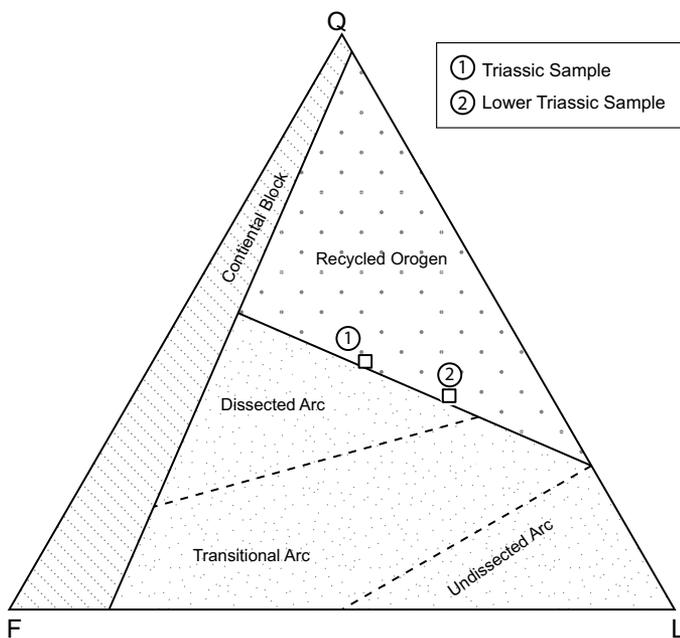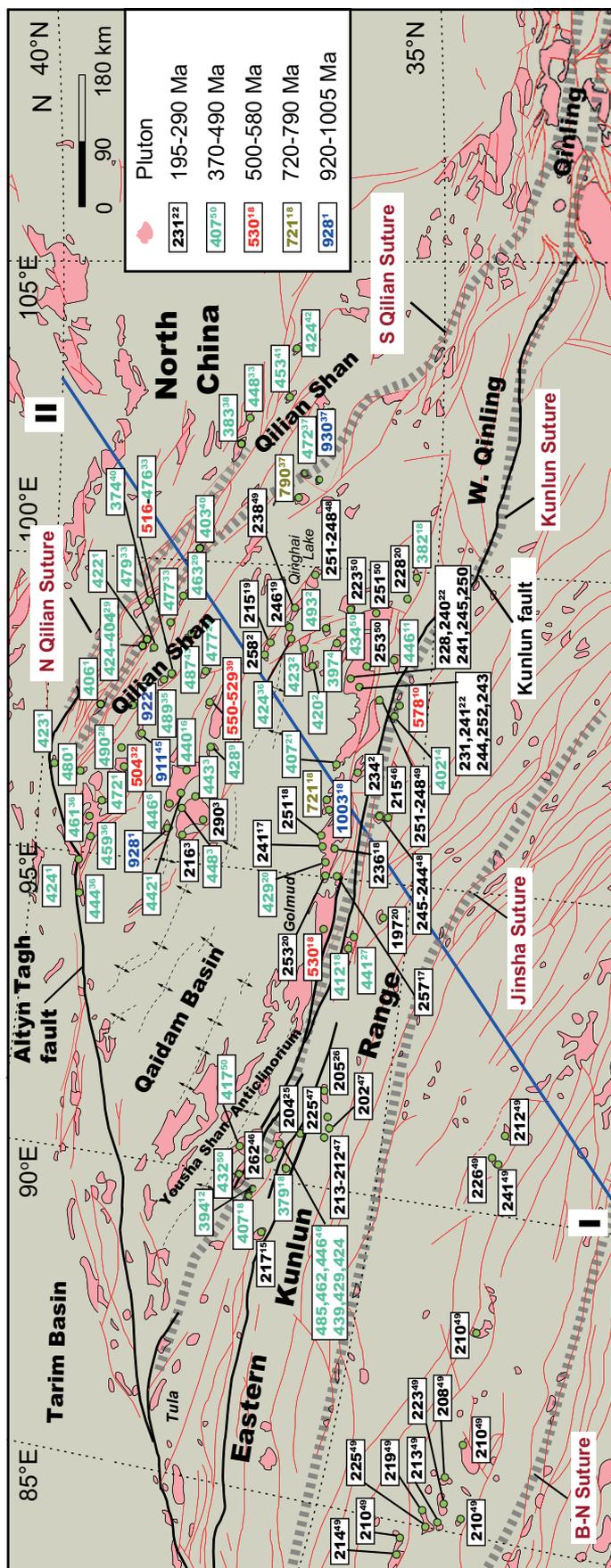
Figure 18. Crystallization ages of Paleozoic and Mesozoic plutons across central and northern Tibet. NZF—north Zongwulongshan fault; NQF—north Qaidam fault; QTF—north Qimantag fault; SQF—south Qaidam fault; KLF—Kunlun fault; ATF—Altyn Tagh fault; WHF—Wahongshan fault (Wenquan fault); LDF—Lapeiquan detachment fault of Chen et al. (2003). B-N—Bangong-Nujiang. Correspondence between data location and the source of information is as follows: 1—Gehrels et al. (2003a); 2—X.H. Chen et al. (2012); 3—Menold (2006) and Menold et al. (2009); 4—Wu et al. (2004a); 5—Liu et al. (2004); 6—C.L. Wu et al. (2001); 7—J.Wu et al. (2001); 8—Yang and Song (2002); 9—Meng et al. (2005); 10—Bian et al. (2000); 11—Wang et al. (2003); 12—H.W. Chen et al. (2006); 13—Wu et al. (2005); 14—Bian et al. (2004); 15—Roger et al. (2003); 16—Lu et al. (2007); 17—Harris et al. (1988); 18—Zhang et al. (2005); 19—Guo et al. (2009); 20—Dai et al. (2013b); 21—Liu et al. (2012); 22—Zhang et al. (2012); 23—Li et al. (2012); 24—Liu et al. (2005); 25—Lu et al. (2010); 26—Chen et al. (2002); 27—B.Z. Wang et al. (2012); 28—Xia and Song (2010); 29—Wu et al. (2011); 30—Qinghai BGMR (1991); 31—Tseng et al. (2007); 32—Xiang et al. (2007); 33—Song et al. (2013); 34—Y.J. Liu et al. (2006); 35—Zhang et al. (2007); 36—Cowgill et al. (2003); 37—Tung et al. (2007b); 38—Wu et al. (2004b); 39—Shi et al. (2004); 40—Hu et al. (2005); 41—Tseng et al. (2009a); 42—Qian et al. (1998); 43—Xia et al. (2012); 44—Lin et al. (2010); 45—Zuza et al. (2013); 46—Li et al. (2013); 47—Ding et al. (2014); 48—Huang et al. (2014); 49—Zhang et al. (2014); and 50—this study.

the evolution of the Kunlun arc along the southern margin of the Kunlun-Qaidam Terrane must be placed in a broader context that includes the coeval development of the Qilian arc system in the north and the Kunlun arc in the south. Figure 19 is a compilation of all available ages of igneous rocks from northern Tibet. The plot shows five phases of igneous activity since the Proterozoic (see references listed in Figs. 4 and 18): at 1005–910 Ma and 940–820 Ma along the northern and southern margins of the Kunlun-Qaidam Terrane, at 790–720 Ma across mostly the eastern Central Qilian Terrane, and at 580–500 Ma, 490–375 Ma, and 290–195 Ma across the Kunlun-Qaidam Terrane and the Qilian orogen.

A 790 Ma granitic gneiss, which intrudes into a sequence of metasedimentary strata with a maximum depositional age of ca. 882 Ma, is exposed in the basement along the northern margin of the Kunlun-Qaidam Terrane (Fig. 18; Tung et al., 2007b). Because there is no information on the geochemistry of this pluton, its origin is uncertain. Another 720 Ma granitoid in the basement is exposed along the southern margin of the Kunlun-Qaidam Terrane in the Eastern Kunlun Range (Zhang et al., 2005). Again, its geochemistry has not been analyzed, and thus its origin is also unknown. The 720 Ma and 790 Ma ages of the basement of the Kunlun-Qaidam Terrane provide a lower limit for the timing of the passive-margin formation along the northern and southern parts of this continental block (i.e., the Kunlun-Qaidam Terrane). Specifically, the Neoproterozoic metasedimentary sequence, consisting of marble, meta-sandstone, and slate in the Eastern Kunlun Range, and a shallow-marine sequence in northern Qaidam Basin and the central Qilian Shan (Wang et al., 2013) are interpreted in this study as passive-margin sediments along the southern and northern margins of the Kunlun-Qaidam Terrane.

Two plutons with ages of 530 Ma and 578 Ma are observed along the Kunlun suture zone. These rocks have much older ages than the nearby Paleozoic plutonic rocks, which have an oldest age of ca. 485 Ma (Fig. 18).

It is possible that these older plutonic rocks are relics of an island-arc terrane that was accreted onto the Kunlun-Qaidam Terrane either during northward oceanic subduction or continent-continent collision. However, there is no evidence of oceanic crust associated with these older plutonic rocks, ruling out an oceanic-arc origin. Alternatively, they could represent the oldest magmatism in the Kunlun arc, as we interpret in Figure 19. The apparent age gap between 530 Ma and 485 Ma may be induced by (1) incomplete sampling and (2) burial by a rift sequence deposited during 375–290 Ma in the southern Eastern Kunlun Range (Yin and Harrison, 2000; also see more detailed discussion on this point in our tectonic reconstruction). In any case, this interpretation requires that the onset of subduction along the southern margin of the Kunlun-Qaidam Terrane could have occurred as early as ca. 580 Ma in the terminal Neoproterozoic, and the protracted arc magmatism lasted until ca. 380 Ma.

A prominent magmatic lull exists between 375 Ma and 290 Ma in both the Eastern Kunlun Range and Qilian Shan areas (Fig. 19). Arc magmatism resumed at 290–280 Ma across the Kunlun-Qaidam Terrane; the onset age is constrained by the age of our dated volcanic sample in the Kunlun area and by a 290 Ma pluton in the Qilian Shan area. Permian–Triassic magmatism across the Kunlun-Qaidam Terrane lasted until ca. 205 Ma in the Eastern Kunlun Range region but finished earlier at ca. 215 Ma in the Qilian Shan (Figs. 18 and 19). We refer to the Permian–Triassic arc in the Kunlun area as the Neo–Kunlun arc, which was generated by the subduction of the traditionally defined Paleo-Tethys Ocean (e.g., Şengör, 1993). We interpret the southward younging trend of magmatic termination ages as a result of southward steepening of the subducting Paleo-Tethyan oceanic slab.

The temporal development of Phanerozoic arc magmatism allows us to test the existing models for the evolution of the Tethyan orogenic system. The two-phase arc development is inconsistent with the protracted
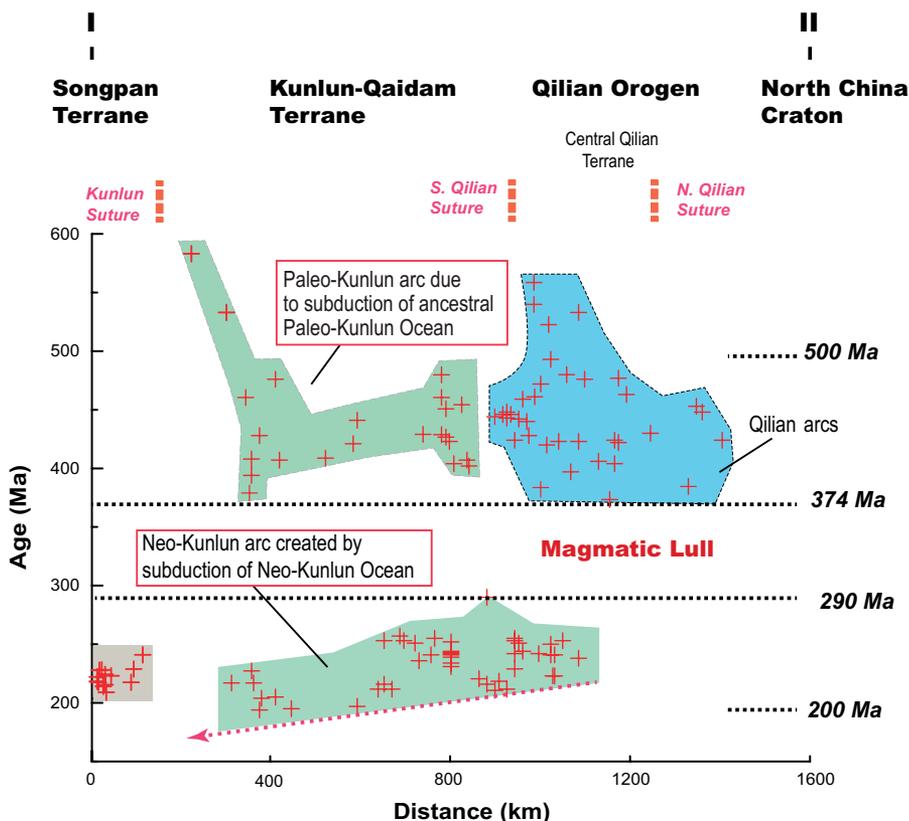
Figure 19. An age-distance plot for Paleozoic–Mesozoic plutonic rocks across central and northern Tibet. The ages are projected along the strike of the suture zones and magmatic arcs onto a cross-section line I–II shown in Figure 18. See text for details.

single-arc model of Şengör (1992) (Fig. 2A) and the double-subduction-zone model of Stampfli and Borel (2002) (Fig. 2D). However, the temporal evolution of arc magmatism in the Kunlun Range area could be explained by the backarc-basin model of Hsü et al. (1995) (Fig. 2B), the two-phase arc model of Yin and Harrison (2000) (Fig. 2C), and/or the double-suture-zone model of Yang et al. (1996) (Fig. 2E). A major issue with the backarc-basin model of Hsü et al. (1995) is that it predicts continuous southward migration of an early Paleozoic arc in the Kunlun region, leading to the opening of an ocean along the southern margin of the older section of the arc. This prediction is not consistent with the nearly random distribution of early Paleozoic plutonic ages in the Kunlun Range area (Fig. 18).

There are two problems with the double-suture-zone model of Yang et al. (1996). First, the model requires southward subduction of the inferred "North Kunlun Terrane" beneath the "South Kunlun Terrane." This tectonic configuration would preclude the occurrence of arc magmatism north of the interpreted suture zone along the "Central Kunlun fault" of Yang et al. (1996). However, as shown in Figure 18, early Paleozoic arc-related plutons are exposed both north and south of their interpreted suture (also see X.H. Chen et al., 2012, 2014). Second, the interpreted suture zone contains ultramafic rocks and high-pressure eclogite. The occurrence of these rocks is only restricted in the eastern end of the Kunlun Range and cannot be traced along strike along the entire range (e.g., Mo et al., 2007). As the structural setting of the high-pressure rocks is not clear, it is difficult to assess their significance. For example, the eclogite terrane could be part of a mélange complex that was first subducted below the Kunlun arc and was later exhumed within the arc. Such a process has been documented in the Paleozoic Altai arc in Central Asia (Briggs et al., 2007, 2009).

Tectonic Settings of the Paleozoic and Mesozoic Sedimentary Strata

Because it was not a main focus of this study, we did not perform detailed and systematic investigations on the stratigraphy, sedimentary structures, sedimentary petrology, and lithofacies of the sedimentary units documented in this work. Thus, our inferences on the tectonic setting and depositional processes are entirely based on U-Pb detrital zircon dating, sandstone composition analyses, and preliminary field observations. With this caveat in mind, we believe that U-Pb detrital zircon dating and preliminary sandstone composition analysis still yield valuable information about the provenance of the Paleozoic and Mesozoic sedimentary strata in the Eastern Kunlun Range. One of our Devonian samples (sample WC051411-10) is dominated by ca. 405 Ma and ca. 856 Ma zircon ages (Fig. 14A). The former can be related to the Paleo-Kunlun arc rocks, whereas the latter can be related to the Proto-Kunlun arc exposed in the crystalline basement complex of the Eastern Kunlun Range. A minor age clustering between 920 and 1130 Ma is also detected from the age spectrum of this sample (Fig. 14A). The younger component of this age range at ca. 920 Ma is correlative with plutonic rocks along both the southern and northern margins of the Kunlun-Qaidam Terrane (Fig. 4C), whereas the older component of the age clustering at ca. 1.0–1.1 Ga is uniquely correlative to plutonic rocks from the Central Qilian Terrane (see Fig. 4B and related text discussed earlier herein).

Our second Devonian sample (sample WC051411-6) lacks zircon grains with 856 Ma ages (Fig. 14B), suggesting that the drainage system in the Eastern Kunlun Range area during Devonian time was highly unstable. The lack of 900–1100 Ma detrital zircon suggests that the basement of the Kunlun-Qaidam and Central Qilian Terranes was covered by younger sedimentary strata that did not contain older basement zircon grains. As the deposition of the Devonian samples examined in this study was broadly contemporaneous with the emplacement of extension-induced A-type

granites in the region, we interpret the Devonian sedimentary strata to have been deposited in an intra-arc extensional basin.

Our two Triassic samples together with the three Triassic samples from Ding et al. (2013) yield rather simple detrital-zircon age spectra characterized by a large number of Permian–Triassic zircon grains (Figs. 14C–14G), which must have been sourced from the nearby Kunlun arc. An intra-arc setting for the deposition of the Triassic strata, where our samples were collected, is consistent with our sandstone composition analysis (Fig. 17).

The age spectrum of the Cretaceous sample (Fig. 14H) suggests that its source area is local in the Eastern Kunlun Range, as indicated by the Kunlun arc zircon. We also note that the Cretaceous sample contains zircon with ages of 700–800 Ma, which are similar to the basement ages of western South China (Fig. 4E). Although the source areas for the Cretaceous strata are generally similar to those of the Triassic sedimentary rocks in the Eastern Kunlun area, the Cretaceous landscape must have been much more subdued than the surface topography of the same area in the Triassic. This is evident from the deposition of the mature Cretaceous arenite versus the immature Triassic arkosic sandstone in the Eastern Kunlun Range (Fig. 16). Note that the Cretaceous sample displays bimodal grain-size distributions, with the frame grains supported by fine-grained quartz and heavy minerals. The sorting may have been related to the hydrodynamic conditions under which the sandstone was deposited. However, this does not affect the conclusion that the sample is dominated by quartz grains as a result of strong chemical weathering that removed all the unstable mineral phases.

Tectonic Evolution of the Combined Kunlun-Qilian Arc System

Based on the data collected from this study and a regional synthesis of tectono-stratigraphic sections of the Proterozoic and early Paleozoic rocks shown in Figure 4, we propose a self-consistent tectonic model that explains the Proterozoic and Phanerozoic geologic history of the central and northern Tibetan Plateau (Fig. 20). In our reconstruction, we avoid assigning the Paleo-Tethys to a specific ocean, as the term implies the existence of a preexisting ocean between the supercontinents Gondwana and Laurasia. As shown below, the major Proterozoic and Phanerozoic oceans created in central and northern Tibet can be best explained by Wilson cycles, with continents repeatedly breaking up and then colliding along the same tectonic belts. This process is fundamentally different from the traditionally envisioned process for the development of the Tethyan orogen (e.g., Şengör, 1984; Şengör and Natal'in, 1996; Yin and Harrison, 2000).

Although the nature of the Songpan-Ganzi Terrane remains debated (e.g., whether it is floored by a continental or oceanic crust and whether it is part of South China; for a recent summary on this problem, see Zhang et al., 2014), we assume this terrane to be a westward extension of the Yangtze craton of western South China since the Mesoproterozoic. This assumption helps to explain the two phases of Phanerozoic arc magmatism as shown in detail in the following. In addition to this key assumption, our model also involves the following features: (1) the suture zones in the Qilian Shan area are linked with the suture zones in the Qinling area (Fig. 1B), (2) the development of the Silurian and Devonian arc in the Eastern Kunlun Range region was associated with intra-arc extension, and (3) the wide (>500 km) Permian–Triassic arc magmatism was caused by flat subduction followed by slab rollback.

Based on our regional synthesis, we infer the existence of a Paleo–Qilian Ocean between North China and the combined Central Qilian and the Kunlun-Qaidam Terranes, referred to in this study as the Proto–Kunlun-Qaidam Terrane (Fig. 20A). The existence of the Paleo–Qilian Ocean is required by the presence of the 1.0–0.9 Ga granitoid belt, interpreted as representing an early Mesoproterozoic arc (i.e., the Paleo–Qilian arc in

Figure 20. (A–M) Tectonic evolution of the Tethyan and Qilian orogenic systems from the onset of the Neoproterozoic to the Early Jurassic. See text for details. (*Continued on following three pages.*)

(E) 740-680 Ma

Future Altyn Tagh Fault
North China
North Tarim
North Qilian Ocean
Opened at ~750 Ma as an intra-continental basin
C. Qilian-N. Qinling Terrane
South Tarim
Future Altyn Tagh Fault
Kunlun-Qaidam Terrane
Central Qinling Terrane
Neoproterozoic passive margins
South Qilian Ocean = Erlangping Ocean in the Qinling region
Opened at ~680 Ma
Paleo-Kunlun Ocean = Shangdan Ocean
Neoproterozoic passive margins
Songpan-Ganzi Terrane
Neoproterozoic passive margins
Jinsha Ocean
Future Longmen Shan Thrust Belt
Yangtze Terrane
South China
Cathaysia Terrane
Future Qiangtang (??)

(F) 550-500 Ma

Future Altyn Tagh Fault
N. Qilian Ocean
North China
North Tarim
C. Qilian Terrane
540-380 Ma Central Qilian arc
South Tarim
S. Qilian Ocean
550-380 Ma Paleo-Kunlun arc
Future Altyn Tagh Fault
Kunlun-Qaidam Terrane
Paleo-Kunlun Ocean
Songpan-Ganzi Terrane
Future Longmen Shan Thrust Belt
Jinsha Ocean
South China
Yangtze Terrane
Cathaysia Terrane

(G) 500-430 Ma

Future Altyn Tagh Fault
North China
North Tarim
N. Qilian Ocean
C. Qilian Terrane
550-430 Ma Paleo-Kunlun arc
South Tarim
540-380 Ma Central Qilian arc
Future Altyn Tagh Fault
Kunlun-Qaidam Terrane
S. Qilian Ocean
480-400 Ma South Qilian-North Qaidam arc
Paleo-Kunlun Ocean
Songpan-Ganzi Terrane
Future Longmen Shan Thrust Belt
Jinsha Ocean
Yangtze Terrane
South China
Cathaysia Terrane

(H) 430-400 Ma

North Tarim
Future Altyn Tagh Fault
North China
N. Qilian Suture
Intra-arc extension and emplacement of 435-410 Ma A-type granites and mafic-ultramafic suites
South Tarim
S. Qilian suture = Erlangping suture
Kunlun-Qaidam Terrane
N. Qinling Terrane
Paleo-Kunlun Ocean
Intra-arc extensional basin for deposition of Devonian strata
Forearc thrusting causing exhumation of ca. 428 Ma eclogite-bearing metamorphic terrane containing 930 Ma protolith
Songpan-Ganzi Terrane
Future Longmen Shan Thrust Belt
Jinsha Ocean
Yangtze Terrane
South China
Cathaysia Terrane

Figure 20 (*continued*).

(I) 400–375 Ma

North Tarim · North China
Future Altyn Tagh Fault
N. Qilian Suture
South Tarim
Kunlun-Qaidam Terrane
N. Qilian Terrane
S. Qilian suture = Erlangping suture
Paleo-Kunlun suture = Shangdan suture
Songpan-Ganzi- Terrane
Yangtze Terrane
Future Longmen Shan Thrust Belt
Jinsha Ocean
South China
Cathaysia Terrane

(J) 375–290 Ma

North Tarim · North China
Future Altyn Tagh Fault
N. Qilian Suture
South Tarim
L. Carboniferous to Early Permian shelf deposits
Kunlun-Qaidam Terrane
N. Qinling Terrane
S. Qilian suture = Erlangping suture
Paleo-Kunlun suture = Shangdan suture
S. Qinling Terrane
Neo-Kunlun Ocean
Neo-Kunlun Ocean = Mianlue Ocean in Qinling Orogen
Songpan-Ganzi- Terrane
Yangtze Terrane
Future Longmen Shan Thrust Belt
Jinsha Ocean
South China
Cathaysia Terrane

(K) 290–225 Ma

Central Asian Orogenic System
Solonker suture
North Tarim · North China
Future Altyn Tagh Fault
N. Qilian Suture
290–225 Ma Neo-Kunlun arc
South Tarim
Kunlun-Qaidam Terrane
N. Qinling Terrane
S. Qilian suture = Erlangping suture
Paleo-Kunlun suture = Shangdan suture
255–222 Ma I- and S- type granitoids examined in this study
Triassic intra-arc basins
S. Qinling Terrane
Neo-Kunlun Ocean = Mianlue Ocean in Qinling Orogen
Neo-Kunlun Ocean
Songpan-Ganzi- Terrane
Yangtze Terrane
Future Longmen Shan Thrust Belt
Jinsha Ocean
South China
Qiangtang Terrane
Cathaysia Terrane

(L) 225–195 Ma

North Tarim · North China
Future Altyn Tagh Fault
N. Qilian Suture
South Tarim
Kunlun-Qaidam Terrane
N. Qinling Terrane
S. Qilian suture = Erlangping suture
Paleo-Kunlun suture = Shangdan suture
Neo-Kunlun suture = Anyimaqen-Kunlun-Muztagh suture = Mianlue suture
S. Qinling Terrane
Songpan-Ganzi flysch complex
Qiangtang Terrane
Yangtze Terrane
Future Longmen Shan Thrust Belt
South China
Spill-over of the Songpan-Ganzi flysch deposits over the adjacent terranes
Plutons emplaced during extreme crustal extension induced by slab rollback
Jinsha suture
Cathaysia Terrane

Figure 20 (*continued*).

(M) 145–120 Ma

Figure 20 (*continued*).

Fig. 20A). The closure of the Paleo–Qilian Ocean must have been accomplished by a south-dipping (present-day coordinate) subduction zone, as the southern margin of the North China craton lacks plutonic rocks of this age (Fig. 4A). An ocean, named here as the Southern Qaidam Ocean, is inferred to lie on the south side of the Proto–Kunlun-Qaidam Terrane (Fig. 20A); its southward subduction below the combined Songpan-Ganzi and Yangtze Terranes created the 940–820 Ma Proto–Kunlun arc that was eventually accreted onto the southern margin of the Proto–Kunlun-Qaidam Terrane at ca. 820 Ma (Fig. 20B). Although it is not the focus of this study, we also place the amalgamation of the Yangtze and Cathaysia Terranes in the context of our reconstruction (Fig. 1B). The timing of the Jiangnan arc is assumed to be 900–830 Ma, and the final closure of the Jiangnan Ocean occurred between 830 Ma and 800 Ma along a single west-dipping subduction (e.g., Zheng et al., 2008; X.L. Wang et al., 2012; Cawood et al., 2013; Yao et al., 2013, 2015). However, we are aware of the current debates on the polarity and timing of the collision between the Yangtze and Cathaysia Terranes (e.g., Zhao, 2015; Dong et al., 2015). In our reconstruction, we suggest that the 950–900 Ma Xixiang volcanic arc complex of Ling et al. (2003) in the northwestern corner of the Yangtze craton was deposited in a backarc setting during the development of the Proto–Kunlun arc (Fig. 20B; cf. Zhao et al., 2011).

The southward subduction of the Southern Qaidam Ocean created a backarc basin (i.e., the Proto–Kunlun Ocean in Figs. 20B and 20C). Termination of magmatism along the 940–820 Ma Proto–Kunlun arc occurred during the collision of the Proto–Kunlun arc with the Proto–Kunlun-Qaidam Terrane along a south-dipping subduction zone. This subduction polarity explains the general lack of 900–820 Ma plutonic rocks north of the Eastern Kunlun Range across the Proto–Kunlun-Qaidam Terrane (Figs. 4A, 4B, and 4C). Bimodal volcanism and passive-margin deposition in North Tarim and North China suggest that the opening of the Paleo–Asian Ocean started by ca. 800 Ma (Fig. 20C; Li et al., 2005; Zhu et al., 2008; Turner, 2010; Shu et al., 2011; Zuza and Yin, 2014).

The inferred suture zone may be exposed at the eastern end of Qaidam Basin, but it would not be easily recognizable because it may have been strongly modified by the younger phases of arc magmatism and collision-induced deformation. Between 830 Ma and 760 Ma, subduction along the northern and western margins of the Yangtze Terrane and the north and south sides of the Songpan-Ganzi Terrane created continental arcs (Fig. 3C), as documented in Zhou et al. (2002a, 2006), Yan et al. (2006), and Zhao and Zhou (2007). Collision between the combined Songpan-Ganzi Terrane and South China and the combined Proto–Kunlun arc and Proto–Kunlun-Qaidam Terrane led to the termination of arc magmatism along the northern and western margins of South China (Fig. 20D).

The North Qilian Ocean started opening during the deposition of a tillite-bearing sequence in the middle Qingbaikou to middle Nanhua (860–680 Ma) (Chinese Geological Survey, 2014). As the section was deposited on a basement that experienced a metamorphic event ca. 758 Ma (Fig. 4A), so its maximum deposition age must be younger than ca. 758 Ma. A passive-margin sequence of a similar age was deposited across the Central Qilian Terrane, which lies above a basement containing ca. 775 Ma orthogneiss (Fig. 4B). This information suggests that the opening of the North Qilian Ocean must have occurred after ca. 758 Ma but before ca. 680 Ma. We assume an age of 750 Ma in our reconstruction (Figs. 4A, 4B, and 20D). It is important to note that the trace of the South Qilian Ocean follows closely the tectonic contact between the North China craton and the Paleo–Qilian arc (Fig. 20D). Our reconstruction also assumes that Cathaysia was part of a superterrane that included the Qiangtang Terrane, Lhasa Terrane, and India (Fig. 20D). This inference is supported by the suggestion that South China was located near Qiangtang, Lhasa, and India in the Neoproterozoic (Jiang et al., 2003; Yu et al., 2008; Guynn et al., 2012; Cawood et al., 2013).

The opening of the South Qilian Ocean may have started at ca. 740 Ma, which is indicated by the deposition of the tillite-bearing Neoproterozoic Quanji Group along the northern margin of the Kunlun-Qaidam Terrane, which was associated with eruption of ca. 738 Ma basalt interpreted here to have been induced by rifting (Fig. 4C). As the lithology and ages of the Paleoproterozoic and Mesoproterozoic basement rocks north and south of the South Qilian suture are similar (Figs. 4B and 4C; Wang et al., 2013), the opening of the South Qilian Ocean likely occurred within the Proto–Kunlun-Qaidam Terrane as shown in Figure 20E. The opening of the Paleo–Kunlun Ocean is inferred to have started at ca. 730 Ma, which is evidenced by the emplacement of ca. 733 Ma mafic dikes in the Eastern Kunlun Range (Fig. 4D) associated with the development of a passive margin as diking was coeval with the deposition of the shallow-marine sequence (Fig. 20E; Wang et al., 2013). However, the lack of a definitively recognizable passive-margin sequence along the southern margin of the Kunlun-Qaidam Terrane makes this interpretation uncertain. The opening site of the Paleo–Kunlun Ocean follows the trace of the 940–820 Ma Proto–Kunlun arc (Fig. 4D), suggesting that its development was controlled by the preexisting tectonic fabrics in the continental lithosphere.

The timing for continental breakup along the western margin of South China must have occurred after the termination of arc magmatism from 825 Ma to 760 Ma and during the deposition of Upper Nanhua to Sinian (ca. 680–550 Ma) (equivalent to the middle Cryogenian to the end of the Ediacaran; Gradstein et al., 2012) shallow-marine strata (Fig. 4E). The lack of tillite-bearing sedimentary strata in the passive-margin sequences suggests that the continental breakup event along the western margin of South China occurred after the Qingbaikou-Nanhua period (ca. 850–680 Ma). As the southern margin of the Kunlun-Qaidam Terrane and the northern margin of South China were conjugate in our model, we suggest that the opening of the Kunlun Ocean occurred later than the Qilian Oceans at ca. 680 Ma (Fig. 20E).

Arc magmatism started at ca. 580 Ma in the Eastern Kunlun Range and ca. 550–520 Ma along the northern margin of the Kunlun-Qaidam Terrane and within the Central Qilian Terrane (Fig. 19) as a result of northward subduction of the Paleo–Kunlun Ocean and southward subduction of the North and South Qilian Oceans (Fig. 20F). Northward subduction of the North Qilian Ocean did not start until ca. 500–480 Ma, creating a dominant Ordovician arc along the southern margin of North China (Figs. 4A and 20G). A-type granitoids emplaced at 430–410 Ma during extension were coeval with deposition of Devonian intra-arc extensional basins (this study) and the emplacement of mafic and ultramafic bodies (Meng et al., 2013b) in the Eastern Kunlun Range area (Fig. 20H). Exhumation of ca. 428 Ma eclogite-bearing high-grade metamorphic rocks with a 930 Ma protolith age (Meng et al., 2013a) in the eastern part of the Eastern Kunlun Range may have been associated with forearc thrusting (Fig. 20H). The final elimination of the Paleo-Kunlun and South Qilian Oceans occurred at 400–375 Ma, which is expressed by the cessation of arc activities across the Kunlun-Qaidam Terrane and the Qilian orogen (Figs. 19 and 20I).

The magmatic lull across the central and northern Tibetan region from ca. 375 Ma to ca. 290 Ma was accompanied by the development of a passive continental margin along the southern edge of the Kunlun-Qaidam Terrane, which is interpreted in this study as a result of continental drifting of the Songpan-Ganzi Terrane (Figs. 20J). This process created the Neo–Kunlun Ocean referred to in this study, but it has been assigned as the Paleo-Tethys by Şengör (1984). The Neo–Kunlun Ocean is interpreted in this study as the western extension of the Mianlue Ocean in the Qinling region (e.g., Ratschbacher et al., 2003; Dong and Santosh, 2015), which was generated within the Laurasia supercontinent.

The consumption of the Neo–Kunlun Ocean (= Anymaqen-Kunlun-Muztagh Ocean of Yin and Harrison, 2000) created a wide zone of arc magmatism (Fig. 20K), stretching from the Qilian Shan in the north to the Kunlun Range in the south over a distance >800 km (Fig. 19), which does not consider the effect of Cenozoic shortening across the Qilian Shan, Qaidam Basin, and the Kunlun Range (Yin et al., 2008b; Zuza et al., 2016). Note that 250–200 Ma arc magmatism induced by a different subduction system from the Jinsha Ocean to the south (see discussion below) also occurred south of the Kunlun suture zone (Fig. 19), which should not be confused with the coeval arc magmatism generated by our inferred shallow to flat north-dipping subduction. The emplacement of 255–222 Ma I- and S-type granitoids examined in this study and deposition of Triassic sediments in intra-arc basins occurred during the development of the Neo–Kunlun arc.

The consumption of the Jinsha Ocean south of the Songpan-Ganzi Terrane was mostly accomplished by both northward and southward subduction from the Triassic to possibly the earliest Jurassic (Kapp et al., 2000, 2003; Pullen et al., 2008; Ding et al., 2013; Zhang et al., 2014). This stage of arc development must have involved flat-slab subduction below the Kunlun-Qaidam Terrane; the associated slab rollback may have occurred from ca. 225 Ma in the Qilian Shan to ca. 195 Ma to the Eastern Kunlun Range, as indicated by the trend of the youngest igneous activities in these regions (Fig. 19). Latest Triassic and earliest Jurassic northward subduction of the Jinsha oceanic plate may have also involved slab rollback (Fig. 20L), causing extreme extension of the Songpan-Ganzi crust on which a thick (5–10 km) flysch pile was deposited in the Triassic during the extension (Pullen et al., 2008; Zhang et al., 2014). The deposition of the Triassic flysch complex may have spilled over to the adjacent terranes and buried the suture zones separating the Songpan-Ganzi Terrane from its neighboring terranes, as suggested by Şengör (1990) and shown in Figure 20L. During the Early Cretaceous (145–120 Ma), the topographic barriers created by the Triassic closure of the Neo–Kunlun

Ocean between South China and the Kunlun-Qaidam terrane must have been removed, allowing a through-going drainage system linking the western margin of South China as a source area to the Eastern Kunlun Range area (Fig. 20M).

The tectonic model proposed here involves five stages of arc magmatism at 1005–910 Ma, 790–720 Ma, 580–500 Ma, 490–375 Ma, and 290–195 Ma, respectively. However, arc magmatism for the first three stages is mainly based on the general petrological characteristics of the plutonic rocks without the support of systematic geochemical analysis and more importantly geologic field documentation of the presence of the arcs and associated tectonic features such as the suture zones and forearc/backarc basins. The main difficulties of establishing the presence of the three older arc systems are that (1) their exposure is highly incomplete due to widespread occurrences of younger sedimentary covers (e.g., Cenozoic Qaidam Basin and Triassic Songpan-Ganzi flysch deposits) and (2) severe tectonic modification and juxtaposition due to the development of the early Paleozoic Qilian orogen and Paleozoic to early Mesozoic Paleo- and Neo-Kunlun orogens. In this regard, a detailed geochemical analysis of the Proterozoic to early Paleozoic plutonic rocks should provide further tests of our proposed model.

Another cautious note about our proposed model is a lack of incorporation of potentially large-scale strike-slip faulting associated with the development of the Qilian Shan and Qinling orogenic belts. For example, Yin and Nie (1996) suggested that the Kunlun-Qaidam Terrane was once located directly south of the Qinling-Dabie region and was extruded westward during the Triassic collision between North China and South China. Although this model successfully explains the timing of strike-slip faulting in the Qinling region and the absence of a pre-Triassic arc in the Dabie Shan region, the model has not been systematically tested in the Qilian Shan and the Eastern Kunlun Range. The existence of the kind of strike-slip faults as predicted by Yin and Nie (1996) would significantly alter the tectonic model proposed in this study.

CONCLUSIONS

The Qilian Shan, Qaidam Basin, and the Eastern Kunlun Range of northern Tibet have experienced five stages of magmatism: (1) at 1005–910 Ma, (2) at 790–720 Ma, (3) at 580–500 Ma, (4) at 490–375 Ma, and (5) at 290–195 Ma. The magmatic history, together with the geologic constraints obtained from this study and early work in the neighboring regions (i.e., Qinling orogen, South China, and North China), allows us to construct a coherent tectonic model that explains the evolution of the southern margin of the supercontinent Laurasia from the onset of the Neoproterozoic to the earliest Jurassic. Our model has the following key features. (1) The linked South Qilian and North Qinling suture zone bounded the coherent Kunlun–Qaidam–North Qinling Terrane in the early Paleozoic. (2) The Songpan-Ganzi Terrane, which experienced extreme extension in the Triassic, has been the western extension of the Yangtze craton of South China since the Neoproterozoic. (3) The development of the wide (>800 km) Permian–Triassic arc across the Kunlun-Qaidam Terrane was induced by flat northward subduction followed by rapid slab rollback. (4) The formation of the Anymaqen-Kunlun-Muztagh Ocean was created within the Laurasia supercontinent rather than being a pre-existing ocean between the supercontinents of Gondwana and Laurasia. The tectonic history of the Kunlun and Qilian Shan regions as unraveled in this study requires that Wilson cycles had played a controlling role in constructing the southern Asian continent from the Neoproterozoic to the early Mesozoic. This conclusion contrasts sharply to the early studies that infer the closure of a preexisting Proterozoic ocean as a fundamental process of the "Paleo-Tethys" development.

REFERENCES CITED

Arculus, R.J., 2003, Use and abuse of the terms calcalkaline and calcalkalic: Journal of Petrology, v. 44, no. 5, p. 929–935, doi:10.1093/petrology/44.5.929.

Badarch, G., Cunningham, W.D., and Windley, B.F., 2002, A new terrane subdivision for Mongolia: Implications for the Phanerozoic crustal growth of Central Asia: Journal of Asian Earth Sciences, v. 21, p. 87–110, doi:10.1016/S1367-9120(02)00017-2.

Bader, T., Franz, L., Ratschbacher, L., Capitani, C., Webb, A.A.G., Yang, Z., Pfander, A.J., Hofmann, M., and Linnemann, U., 2013, The Heart of China revisited: II. Early Paleozoic (ultra) high-pressure and (ultra) high-temperature metamorphic Qinling orogenic collage: Tectonics, v. 32, p. 922–947.

Baksi, A.K., 2001, Search for a deep-mantle component in mafic lavas using a Nb Y Zr plot: Canadian Journal of Earth Sciences, v. 38, no. 5, p. 813–824.

Bian, Q.T., Luo, X.Q., Li, D.H., Zhao, D.S., Chen, H.H., Xu, G.Z., Chang, C.F., and Gao, Y.L., 2000, Discovery of Caledonian island-arc granodiorite-tonalite in Buqingshan, Qinghai Province: Progress in Natural Science, v. 10, p. 74–78.

Bian, Q.T., Gao, S.L., Li, D.H., Ye, Z.G., Chang, C.F., and Luo, X.Q., 2001, A study of the Kunlun-Qilian-Qinling suture system: Acta Geologica Sinica, v. 75, p. 364–374 [English edition].

Bian, Q.T., Li, D.H., Pospelov, I., Yin, L.M., Li, H.S., Zhao, D.S., Chang, C.F., Luo, X.Q., Gao, S.L., Astrakhantsev, O., and Chamov, N., 2004, Age, geochemistry and tectonic setting of Buqingshan ophiolites, North Qinghai–Tibet Plateau, China: Journal of Asian Earth Sciences, v. 23, p. 577–596, doi:10.1016/j.jseaes.2003.09.003.

Bian, Q.T., Zhu, S.X., Pospelov, I.I., Semikhatov, M.A., Sun, S.F., Chen, D.Z., and Na, C.G., 2006, Discovery of late Mesoproterozoic–early Neoproterozoic stromatolite assemblage in the southern belt of the Eastern Kunlun: Chinese Journal of Geology, v. 41, no. 3, p. 500–510 [in Chinese with English abstract].

Boynton, W.V., 1984, Cosmochemistry of the rare earth elements: Meteorite studies, in Henderson, P., ed., Rare Earth Element Geochemistry: Amsterdam, Netherlands, Elsevier, p. 63–114, doi:10.1016/B978-0-444-42148-7.50008-3.

Briggs, S.M., Yin, A., Manning, C.E., Chen, Z.L., Wang, X.F., and Grove, M., 2007, Late Paleozoic tectonic history of the Ertix fault in the Chinese Altai and its implications for the development of the Central Asian orogenic system: Geological Society of America Bulletin, v. 119, p. 944–960, doi:10.1130/B26044.1.

Briggs, S.M., Yin, A., Manning, C.E., Chen, Z.L., and Wang, X.F., 2009, Tectonic development of the southern Chinese Altai Range as determined by structural geology, thermobarometry, ⁴⁰Ar/³⁹Ar thermochronology, and Th/Pb ion-microprobe monazite geochronology: Geological Society of America Bulletin, v. 121, p. 1381–1393, doi:10.1130/B26385.1.

Cawood, P.A., Wang, Y., Xu, Y., and Zhao, G., 2013, Locating South China in Rodinia and Gondwana: A fragment of greater India lithosphere?: Geology, v. 41, no. 8, p. 903–906, doi:10.1130/G34395.1.

Chen, H.W., Luo, Z.H., Mo, X.X., Zhang, X.T., Wang, J., and Wang, B.Z., 2006, SHRIMP ages of Kayakedengtage complex in the East Kunlun Mountains and their geological implications: Acta Petrologica et Mineralogica, v. 25, p. 25–32 [in Chinese with English abstract].

Chen, N.S., Sun, M., He, L., Zhang, K.X., and Wang, G.C., 2002, Precise timing of the Early Paleozoic metamorphism and thrust deformation in the Eastern Kunlun orogen: Chinese Science Bulletin, v. 47, p. 1130–1133, doi:10.1360/02tb9253.

Chen, N.S., Li, X.Y., Wang, X.Y., Chen, Q., Wang, Q.Y., and Wan, Y.S., 2006a, Zircon U-Pb SHRIMP dating of Neoproterozoic metagranite in the North Kunlun unit on the southern margin of the Qaidam block in China: Geological Bulletin of China, v. 25, p. 1311–1314.

Chen, N.S., Li, X.Y., Zhang, K.X., Wang, G.C., Zhu, Y.H., Hou, G.J., and Bai, Y.S., 2006b, Lithological characteristics of the Baishahe Formation south of Xiangride town, Eastern Kunlun Mountains, and its age constrained from zircon Pb-Pb dating: Geological Science and Technology Information, v. 25, p. 1–7 [in Chinese with English abstract].

Chen, N.S., Sun, M., Wang, Q.Y., Zhang, K.X., Wan, Y.S., and Chen, H.H., 2008, U-Pb dating of zircon from the Central zone of the East Kunlun orogen and its implications for tectonic evolution: Science in China Series D, Earth Sciences, v. 51, p. 929–938, doi:10.1007/s11430-008-0072-x.

Chen, N.S., Zhang, L., Sun, M., Wang, Q., and Kusky, T.M., 2012, U-Pb and Hf isotopic compositions of detrital zircons from the paragneisses of the Quanji Massif, NW China: Implications for its early tectonic evolutionary history: Journal of Asian Earth Sciences, v. 54, p. 110–130, doi:10.1016/j.jseaes.2012.04.006.

Chen, N.S., Liao, F.X., Wang, L., Santosh, M., Sun, M., Wang, Q.Y., and Mustafa, H.A., 2013a, Late Paleoproterozoic multiple metamorphic events in the Quanji Massif: Links with Tarim and North China cratons and implications for assembly of the Columbia supercontinent: Precambrian Research, v. 228, p. 102–116, doi:10.1016/j.precamres.2013.01.013.

Chen, N.S., Gong, S.L., Xia, X.P., Geng, H.Y., Wang, L., Sun, M., and Kusky, M.T., 2013b, Zircon Hf isotope of Yingfeng rapakivi granites from the Quanji Massif and ~2.7 Ga crustal growth: Journal of Earth Science, v. 24, p. 29–41, doi:10.1007/s12583-013-0309-2.

Chen, X.H., Yin, A., Gehrels, G.E., Cowgill, E.S., Grove, M., Harrison, T.M., and Wang, X.F., 2003, Two phases of Mesozoic north-south extension in the eastern Altyn Tagh range, northern Tibetan Plateau: Tectonics, v. 22, no. 5, p. 1053, doi:10.1029/2001TC001336.

Chen, X.H., Gehrels, G.E., Yin, A., Li, L., and Jiang, R.B., 2012, Paleozoic and Mesozoic basement magmatisms of Eastern Qaidam Basin, Northern Qinghai–Tibet Plateau: LA-ICP-MS zircon U-Pb geochronology and its geological significance: Acta Geologica Sinica, v. 86, p. 350–369, doi:10.1111/j.1755-6724.2012.00665.x.

Chen, X.H., Gehrels, G.E., Yin, A., Zhou, Q., and Huang, P.H., 2014, Geochemical and Nd-Sr-Pb-O isotopic constraints on Permo–Triassic magmatism in eastern Qaidam Basin, Northern Qinghai–Tibetan Plateau: Implications for the evolution of the Paleo-Tethys: Journal of Asian Earth Sciences, v. 114, p. 674–692, doi:10.1016/j.jseaes.2014.11.013.

Chen, Y.X., Pei, X.Z., Li, R.B., Liu, Z.Q., Li, Z.C., Zhang, X.F., Chen, G.C., Liu, Z.G., Ding, S.P., and Guo, J.F., 2011, Zircon U-Pb age of Xiaomiao Formation of Proterozoic in the eastern section of the East Kunlun orogenic belt: Geoscience, v. 25, p. 510–521 [in Chinese with English abstract].

Chinese Geological Survey, 2014, Geologic Time Units in China: Geological Publishing House, Beijing.

Chinese State Bureau of Seismology (CSBS), 1992, The Altyn Tagh Active Fault System: Beijing, Seismology Publishing House, 319 p.

Christiansen, E.H., Sheridan, M.F., and Burt, D.M., 1986, The Geology and Geochemistry of Cenozoic Topaz Rhyolites from the Western United States: Geological Society of America Special Paper 205, 82 p., doi:10.1130/SPE205-p1.

Clark, M.K., Farley, K.A., Zheng, D., Wang, Z., and Duvall, A.R., 2010, Early Cenozoic faulting of the northern Tibetan Plateau margin from apatite (U-Th)/He ages: Earth and Planetary Science Letters, v. 296, p. 78–88, doi:10.1016/j.epsl.2010.04.051.

Cowgill, E., 2001, Tectonic Evolution of the Altyn Tagh–Western Kunlun Fault System, Northwestern China [Ph.D. thesis]: Los Angeles, California, University of California, 311 p.

Cowgill, E., Yin, A., Harrison, T.M., and Wang, X.F., 2003, Reconstruction of the Altyn Tagh fault based on U-Pb geochronology: Role of back thrusts, mantle sutures, and heterogeneous crustal strength in forming the Tibetan Plateau: Journal of Geophysical Research, v. 108, p. 2346, doi:10.1029/2002JB002080.

Dai, J., Yin, A., Liu, W., and Wang, C., 2008, Nd isotopic compositions of the Tethyan Himalayan Sequence in southeastern Tibet: Science in China, ser. D, Earth Sciences, v. 51, no. 9, p. 1306–1316, doi:10.1007/s11430-008-0103-7.

Dai, J., Wang, C., Polat, A., Santosh, M., Li, Y., and Ge, Y., 2013a, Rapid forearc spreading between 130 and 120 Ma: Evidence from geochronology and geochemistry of the Xigaze ophiolite, southern Tibet: Lithos, v. 172, p. 1–16, doi:10.1016/j.lithos.2013.03.011.

Dai, J.G., Wang, C.S., Hourigan, J., and Santosh, M., 2013b, Multi-stage tectono-magmatic events of the Eastern Kunlun Range, northern Tibet: Insights from U-Pb geochronology and (U-Th)/He thermochronology: Tectonophysics, v. 599, p. 97–106, doi:10.1016/j.tecto.2013.04.005.

Dickinson, W.R., 1970, Interpreting detrital modes of graywacke and arkose: Journal of Sedimentary Research, v. 40, p. 695–707.

Dickinson, W.R., 1985, Interpreting provenance relations from detrital modes of sandstones, in Zuffa, G.G., ed., Provenance of Arenites: NATO ASI Series C Volume 148: Dordrecht, Netherlands, D. Reidel Publishing Company, p. 333–361, doi:10.1007/978-94-017-2809-6_15.

Dickinson, W.R., and Gehrels, G.E., 2009, Use of U-Pb ages of detrital zircons to infer maximum depositional ages of strata: A test against a Colorado Plateau Mesozoic database: Earth and Planetary Science Letters, v. 288, p. 115–125, doi:10.1016/j.epsl.2009.09.013.

Ding, L., Yang, D., Cai, F.L., Pullen, A., Kapp, P., Gehrels, G.E., Zhang, L.Y., Zhang, Q.H., Lai, Q.Z., Yue, Y.H., and Shi, R.D., 2013, Provenance analysis of the Mesozoic Hoh-Xil-Songpan-Ganzi turbidites in northern Tibet: Implications for the tectonic evolution of the eastern Paleo-Tethys Ocean: Tectonics, v. 32, p. 34–48, doi:10.1002/tect.20013.

Ding, Q.F., Jiang, S.Y., and Sun, F.Y., 2014, Zircon U-Pb geochronology, geochemical and Sr-Nd-Hf isotopic compositions of the Triassic granite and diorite dikes from the Wulonggou mining area in the Eastern Kunlun orogen, NW China: Petrogenesis and tectonic implications: Lithos, v. 205, p. 266–283, doi:10.1016/j.lithos.2014.07.015.

Dong, S.W., Gao, R., Yin, A., Guo, T.L., Zhang, Y.Q., Hu, J.M., Li, J.H., Shi, W., and Li, Q.S., 2013, What drove continued continent-continent convergence after ocean closure? Insights from high-resolution seismic-reflection profiling across the Daba Shan in central China: Geology, v. 41, p. 671–674, doi:10.1130/G34161.1.

Dong, S.W., Zhang, Y.Q., Gao, R., Su, J.B., Liu, M., and Li, J.H., 2015, A possible buried Paleoproterozoic collisional orogen beneath central South China: Evidence from seismic-reflection profiling: Precambrian Research, v. 264, p. 1–10.

Dong, Y.P., and Santosh, M., 2015, Tectonic architecture and multiple orogeny of the Qinling orogenic belt, Central China: Gondwana Research, v. 29, no. 1, p. 1–40, doi:10.1016/j.gr.2015.06.009.

Drake, M.J., and Weill, D.F., 1975, Partition of Sr, Ba, Ca, Y, Eu²⁺, Eu³⁺, and other REE between plagioclase feldspar and magmatic liquid: An experimental study: Geochimica et Cosmochimica Acta, v. 39, no. 5, p. 689–712, doi:10.1016/0016-7037(75)90011-3.

Dupont-Nivet, G., Lippert, P.C., Van Hinsbergen, D.J., Meijers, M.J., and Kapp, P., 2010, Palaeolatitude and age of the Indo-Asia collision: Palaeomagnetic constraints: Geophysical Journal International, v. 182, p. 1189–1198, doi:10.1111/j.1365-246X.2010.04697.x.

Duvall, A.R., Clark, M.K., Kirby, E., Farley, K.A., Craddock, W.H., Li, C., and Yuan, D.Y., 2013, Low-temperature thermochronometry along the Kunlun and Haiyuan faults, NE Tibetan Plateau: Evidence for kinematic change during late-stage orogenesis: Tectonics, v. 32, p. 1190–1211, doi:10.1002/tect.20072.

Eby, G.N., 1990, The A-type granitoids: A review of their occurrence and chemical characteristics and speculations on their petrogenesis: Lithos, v. 26, p. 115–134, doi:10.1016/0024-4937(90)90043-Z.

Eby, G.N., 1992, Chemical subdivision of the A-type granitoids: Petrogenetic and tectonic implications: Geology, v. 20, p. 641–644, doi:10.1130/0091-7613(1992)020<0641:CSOTAT>2.3.CO;2.

Enkelmann, E., Weislogel, A., Ratschbacher, L., Eide, E., Renno, A., and Wooden, J., 2007, How was the Triassic Songpan-Ganzi basin filled? A provenance study: Tectonics, v. 26, no. 4, doi:10.1029/2006TC002078.

Enkin, R.J., Yang, Z., Chen, Y., and Courtillot, V., 1992, Paleomagnetic constraints on the geodynamic history of the major blocks of China from the Permian to the present: Journal of Geophysical Research, v. 97, p. 13,953–13,989, doi:10.1029/92JB00648.

Fitton, J.G., Saunders, A.D., Norry, M.J., Hardarson, B.S., and Taylor, R.N., 1997, Thermal and chemical structure of the Iceland plume: Earth and Planetary Science Letters, v. 153, p. 197–208, doi:10.1016/S0012-821X(97)00170-2.

Gehrels, G.E., Yin, A., and Wang, X.F., 2003a, Magmatic history of the northeastern Tibetan Plateau: Journal of Geophysical Research, v. 108, 2423, p. 1978–2012, doi:10.1029/2002JB001876.

Gehrels, G.E., Yin, A., and Wang, X.F., 2003b, Detrital-zircon geochronology of the northeastern Tibetan Plateau: Geological Society of America Bulletin, v. 115, p. 881–896, doi:10.1130/0016-7606(2003)115<0881:DGOTNT>2.0.CO;2.

Gehrels, G.E., Kapp, P., DeCelles, P., Pullen, A., Blakey, R., Weislogel, A., Ding, L., Guynn, J., Martin, A., McQuarrie, N., and Yin, A., 2011, Detrital zircon geochronology of pre-Tertiary strata in the Tibetan-Himalayan orogen: Tectonics, v. 30, TC5016, doi:10.1029/2011TC002868.

Gilotti, J.A., and McClelland, W.C., 2007, Characteristics of, and a tectonic model for, ultrahigh-pressure metamorphism in the overriding plate of the Caledonian orogen: International Geology Review, v. 49, p. 777–797, doi:10.2747/0020-6814.49.9.777.

Gong, S.L., Chen, N.S., Wang, Q.Y., Kusky, T.M., Wang, L., Zhang, L., Ba, J., and Liao, F.X., 2012, Early Paleoproterozoic magmatism in the Quanji Massif, northeastern margin of the Qinghai–Tibet Plateau and its tectonic significance: LA-ICPMS U-Pb zircon geochronology and geochemistry: Gondwana Research, v. 21, p. 152–166, doi:10.1016/j.gr.2011.07.011.

Gradstein, F.M., Ogg, J.G., Schmitz, M., and Ogg, G., 2012, On the geologic time scale: Newsletters on Stratigraphy, v. 45, no. 2, p. 171–188, doi:10.1127/0078-0421/2012/0020.

Guo, A.L., Zhang, G.W., Qiang, J., Sun, Y.G., Li, G., and Yao, A.P., 2009, Indosinian Zongwulong orogenic belt on the northeastern margin of the Qinghai-Tibet Plateau: Yanshi Xuebao, v. 25, p. 1–12 [in Chinese with English abstract].

Guo, X.Q., Yan, Z., Wang, Z.Q., Wang, T., Hou, K.J., Fu, C.L., and Li, J.L., 2012, Middle Triassic arc magmatism along the northeastern margin of Tibet: U-Pb and Lu-Hf zircon characterization of the Gangcha complex in the West Qinling terrane, Central China: Journal of the Geological Society of London, v. 169, p. 327–336, doi:10.1144/0016-76492011-083.

Guo, Z.J., Yin, A., Robinson, A., and Jia, C.Z., 2005, Geochronology and geochemistry of deep-drill-core samples from the basement of the central Tarim Basin: Journal of Asian Earth Sciences, v. 25, p. 45–56, doi:10.1016/j.jseaes.2004.01.016.

Guynn, J., Kapp, P., Gehrels, G.E., and Ding, L., 2012, U-Pb geochronology of basement rocks in central Tibet and paleogeographic implications: Journal of Asian Earth Sciences, v. 43, no. 1, p. 23–50, doi:10.1016/j.jseaes.2011.09.003.

Hacker, B.R., Ratschbacher, L., Webb, L., McWilliams, M.O., Ireland, T., Calvert, A., Dong, S.W., Wenk, H.R., and Chateigner, D., 2000, Exhumation of ultrahigh-pressure continental crust in east central China: Late Triassic–Early Jurassic tectonic unroofing: Journal of Geophysical Research, v. 105, p. 13,339–13,364, doi:10.1029/2000JB900039.

Harris, N.B.W., Xu, R.H., Lewis, C.L., Hawkesworth, C.J., and Zhang, Y.Q., 1988, Isotope geochemistry of the 1985 Tibet Geotraverse, Lhasa to Golmud: Philosophical Transactions of the Royal Society of London, v. 327, p. 263–285, doi:10.1098/rsta.1988.0129.

Harrison, T.M., Copeland, P., Kidd, W.S.F., and Yin, A., 1992, Raising Tibet: Science, v. 255, p. 1663–1670, doi:10.1126/science.255.5052.1663.

He, S.P., Wang, H.L., Chen, J.L., Xu, X.Y., Zhang, H.F., Ren, G.M., and Yu, J.Y., 2007, LA-ICP-MS U-Pb zircon geochronology of basic dikes within Maxianshan rock group in the central Qilian orogenic belt and its tectonic implications: Journal of China University of Geosciences, v. 18, p. 19–29, doi:10.1016/S1002-0705(07)60015-6.

Heubeck, C., 2001, Assembly of Central Asia during the middle and late Paleozoic, in Hendrix, M.S., and Davis, G.A., eds., Paleozoic and Mesozoic Tectonic Evolution of Central and Eastern Asia: From Continental Assembly to Intracontinental Deformation: Geological Society of America Memoir 194, p. 1–22.

Hildreth, W., and Moorbath, S., 1988, Crustal contributions to arc magmatism in the Andes of central Chile: Contributions to Mineralogy and Petrology, v. 98, no. 4, p. 455–489, doi:10.1007/BF00372365.

Hsü, K.J., Guitang, P., and Şengör, A.M.C., 1995, Tectonic evolution of the Tibetan Plateau: A working hypothesis based on the archipelago model of orogenesis: International Geology Review, v. 37, p. 473–508, doi:10.1080/00206819509465414.

Hu, N.G., Xu, A.D., and Yang, J.X., 2005, Characteristics and tectonic environment of Zhigoumen pluton in Longshoushan area: Journal of Earth Sciences and Environment, v. 27, p. 5–11 [in Chinese with English abstract].

Huang, H., Niu, Y.L., Nowell, G., Zhao, Z.D., Yu, X.H., Zhu, D.C., Mo, X.X., and Ding, S., 2014, Geochemical constraints on the petrogenesis of granitoids in the East Kunlun orogenic belt, northern Tibetan Plateau: Implications for continental crust growth through syn-collisional felsic magmatism: Chemical Geology, v. 370, p. 1–18, doi:10.1016/j.chemgeo.2014.01.010.

Ingersoll, R.V., Bullard, T.F., Ford, R.L., Grimm, J.P., Pickle, J.D., and Sares, S.W., 1984, The effect of grain size on detrital modes: A test of the Gazzi-Dickinson point-counting method: Journal of Sedimentary Research, v. 54, p. 103–116.

Irvine, T., and Baragar, W., 1971, A guide to the chemical classification of the common volcanic rocks: Canadian Journal of Earth Sciences, v. 8, no. 5, p. 523–548, doi:10.1139/e71-055.

Ji, W.H., Li, R.S., Chen, S.J., He, S.P., Zhao, Z.M., Bian, X.W., Zhu, H.P., Cui, J.G., and Ren, J.G., 2011, The discovery of Palaeoproterozoic volcanic rocks in the Bulunkuoler Group from the Tianshuihai Massif in Xinjiang of Northwest China and its geological significance: Science China Earth Sciences, v. 54, p. 61–72, doi:10.1007/s11430-010-4043-7.

Jiang, C.F., Yang, J.S., Feng, B.G., Zhu, Z.Z., Zhao, M., Chai, Y.C., Shi, X.D., Wang, H.D., and Ha, J.Q., 1992, Opening Closing Tectonics of Kunlun Mountains: Geological Memoirs: Beijing, Geological Publishing House, 224 p. [in Chinese with English abstract].

Jiang, G., Sohl, L.E., and Christie-Blick, N., 2003, Neoproterozoic stratigraphic comparison of the Lesser Himalaya (India) and Yangtze block (south China): Paleogeographic implications: Geology, v. 31, no. 10, p. 917–920, doi:10.1130/G19790.1.

Jiang, M., Galvé, A., Hirn, A., De Voogd, B., Laigle, M., Su, H.P., Diaz, J., Lépine, J.C., and Wang, Y.X., 2006, Crustal thickening and variations in architecture from the Qaidam Basin to the Qang Tang (north-central Tibetan Plateau) from wide-angle reflection seismology: Tectonophysics, v. 412, p. 121–140, doi:10.1016/j.tecto.2005.09.011.

Jiang, R.B., Chen, X.H., Dang, Y.Q., Yin, A., Wang, L.Q., Jiang, W.M., Wan, J.L., and Wang, X.F., 2008, Apatite fission track evidence for two phases Mesozoic–Cenozoic thrust faulting in eastern Qaidam Basin: Chinese Journal of Geophysics, v. 51, p. 116–124.

Kapp, P., Yin, A., Manning, C.E., Murphy, M., Harrison, T.M., Spurlin, M., Ding, L., Deng, X.G., and Wu, C.M., 2000, Blueschist-bearing metamorphic core complexes in the Qiangtang block reveal deep crustal structure of northern Tibet: Geology, v. 28, no. 1, p. 19–22, doi:10.1130/0091-7613(2000)28<19:BMCCIT>2.0.CO;2.

Kapp, P., Yin, A., Manning, C.E., Harrison, T.M., Taylor, M.H., and Ding, L., 2003, Tectonic evolution of the early Mesozoic blueschist-bearing Qiangtang metamorphic belt, central Tibet: Tectonics, v. 22, no. 4, p. 1043, doi:10.1029/2002TC001383.

Kay, S.M., Ramos, V.A., Mpodozis, C., and Sruoga, P., 1989, Late Paleozoic to Jurassic silicic magmatism at the Gondwana margin: Analogy to the Middle Proterozoic in North America?: Geology, v. 17, no. 4, p. 324–328, doi:10.1130/0091-7613(1989)017<0324:LPTJSM>2.3.CO;2.

Kay, S.M., Coira, B., and Viramonte, J., 1994, Young mafic back arc volcanic rocks as indicators of continental lithospheric delamination beneath the Argentine Puna plateau, central Andes: Journal of Geophysical Research, v. 99, p. 24,323–24,339, doi:10.1029/94JB00896.

Kay, S.M., Godoy, E., and Kurtz, A., 2005, Episodic arc migration, crustal thickening, subduction erosion, and magmatism in the south-central Andes: Geological Society of America Bulletin, v. 117, no. 1–2, p. 67–88, doi:10.1130/B25431.1.

Kuno, H., 1968, Differentiation of basaltic magma, in Hess, H.H., and Poldervaart, A.A., eds., The Poldervaart Treatise on Rocks of Basaltic Composition, 2: New York, Interscience, p. 623–688.

Lai, S.C., Liu, C.Y., and Yi, H.S., 2003, Geochemistry and petrogenesis of Cenozoic andesite-dacite associations from the Hoh Xil region, Tibetan Plateau: International Geology Review, v. 45, p. 998–1019, doi:10.2747/0020-6814.45.11.998.

Lai, S.C., Qin, J.F., and Li, Y.F., 2007, Partial melting of thickened Tibetan crust: Geochemical evidence from Cenozoic adakitic volcanic rocks: International Geology Review, v. 49, p. 357–373, doi:10.2747/0020-6814.49.4.357.

Le Maitre, R.W.B., Dudek, P., Keller, A., Lameyre, J., Le Bas, J., Sabine, M.J., Schmid, P.A., Sorensen, R., Streckeisen, A., Woolley, A., and Zanettin, A.R., 1989, A Classification of Igneous Rocks and Glossary of Terms: Recommendations of the International Union of Geological Sciences, Subcommission on the Systematics of Igneous Rocks (No. 552.3 CLA): International Union of Geological Sciences: Oxford, Blackwell, 193 p.

Li, B.L., Sun, F.Y., Yu, X.F., Qian, Y., Wang, G., and Yang, Y.Q., 2012, U-Pb dating and geochemistry of diorite in the eastern section from eastern Kunlun middle uplifted basement and granitic belt: Yanshi Xuebao, v. 28, p. 1163–1172.

Li, J.H., Dong, S.W., Yin, A., Zhang, Y.Q., and Shi, W., 2015, Mesozoic tectonic evolution of the Daba Shan thrust belt in the southern Qinling orogen, central China: Constraints from surface geology and reflection seismology: Tectonics, v. 34, no. 8, p. 1545–1575, doi:10.1002/2014TC003813.

Li, W., Neubauer, F., Liu, Y.J., Genser, J., Ren, S.M., Han, G.Q., and Liang, C.Y., 2013, Paleozoic evolution of the Qimantagh magmatic arcs, Eastern Kunlun Mountains: Constraints from zircon dating of granitoids and modern river sands: Journal of Asian Earth Sciences, v. 77, p. 183–202, doi:10.1016/j.jseaes.2013.08.030.

Li, X.H., Su, L., Chung, S.L., Li, Z.X., Liu, Y., Song, B., and Liu, D.Y., 2005, Formation of the Jinchuan ultramafic intrusion and the world's third largest Ni-Cu sulfide deposit: Associated with the ~825 Ma south China mantle plume?: Geochemistry Geophysics Geosystems, v. 6, Q11004, doi:10.1029/2005GC001006.

Liao, F.X., Zhang, L., Chen, N.S., Sun, M., Santosh, M., Wang, Q.Y., and Mustafa, H.A., 2014, Geochronology and geochemistry of meta-mafic dykes in the Quanji Massif, NW China: Paleoproterozoic evolution of the Tarim craton and implications for the assembly of the Columbia supercontinent: Precambrian Research, v. 249, p. 33–56, doi:10.1016/j.precamres.2014.04.015.

Lin, Y.H., Zhang, L.F., Ji, J.Q., and Song, S.G., 2010, 40Ar/39Ar Age of Jiugequan lawsonite blueschists in northern Qilian Mountains and its petrologic significance: Chinese Science Bulletin, v. 55, p. 2021–2027, doi:10.1007/s11434-010-3239-8.

Ling, W., Gao, S., Zhang, B., Li, H., Liu, Y., and Cheng, J., 2003, Neoproterozoic tectonic evolution of the northwestern Yangtze craton, South China: Implications for amalgamation and break-up of the Rodinia supercontinent: Precambrian Research, v. 122, no. 1, p. 111–140, doi:10.1016/S0301-9268(02)00222-X.

Liu, B., Ma, C.Q., Zhang, J.Y., Xiong, F.H., Huang, J., and Jiang, H.A., 2012, Petrogenesis of Early Devonian intrusive rocks in the east part of Eastern Kunlun orogen and implication for early Palaeozoic orogenic processes: Yanshi Xuebao, v. 28, p. 1785–1807.

Liu, C.D., Mo, X.X., Luo, Z.H., Yu, X.H., Chen, H.W., Li, S.W., and Zhao, X., 2004, Mixing events between the crust- and mantle-derived magmas in Eastern Kunlun: Evidence from zircon SHRIMP Π chronology: Chinese Science Bulletin, v. 49, p. 828–834.

Liu, M., Mooney, W.D., Li, S., Okaya, N., and Detweiler, S., 2006, Crustal structure of the northeastern margin of the Tibetan Plateau from the Songpan-Ganzi terrane to the Ordos basin: Tectonophysics, v. 420, p. 253–266, doi:10.1016/j.tecto.2006.01.025.

Liu, Y.J., Genser, J., Neubauer, F., Jin, W., Ge, X., Handler, R., and Takasu, A., 2005, 40Ar/39Ar mineral ages from basement rocks in the Eastern Kunlun Mountains, NW China, and their tectonic implications: Tectonophysics, v. 398, p. 199–224, doi:10.1016/j.tecto.2005.02.007.

Liu, Y.J., Neubauer, F., Genser, J., Takasu, A., Ge, X.H., and Handler, R., 2006, 40Ar/39Ar ages of blueschist facies politic schists from Qingshuigou in the Northern Qilian Mountains, western China: The Island Arc, v. 15, p. 187–198, doi:10.1111/j.1440-1738.2006.00508.x.

Loiselle, M.C., and Wones, D.R., 1979, Characteristics and origin of anorogenic granites: Geological Society of America Abstracts with Programs, v. 11, no. 7, p. 468.

Lu, L., Wu, Z.H., Hu, D.G., Barosh, P.J., Hao, S., and Zhou, C.J., 2010, Zircon U-Pb age for rhyolite of the Maoniushan Formation and its tectonic significance in the East Kunlun Mountains: Yanshi Xuebao, v. 26, p. 1150–1158.

Lu, S.N., 2002, Preliminary Study of Precambrian Geology in the North Tibet–Qinghai Plateau: Beijing, Geological Publishing House, 125 p. [in Chinese].

Lu, S.N., Yu, H.F., and Li, H.K., 2006, Research on Precambrian Major Problems in China: Beijing, Geological Publishing House, 206 p. [in Chinese].

Lu, S.N., Li, H.K., Zhang, C.L., and Niu, G.H., 2008, Geological and geochronological evidence for the Precambrian evolution of the Tarim craton and surrounding continental fragments: Precambrian Research, v. 160, p. 94–107, doi:10.1016/j.precamres.2007.04.025.

Lu, X.X., Sun, Y.G., Zhang, X.T., Xiao, Q.H., Wang, X.X., Wei, X.D., and Gu, D., 2007, The SHRIMP age of Tatalin rapakivi granite at the north margin of Qaidam Basin: Acta Geologica Sinica, v. 81, p. 626–634 [in Chinese with English abstract].

Ma, C.Q., Xiong, F.H., Zhang, J.Y., Liu, B., Huang, J., and Jiang, H.A., 2013, The effect of magmatism from the plate subduction to the post orogenic stage: The evidence of Early Permian–Late Triassic mafic dyke swarms in Eastern Kunlun: Acta Geologica Sinica, v. 87, supplement, p. 79–81 [in Chinese].

Maniar, P.D., and Piccoli, P.M., 1989, Tectonic discrimination of granitoids: Geological Society of America Bulletin, v. 101, p. 635–643, doi:10.1130/0016-7606(1989)101<0635:TDOG>2.3.CO;2.

Meng, F.C., Zhang, J.X., and Yang, J.S., 2005, Tectonothermal event of post-HP/UHP metamorphism in the Xitieshan area of the North Qaidam Mountains, western China: Isotopic and geochemical evidence of granite and gneiss: Yanshi Xuebao, v. 21, p. 45–56 [in Chinese with English abstract].

Meng, F.C., Zhang, J.X., and Cui, M.H., 2013a, Discovery of early Paleozoic eclogite from the East Kunlun, western China, and its tectonic significance: Gondwana Research, v. 23, p. 825–836, doi:10.1016/j.gr.2012.06.007.

Meng, F.C., Cui, M.H., Wu, X.K., Wu, J.F and Wang, J.H., 2013b, Magmatic and metamorphic events recorded in granitic gneisses from the Qimentagh, East Kunlun Mountains, Northwest China: Acta Petrologica Sinica, v. 29, no. 6, p. 2107–2122.

Meng, F.C., Cui, M.H., Wu, X.K., and Ren, Y.F., 2015, Heishan mafic-ultramafic rocks in the Qimantag area of Eastern Kunlun, NW China: Remnants of an early Paleozoic incipient island arc: Gondwana Research, v. 27, p. 745–759, doi:10.1016/j.gr.2013.09.023.

Meng, Q.R., and Zhang, G.W., 1999, Timing of collision of the North and South China blocks: Controversy and reconciliation: Geology, v. 27, p. 123–126, doi:10.1130/0091-7613(1999)027<0123:TOCOTN>2.3.CO;2.

Menold, C.A., 2006, Tectonic and Metamorphic Evolution of the North Qaidam Ultrahigh-Pressure Metamorphic Terrane, Western China [Ph.D. thesis]: Los Angeles, California, University of California, 261 p.

Menold, C.A., Manning, C.E., Yin, A., Tropper, P., Chen, X.H., and Wang, X.F., 2009, Metamorphic evolution, mineral chemistry and thermobarometry of orthogneiss hosting ultrahigh-pressure eclogites in the North Qaidam metamorphic belt, western China: Journal of Asian Earth Sciences, v. 35, p. 273–284, doi:10.1016/j.jseaes.2008.12.008.

Middlemost, E.A.K., 1994, Naming materials in the magma/igneous rock system: Earth-Science Reviews, v. 37, p. 215–224, doi:10.1016/0012-8252(94)90029-9.

Mo, X.X., Luo, Z.H., Deng, J.F., Yu, X.H., Liu, C.D., Chen, H.W., Yuan, W.M., and Liu, Y.H., 2007, Granitoids and crustal growth in the east Kunlun orogenic belt: Geological Journal of China Universities, v. 3, p. 403–414 [in Chinese with English abstract].

Molnar, P., England, P., and Martinod, J., 1993, Mantle dynamics, uplift of the Tibetan Plateau, and the Indian monsoon: Reviews of Geophysics, v. 31, p. 357–396, doi:10.1029/93RG02030.

Nie, S.Y., Yin, A., Rowley, D.B., and Jin, Y.G., 1994, Exhumation of the Dabie Shan ultra-high-pressure rocks and accumulation of the Songpan-Ganzi flysch sequence, central China: Geology, v. 22, p. 999–1002, doi:10.1130/0091-7613(1994)022<0999:EOTDSU>2.3.CO;2.

Osen, A.K., Winguth, A.M., Winguth, C., and Scotese, C.R., 2013, Sensitivity of Late Permian climate to bathymetric features and implications for the mass extinction: Global and Planetary Change, v. 105, p. 171–179, doi:10.1016/j.gloplacha.2012.01.011.

Patiño Douce, A.E., 1997, Generation of metaluminous A-type granites by low-pressure melting of calc-alkaline granitoids: Geology, v. 25, p. 743–746, doi:10.1130/0091-7613(1997)025<0743:GOMATG>2.3.CO;2.

Pearce, J.A., 1996, Sources and settings of granitic rocks: Episodes, v. 19, p. 120–125.

Pearce, J.A., Harris, N.B.W., and Tindle, A.G., 1984, Trace element discrimination diagrams for the tectonic interpretation of granitic rocks: Journal of Petrology, v. 25, p. 956–983, doi:10.1093/petrology/25.4.956.

Pullen, A., Kapp, P., Gehrels, G.E., Vervoort, J.D., and Ding, L., 2008, Triassic continental subduction in central Tibet and Mediterranean-style closure of the Paleo-Tethys Ocean: Geology, v. 36, p. 351–354, doi:10.1130/G24435A.1.

Qian, Q., Wang, Y.M., Li, H.M., Jia, X.Q., Han, S., and Zhang, Q., 1998, Geochemical characteristics and genesis of diorites from Laohushan, Gansu Province: Yanshi Xuebao, v. 14, p. 520–528 [in Chinese with English abstract].

Qinghai Bureau of Geology and Mineral Resources (Qinghai BGMR), 1991, Regional Geology of Qinghai Province: Beijing, Geological Publishing House, 662 p.

Ratschbacher, L., Hacker, B.R., Calvert, A., Webb, L.E., Grimmer, J.C., McWilliams, M.O., Dong, S.W., and Hu, J., 2003, Tectonics of the Qinling (Central China): Tectonostratigraphy, geochronology, and deformation history: Tectonophysics, v. 366, p. 1–53, doi:10.1016/S0040-1951(03)00053-2.

Ren, J.H., Liu, Y.Q., Zhou, D.W., Feng, Q., Zhang, K., Dong, Z.L., and Qin, P.L., 2010, Geochemical characteristics and LA-ICP-MS zircon U-Pb dating of basic dykes in the Xiaomian area: Eastern Kunlun: Journal of Jilin University, Earth Science Edition, v. 40, p. 856–868.

Rickwood, P.C., 1989, Boundary lines within petrologic diagrams which use oxides of major and minor elements: Lithos, v. 22, p. 247–263, doi:10.1016/0024-4937(89)90028-5.

Robinson, A.C., 2015, Mesozoic tectonics of the Gondwanan terranes of the Pamir plateau: Journal of Asian Earth Sciences, v. 102, p. 170–179, doi:10.1016/j.jseaes.2014.09.012.

Robinson, A.C., Yin, A., Manning, C.E., Harrison, T.M., Zhang, S.H., and Wang, X.F., 2004, Tectonic evolution of the northeastern Pamir: Constraints from the northern portion of the Cenozoic Kongur Shan extensional system, western China: Geological Society of America Bulletin, v. 116, no. 7–8, p. 953–973, doi:10.1130/B25375.1.

Robinson, A.C., Yin, A., Manning, C.E., Harrison, T.M., Zhang, S.H., and Wang, X.F., 2007, Cenozoic evolution of the eastern Pamir: Implications for strain-accommodation mechanisms at the western end of the Himalayan-Tibetan orogen: Geological Society of America Bulletin, v. 119, no. 7–8, p. 882–896, doi:10.1130/B25981.1.

Robinson, A.C., Ducea, M., and Lapen, T.J., 2012, Detrital zircon and isotopic constraints on the crustal architecture and tectonic evolution of the northeastern Pamir: Tectonics, v. 31, TC2016, doi:10.1029/2011TC003013.

Roger, F., Arnaud, N., Gilder, S., Tapponnier, P., Jolivet, M., Brunel, M., Malavieille, J., Xu, Z.Q., and Yang, J.S., 2003, Geochronological and geochemical constraints on Mesozoic suturing in east central Tibet: Tectonics, v. 22, no. 4, p. 1037, doi:10.1029/2002TC001466.

Roger, F., Malavieille, J., Leloup, P.H., Calassou, S., and Xu, Z., 2004, Timing of granite emplacement and cooling in the Songpan-Garzê fold belt (eastern Tibetan Plateau) with tectonic implications: Journal of Asian Earth Sciences, v. 22, p. 465–481, doi:10.1016/S1367-9120(03)00089-0.

Rollinson, H.R., 2014, Using Geochemical Data: Evaluation, Presentation, Interpretation: Routledge, 352 p.

Rudnick, R., and Gao, S., 2003, Composition of the continental crust, in Rudnick, R.L., ed., Treatise on Geochemistry, Volume 3: Oxford, UK, Elsevier-Pergamon, 64 p.

Schwab, M., Ratschbacher, L., Siebel, W., McWilliams, M., Minaev, V., Lutkov, V., Chen, O.K., Stanek, K., Nelson, B., Frisch, W., and Wooden, J.L., 2004, Assembly of the Pamirs: Age and origin of magmatic belts from the southern Tien Shan to the southern Pamirs and their relation to Tibet: Tectonics, v. 23, TC4002, doi:10.1029/2003TC001583.

Şengör, A.M.C., 1984, The Cimmeride Orogenic System and the Tectonics of Eurasia: Geological Society of America Special Paper 195, 74 p., doi:10.1130/SPE195-p1.

Şengör, A.M.C., 1990, A new model for the late Palaeozoic–Mesozoic tectonic evolution of Iran and implications for Oman, in Robertson, A.H.F., Searle, M.P., and Ries, A.C., eds., The Geology and Tectonics of the Oman Region: Geological Society of London Special Publication 49, p. 797–831, doi:10.1144/GSL.SP.1992.049.01.49.

Şengör, A.M.C., 1992, The Palaeo-Tethyan suture: A line of demarcation between two fundamentally different architectural styles in the structure of Asia: The Island Arc, v. 1, p. 78–91, doi:10.1111/j.1440-1738.1992.tb00060.x.

Şengör, A.M.C., and Natal'in, B.A., 1996, Paleotectonics of Asia: Fragments of a synthesis, in Yin, A., and Harrison, T.M., eds., The Tectonic Evolution of Asia: New York, Cambridge University Press, p. 486–640.

Şengör, A.M.C., Altıner, D., Cin, A., Ustaömer, T., and Hsü, K.J., 1988, Origin and assembly of the Tethyside orogenic collage at the expense of Gondwana Land, in Audley-Charles, M.G., and Hallam, A., eds., Gondwana and Tethys: Geological Society of London Special Publication 37, p. 119–181, doi:10.1144/GSL.SP.1988.037.01.09.

Şengör, A.M.C., Atayman, S., and Özeren, S., 2008, A scale of greatness and causal classification of mass extinctions: Implications for mechanisms: Proceedings of the National Academy of Sciences of the United States of America, v. 105, p. 13,736–13,740, doi:10.1073/pnas.0805482105.

Shen, B., Xiao, S.H., Zhou, C.M., Kaufman, A.J., and Yuan, X.L., 2010, Carbon and sulfur isotope chemostratigraphy of the Neoproterozoic Quanji Group of the Chaidam Basin, NW China: Basin stratification in the aftermath of an Ediacaran glaciation postdating the Shuram event?: Precambrian Geology, v. 177, p. 241–252, doi:10.1016/j.precamres.2009.12.006.

Shervais, J.W., 1982, Ti-V plots and the petrogenesis of modern and ophiolitic lavas: Earth and Planetary Science Letters, v. 59, no. 1, p. 101–118, doi:10.1016/0012-821X(82)90120-0.

Shi, R.D., Yang, J.S., and Wu, C.L., 2004, First SHRIMP dating for the formation of the late Sinian Yushigou ophiolite North Qilian Mountains: Acta Geologica Sinica, v. 78, p. 649–657 [in Chinese with English abstract].

Shu, L.S., Deng, X.L., Zhu, W.B., Ma, D.S., and Xiao, W.J., 2011, Precambrian tectonic evolution of the Tarim block, NW China: New geochronological insights from the Quruqtagh domain: Journal of Asian Earth Sciences, v. 42, p. 774–790, doi:10.1016/j.jseaes.2010.08.018.

Smith, A.D., 2006, The geochemistry and age of ophiolitic strata of the Xinglongshan Group: Implications for the amalgamation of the Central Qilian belt: Journal of Asian Earth Sciences, v. 28, p. 133–142, doi:10.1016/j.jseaes.2005.09.014.

Sobel, E.R., and Arnaud, N., 1999, A possible middle Paleozoic suture in the Altyn Tagh, NW China: Tectonics, v. 18, p. 64–74, doi:10.1029/1998TC900023.

Sone, M., and Metcalfe, I., 2008, Parallel Tethyan sutures in mainland Southeast Asia: New insights for Palaeo-Tethys closure and implications for the Indosinian orogeny: Comptes Rendus Geoscience, v. 340, p. 166–179, doi:10.1016/j.crte.2007.09.008.

Song, S.G., Niu, Y.L., Su, L., and Xia, X.H., 2013, Tectonics of the North Qilian orogen, NW China: Gondwana Research, v. 23, p. 1378–1401, doi:10.1016/j.gr.2012.02.004.

Stampfli, G.M., and Borel, G.D., 2002, A plate tectonic model for the Paleozoic and Mesozoic constrained by dynamic plate boundaries and restored synthetic oceanic isochrones: Earth and Planetary Science Letters, v. 196, p. 17–33, doi:10.1016/S0012-821X(01)00588-X.

Stampfli, G.M., Hochard, C., Vérard, C., and Wilhem, C., 2013, The formation of Pangea: Tectonophysics, v. 593, p. 1–19, doi:10.1016/j.tecto.2013.02.037.

Sun, S.S., and McDonough, W.F., 1989, Chemical and isotopic systematics of oceanic basalts: Implications for mantle composition and processes, in Saunders, A.D., and Norry, M.J., eds., Magmatism in the Ocean Basins: Geological Society of London Special Publication 42, p. 313–345, doi:10.1144/GSL.SP.1989.042.01.19.

Tan, S.X., Bai, Y.S., Chang, G.H., Tong, H.K., and Bao, G.P., 2004, Discovery and geological significance of metamorphic and intrusive rock (system) of Qimantagh region in Jinning epoch: Northwest Geology, v. 37, p. 69–73 [in Chinese with English abstract].

Tseng, C.Y., Yang, H.Y., Wan, Y., Liu, D., Wen, D.J., Lin, T.C., and Tung, K.A., 2006, Finding of Neoproterozoic (775 Ma) magmatism recorded in metamorphic complexes from the North Qilian orogen: Evidence from SHRIMP zircon U-Pb dating: Chinese Science Bulletin, v. 51, no. 8, p. 963–970, doi:10.1007/s11434-006-0963-1.

Tseng, C.Y., Yang, H.J., Yang, H.Y., Liu, D., Tsai, C.L., Wu, H., and Zuo, G., 2007, The Dongcaohe ophiolite from the North Qilian Mountains: A fossil oceanic crust of the Paleo-Qilian ocean: Chinese Science Bulletin, v. 52, p. 2390–2401, doi:10.1007/s11434-007-0300-3.

Tseng, C.Y., Yang, H.J., Yang, H.Y., Liu, D., Wu, C., Cheng, C.K., Chen, C.H., and Ker, C.M., 2009a, Continuity of the North Qilian and North Qinling orogenic belts, Central orogenic system of China: Evidence from newly discovered Paleozoic adakitic rocks: Gondwana Research, v. 16, p. 285–293, doi:10.1016/j.gr.2009.04.003.

Tseng, C.Y., Zuo, G.C., Yang, H.J., Yang, H.Y., Tung, K.A., Liu, D.Y., and Wu, H.Q., 2009b, Occurrence of Alaskan-type mafic-ultramafic intrusions in the North Qilian Mountains, northwest China: Evidence of Cambrian arc magmatism on the Qilian block: The Island Arc, v. 18, p. 526–549, doi:10.1111/j.1440-1738.2009.00675.x.

Tung, K.A., Yang, H.J., Liu, D.Y., Zhang, J.X., Tseng, C.Y., and Wan, Y.S., 2007a, SHRIMP U-Pb geochronology of the detrital zircons from the Longshoushan Group and its tectonic significance: Chinese Science Bulletin, v. 52, p. 1415–1425.

Tung, K.A., Yang, H.J., Yang, H.Y., Liu, D.Y., Zhang, J.X., Wan, Y., and Tseng, C.Y., 2007b, SHRIMP U-Pb geochronology of the zircons from the Precambrian basement of the Qilian block and its geological significances: Chinese Science Bulletin, v. 52, p. 2687–2701, doi:10.1007/s11434-007-0356-0.

Tung, K.A., Yang, H.J., Yang, H.Y., Liu, D.Y., Zhang, J.X., Yang, H.J., Shau, Y.H., and Tseng, C.Y., 2012, The amphibolite-facies metamorphosed mafic rocks from the Maxianshan area, Qilian block, NW China: S record of early Neoproterozoic arc magmatism: Journal of Asian Earth Sciences, v. 46, p. 177–189, doi:10.1016/j.jseaes.2011.12.006.

Turner, S.A., 2010, Sedimentary record of late Neoproterozoic rifting in the NW Tarim Basin, China: Precambrian Research, v. 181, no. 1, p. 85–96, doi:10.1016/j.precamres.2010.05.015.

Turner, S.P., Foden, J.D., and Morrison, R.S., 1992, Derivation of some A-type magmas by fractionation of basaltic magma—An example from the Padthaway Ridge, South Australia: Lithos, v. 28, p. 151–179, doi:10.1016/0024-4937(92)90029-X.

van Hinsbergen, D.J.J., Kapp, P., Dupont-Nivet, G., Lippert, P.C., DeCelles, P.G., and Torsvik, T.H., 2011, Restoration of Cenozoic deformation in Asia and the size of Greater India: Tectonics, v. 30, TC5003, doi:10.1029/2011TC002908.

Vavra, G., Gebauer, D., Schmid, R., and Compston, W., 1996, Multiple zircon growth and recrystallization during polyphase late Carboniferous to Triassic metamorphism in granulites of the Ivrea zone (Southern Alps): An ion microprobe (SHRIMP) study: Contributions to Mineralogy and Petrology, v. 122, no. 4, p. 337–358, doi:10.1007/s004100050132.

Wang, G.C., Chen, N.S., Zhu, Y.H., and Zhang, K.X., 2003, Late Caledonian ductile thrusting deformation in the central East Kunlun belt, Qinghai, China, and its significance: Evidence from geochronology: Acta Geologica Sinica, v. 77, p. 311–319, doi:10.1111/j.1755-6724.2003.tb00747.x.

Wang, L.Q., Pan, G.T., Ding, J., and Yao, D.S., compiler, 2013, Geological Map of the Tibetan Plateau at a Scale of 1:1.5 M with Explanations: Beijing, Geological Publishing House, 288 p.

Wang, Q., McDermott, F., Xu, J.F., Bellon, H., and Zhu, Y.T., 2005, Cenozoic K-rich adakitic volcanic rocks in the Hohxil area, northern Tibet: Lower-crustal melting in an intracontinental setting: Geology, v. 33, p. 465–468, doi:10.1130/G21522.1.

Wang, X.L., Shu, L.S., Xing, G.F., Zhou, J.C., Tang, M., Shu, X.J., Qi, L., and Hu, Y.H., 2012, Post-orogenic extension in the eastern part of the Jiangnan orogen: Evidence from ca. 800–760 Ma volcanic rocks: Precambrian Research, v. 222, p. 404–423, doi:10.1016/j.precamres.2011.07.003.

Wang, B.Z., Luo, Z.H., Pan, T., Song, T.Z., Xiao, P.X., and Zhang, Z.Q., 2012, Petrotectonic assemblages and LA-ICP-MS zircon U-Pb age of Early Paleozoic volcanic rocks in Qimantagh area, Tibetan Plateau: Geological Bulletin of China, v. 31, p. 860–874 (in Chinese with English abstract).

Webb, A.A.G., Yin, A., Harrison, T.M., Célérier, J., Gehrels, G.E., Manning, C.E., and Grove, M., 2011, Cenozoic tectonic history of the Himachal Himalaya (northwestern India) and its constraints on the formation mechanism of the Himalayan orogen: Geosphere, v. 7, p. 1013–1061, doi:10.1130/GES00627.1.

Webb, A.A.G., Yin, A., and Dubey, C.S., 2013, U-Pb zircon geochronology of major lithologic units in the eastern Himalaya: Implications for the origin and assembly of Himalayan rocks: Geological Society of America Bulletin, v. 125, p. 499–522, doi:10.1130/B30626.1.

Weill, D.F., and Drake, M.J., 1973, Europium anomaly in plagioclase feldspar: Experimental results and semiquantitative model: Science, v. 180, p. 1059–1060, doi:10.1126/science.180.4090.1059.

Weislogel, A.L., 2008, Tectonostratigraphic and geochronologic constraints on evolution of the northeast Paleotethys from the Songpan-Ganzi complex, central China: Tectonophysics, v. 451, p. 331–345, doi:10.1016/j.tecto.2007.11.053.

Weislogel, A.L., Graham, S.A., Chang, E.Z., Wooden, J.L., Gehrels, G.E., and Yang, H., 2006, Detrital zircon provenance of the Late Triassic Songpan-Ganzi complex: Sedimentary record of collision of the North and South China blocks: Geology, v. 34, no. 2, p. 97–100, doi:10.1130/G21929.1.

Weislogel, A.L., Graham, S.A., Chang, E.Z., Wooden, J.L., and Gehrels, G.E., 2010, Detrital zircon provenance from three turbidite depocenters of the Middle–Upper Triassic Songpan-Ganzi complex, central China: Record of collisional tectonics, erosional exhumation, and sediment production: Geological Society of America Bulletin, v. 122, no. 11–12, p. 2041–2062, doi:10.1130/B26606.1.

Whalen, J.B., Currie, K.L., and Chappell, B.W., 1987, A-type granites: Geochemical characteristics, discrimination and petrogenesis: Contributions to Mineralogy and Petrology, v. 95, p. 407–419, doi:10.1007/BF00402202.

Wu, C.L., Yang, J.S., Ireland, T., Wooden, J., Li, H.B., Wan, Y.S., and Shi, R.D., 2001, Zircon SHRIMP ages of Aolanshao granite from the south margin of Qilian Shan and its geological significance: Yanshi Xuebao, v. 17, p. 215–221 [in Chinese with English abstract].

Wu, C.L., Yang, J.S., Wooden, J.L., Shi, R.D., Chen, S.Y., Meibom, A., and Mattinson, C., 2004a, Zircon U-Pb SHRIMP dating of the Yematan Batholith in Dulan, north Qaidam, NW China: Chinese Science Bulletin, v. 49, p. 1736–1740, doi:10.1007/BF03184308.

Wu, C.L., Yang, J.S., Yang, H.Y., Wooden, J., Shi, R.D., and Zheng, Q.G., 2004b, Dating of two types of granite from north Qilian, China: Yanshi Xuebao, v. 20, p. 425–432 [in Chinese with English abstract].

Wu, C.L., Wooden, J.L., Yang, J.S., Robinson, P.T., Zheng, L.S., Shi, R.D., and Chen, S.Y., 2006, Granitic magmatism in the North Qaidam early Paleozoic ultrahigh-pressure metamorphic belt, northwestern China: International Geology Review, v. 48, p. 223–240, doi:10.2747/0020-6814.48.3.223.

Wu, C.L., Xu, X.Y., Gao, Q.M., Li, X.M., Lei, M., Gao, Y.H., Frost, R.B., and Wooden, J.L., 2010, Early Palaeozoic granitoid magmatism and tectonic evolution in North Qilian, NW China: Yanshi Xuebao, v. 26, p. 1027–1044 [in Chinese with English abstract].

Wu, J., Lan, C.L., Li, J.L., and Yu, L.J., 2001, Determination of ophiolite at the western margin of Aqikekule lake, East Kunlun of Xinjiang: Geological Science and Technology Information, v. 20, p. 6–10 [in Chinese with English abstract].

Wu, X.K., Meng, F.C., Xu, H., and Cui, M., 2011, Zircon U-Pb dating, geochemistry and Nd-Hf isotopic compositions of the Maxingdaban Late Triassic granitic pluton from Qimantang in the eastern Kunlun: Yanshi Xuebao, v. 27, p. 3380–3394 [in Chinese with English abstract].

Wu, Z.H., Hu, D.G., Song, B., and Zhou, C., 2005, Ages and thermo-chronological evolution of the north Xidatan granite in the South Kunlun Mts: Acta Geologica Sinica, v. 79, p. 628–635 [in Chinese with English abstract].

Xia, X.H., and Song, S.G., 2010, Forming age and tectono-petrogenesis of the Jiugequan ophiolite in the North Qilian Mountain, NW China: Chinese Science Bulletin, v. 55, p. 1899–1907, doi:10.1007/s11434-010-3207-3.

Xia, X.H., Song, S.G., and Niu, Y.L., 2012, Tholeiite-boninite terrane in the North Qilian suture zone: Implications for subduction initiation and back-arc basin development: Chemical Geology, v. 328, p. 259–277, doi:10.1016/j.chemgeo.2011.12.001.

Xiang, Z.Q., Lu, S.N., Li, H.K., Li, H.M., Song, B., and Zheng, J.K., 2007, SHRIMP U-Pb zircon age of gabbro in Aoyougou in the western segment of the North Qilian Mountains, China, and its geological implications: Geological Bulletin of China, v. 26, p. 1686–1691.

Xiao, W.J., Windley, B.F., Yong, Y., Yan, Z., Yuan, C., Liu, C.Z., and Li, J.L., 2009, Early Paleozoic to Devonian multiple-accretionary model for the Qilian Shan, NW China: Journal of Asian Earth Sciences, v. 35, p. 323–333, doi:10.1016/j.jseaes.2008.10.001.

Xiao, X.C., Tang, Y.Q., and Gao, Y.L., 1986, Re-exposition on plate tectonics of the Qinghai–Xizang Plateau: Bulletin of the Chinese Academy of Geological Sciences, v. 14, p. 7–19 [in Chinese].

Xie, L.W., Zhang, Y.B., Zhang, H.H., Sun, J.F., and Wu, F.Y., 2008, In situ simultaneous determination of trace elements, U-Pb and Lu-Hf isotopes in zircon and baddeleyite: Chinese Science Bulletin, v. 53, p. 1565–1573.

Xiong, Q., Zheng, J., Griffin, W.L., O'Reilly, S.Y., and Pearson, N.J., 2012, Decoupling of U-Pb and Lu-Hf isotopes and trace elements in zircon from the UHP North Qaidam orogen, NE Tibet (China): Tracing the deep subduction of continental blocks: Lithos, v. 155, p. 125–145, doi:10.1016/j.lithos.2012.08.022.

Xu, Y.J., Du, Y.S., Cawood, P.A., Guo, H., Huang, H., and An, Z.H., 2010a, Detrital zircon record of continental collision: Assembly of the Qilian orogen, China: Sedimentary Geology, v. 230, p. 35–45, doi:10.1016/j.sedgeo.2010.06.020.

Xu, Y.J., Du, Y.S., Cawood, P.A., and Yang, J.H., 2010b, Provenance record of a foreland basin: Detrital zircon U-Pb ages from Devonian strata in the North Qilian orogenic belt, China: Tectonophysics, v. 495, p. 337–347, doi:10.1016/j.tecto.2010.10.001.

Yan, D.P., Zhou, M.F., Wang, C.Y., and Xia, B., 2006, Structural and geochronological constraints on the tectonic evolution of the Dulong–Song Chay tectonic dome in Yunnan Province, SW China: Journal of Asian Earth Sciences, v. 28, no. 4, p. 332–353, doi:10.1016/j.jseaes.2005.10.011.

Yang, J.S., Robinson, P.T., Jiang, C.F., and Xu, Z.Q., 1996, Ophiolites of the Kunlun Mountains, China, and their tectonic implications: Tectonophysics, v. 258, p. 215–231, doi:10.1016/0040-1951(95)00199-9.

Yang, J.S., Xu, Z.Q., Zhang, J.X., Chu, C.Y., Zhang, R., and Liou, J.G., 2001, Tectonic significance of early Paleozoic high-pressure rocks in Altun-Qaidam-Qilian Mountains, northwest China, in Hendrix, M.S., and Davis, G.A., eds., Paleozoic and Mesozoic Tectonic Evolution of Central Asia: From Continental Assembly to Intracontinental Deformation: Geological Society of America Memoir 194, p. 151–170, doi:10.1130/0-8137-1194-0.151.

Yang, J.H., Du, Y.S., Cawood, P.A., and Xu, Y.J., 2009, Silurian collisional suturing onto the southern margin of the North Craton: Detrital zircon geochronology constraints from the Qilian orogen: Sedimentary Geology, v. 220, p. 95–104, doi:10.1016/j.sedgeo.2009.07.001.

Yang, J.H., Du, Y., Cawood, P.A., and Xu, Y.J., 2012a, Modal and geochemical composition of the Lower Silurian clastic rocks in North Qilian, NW China: Implications for provenance, chemical weathering, and tectonic setting: Journal of Sedimentology, v. 82, p. 92–103.

Yang, J.H., Du, Y., Cawood, P.A., and Xu, Y., 2012b, From subduction to collision in the northern Tibetan Plateau: Evidence from the Early Silurian clastic rocks, northwestern China: The Journal of Geology, v. 120, p. 49–67, doi:10.1086/662717.

Yang, M.H., and Song, J.J., 2002, Petrology of the Lenghu granite mass, northwestern Qaidam Basin, China: Northwest Geology, v. 35, p. 94–98 [in Chinese with English abstract].

Yao, J., Shu, L., Santosh, M., and Li, J., 2013, Geochronology and Hf isotope of detrital zircons from Precambrian sequences in the eastern Jiangnan orogen: Constraining the assembly of Yangtze and Cathaysia blocks in South China: Journal of Asian Earth Sciences, v. 74, p. 225–243, doi:10.1016/j.jseaes.2012.08.010.

Yao, J., Shu, L., Santosh, M., and Li, J., 2015, Neoproterozoic arc-related andesite and orogeny-related unconformity in the eastern Jiangnan orogenic belt: Constraints on the assembly of the Yangtze and Cathaysia blocks in South China: Precambrian Research, v. 262, p. 84–100, doi:10.1016/j.precamres.2015.02.021.

Yin, A., 2006, Cenozoic tectonic evolution of the Himalayan orogen as constrained by along-strike variation of structural geometry, exhumation history, and foreland sedimentation: Earth-Science Reviews, v. 76, p. 1–131, doi:10.1016/j.earscirev.2005.05.004.

Yin, A., 2010, Cenozoic tectonic evolution of Asia: A preliminary synthesis: Tectonophysics, v. 488, p. 293–325, doi:10.1016/j.tecto.2009.06.002.

Yin, A., and Harrison, T.M., 2000, Geologic evolution of the Himalayan-Tibetan orogen: Annual Review of Earth and Planetary Sciences, v. 28, p. 211–280, doi:10.1146/annurev.earth.28.1.211.

Yin, A., and Nie, S.Y., 1993, An indentation model for the North and South China collision and the development of the Tan-Lu and Honam fault systems, eastern Asia: Tectonics, v. 12, p. 801–813, doi:10.1029/93TC00313.

Yin, A., and Nie, S.Y., 1996, A Phanerozoic palinspastic reconstruction of China and its neighboring regions, *in* Yin, A., and Harrison, T.M., eds., The Tectonic Evolution of Asia: New York, Cambridge University Press, p. 442–485.

Yin, A., Manning, C.E., Lovera, O., Menold, C.A., Chen, X.H., and Gehrels, G.E., 2007a, Early Paleozoic tectonic and thermomechanical evolution of ultrahigh-pressure (UHP) metamorphic rocks in the northern Tibetan Plateau, northwest China: International Geology Review, v. 49, p. 681–716, doi:10.2747/0020-6814.49.8.681.

Yin, A., Dang, Y.Q., Zhang, M., McRivette, M.W., Burgess, W.P., and Chen, X.H., 2007b, Cenozoic tectonic evolution of Qaidam Basin and its surrounding regions (part 2): Wedge tectonics in southern Qaidam Basin and the Eastern Kunlun Range, *in* Sears, J.W., Harms, T.A., and Evenchick, C.A., eds., Whence the Mountains? Inquiries into the Evolution of Orogenic Systems: A Volume in Honor of Raymond A. Price: Geological Society of America Special Paper 433, p. 369–390.

Yin, A., Dang, Y.Q., Wang, L.C., Jiang, W.M., Zhou, S.P., Chen, X.H., Gehrels, G.E., and McRivette, M.W., 2008a, Cenozoic tectonic evolution of Qaidam Basin and its surrounding regions (Part 1): The southern Qilian Shan–Nan Shan thrust belt and northern Qaidam Basin: Geological Society of America Bulletin, v. 120, p. 813–846, doi:10.1130/B26180.1.

Yin, A., Dang, Y.Q., Zhang, M., Chen, X.H., and McRivette, M.W., 2008b, Cenozoic tectonic evolution of the Qaidam Basin and its surrounding regions (Part 3): Structural geology, sedimentation, and regional tectonic reconstruction: Geological Society of America Bulletin, v. 120, p. 847–876, doi:10.1130/B26232.1.

Yong, Y., Xiao, W.J., Yuan, C., Yan, Z., and Li, J.L., 2008, Geochronology and geochemistry of Paleozoic granitic plutons from the eastern Central Qilian and their tectonic implications: Yanshi Xuebao, v. 24, no. 4, p. 855–866 [in Chinese with English abstract].

Yu, J.H., O'Reilly, S.Y., Wang, L., Griffin, W.L., Zhang, M., Wang, R., Jiang, S., and Shu, L., 2008, Where was South China in the Rodinia supercontinent?: Evidence from U-Pb geochronology and Hf isotopes of detrital zircons: Precambrian Research, v. 164, no. 1, p. 1–15, doi:10.1016/j.precamres.2008.03.002.

Yuan, C., Zhou, M.F., Sun, M., Zhao, Y.J., Wilde, S., Long, X.P., and Yan, D.P., 2010, Triassic granitoids in the eastern Songpan Ganzi fold belt, SW China: Magmatic response to geodynamics of the deep lithosphere: Earth and Planetary Science Letters, v. 290, p. 481–492, doi:10.1016/j.epsl.2010.01.005.

Yuan, D.Y., Ge, W.P., Chen, Z.W., Li, C.Y., Wang, Z.C., Zhang, H.P., Zhang, P.Z., Zheng, D.W., Zheng, W.J., Craddock, W.H., Dayem, K.E., Duvall, R.A., Hough, B.G., Lease, R.O., Champagnac, J.D., Burbank, D.W., Clark, M.K., Farley, K.A., Garzione, C.N., Kirby, E., Molnar, P., and Roe, G.H., 2013, The growth of northeastern Tibet and its relevance to large-scale continental geodynamics: A review of recent studies: Tectonics, v. 32, p. 1358–1370, doi:10.1002/tect.20081.

Yuan, W.M., Dong, J.Q., Wang, S.C., and Carter, A., 2006, Apatite fission track evidence for Neogene uplift in the eastern Kunlun Mountains, northern Qinghai-Tibet Plateau: Journal of Asian Earth Sciences, v. 27, p. 847–856, doi:10.1016/j.jseaes.2005.09.002.

Zhang, C., Zhang, L.F., Van Roermund, H., Song, S.G., and Zhang, G.B., 2011, Petrology and SHRIMP U-Pb dating of Xitieshan eclogite, North Qaidam UHP metamorphic belt, NW China: Journal of Asian Earth Sciences, v. 42, p. 752–767, doi:10.1016/j.jseaes.2011.04.002.

Zhang, J.X., Meng, F.C., and Wan, Y.S., 2007, A cold early Palaeozoic subduction zone in the North Qilian Mountains, NW China: Petrological and U-Pb geochronological constraints: Journal of Metamorphic Geology, v. 25, p. 285–304, doi:10.1111/j.1525-1314.2006.00689.x.

Zhang, J.Y., Ma, C.Q., Xiong, F.H., and Liu, B., 2012, Petrogenesis and tectonic significance of the Late Permian–Middle Triassic calc-alkaline granites in the Balong region, eastern Kunlun orogen, China: Geological Magazine, v. 149, p. 892–908, doi:10.1017/S0016756811001142.

Zhang, L.Y., Ding, L., Pullen, A., Xu, Q., Liu, D.L., Cai, F.L., Yue, Y.H., Lai, Q.Z., Shi, R.D., Ducea, M.H., Kapp, P., and Chapman, A., 2014, Age and geochemistry of western Hoh-Xil–Songpan-Ganzi granitoids, northern Tibet: Implications for the Mesozoic closure of the Paleo-Tethys ocean: Lithos, v. 190, p. 328–348, doi:10.1016/j.lithos.2013.12.019.

Zhang, L.Y., Ding, L., Pullen, A., and Kapp, P., 2015, Reply to comment by Liu, W., and Xia, B., on "Age and geochemistry of western Hoh-Xil–Songpan-Ganzi granitoids, northern Tibet: Implications for the Mesozoic closure of the Paleo-Tethys ocean": Lithos, v. 212–215, p. 457–461, doi:10.1016/j.lithos.2014.11.016.

Zhang, X.H., 1992, Basic characteristics and evolutionary history of the Longshou Shan paleo-rift zone: Geology of Northwestern China, v. 13, no. 1, p. 6–13 [in Chinese].

Zhang, X.T., Yang, S.D., and Yang, Z.J., 2005, Introduction to Regional Geology of Qinghai Province—Explanatory Notes of Geological Map of Qinghai Province in 1:1,000,000: Beijing, Geological Publishing House, 158 p. [in Chinese with English abstract].

Zhao, G., 2015, Jiangnan orogen in South China: Developing from divergent double subduction: Gondwana Research, v. 27, no. 3, p. 1173–1180, doi:10.1016/j.gr.2014.09.004.

Zhao, J.H., and Zhou, M.F., 2007, Geochemistry of Neoproterozoic mafic intrusions in the Panzhihua district (Sichuan Province, SW China): Implications for subduction-related metasomatism in the upper mantle: Precambrian Research, v. 152, no. 1, p. 27–47, doi:10.1016/j.precamres.2006.09.002.

Zhao, J.H., Zhou, M.F., Yan, D.P., Zheng, J.P., and Li, J.W., 2011, Reappraisal of the ages of Neoproterozoic strata in South China: No connection with the Grenvillian orogeny: Geology, v. 39, no. 4, p. 299–302, doi:10.1130/G31701.1.

Zheng, Y.F., Wu, R.X., Wu, Y.B., Zhang, S.B., Yuan, H., and Wu, F.Y., 2008, Rift melting of juvenile arc-derived crust: Geochemical evidence from Neoproterozoic volcanic and granitic rocks in the Jiangnan orogen, South China: Precambrian Research, v. 163, no. 3, p. 351–383, doi:10.1016/j.precamres.2008.01.004.

Zhou, D., and Graham, S.A., 1996, Extrusion of the Altyn Tagh wedge: A kinematic model for the Altyn Tagh fault and palinspastic reconstruction of northern China: Geology, v. 24, p. 427–430, doi:10.1130/0091-7613(1996)024<0427:EOTATW>2.3.CO;2.

Zhou, M.F., Yan, D.P., Kennedy, A.K., Li, Y., and Ding, J., 2002a, SHRIMP U-Pb zircon geochronological and geochemical evidence for Neoproterozoic arc-magmatism along the western margin of the Yangtze block, South China: Earth and Planetary Science Letters, v. 196, p. 51–67, doi:10.1016/S0012-821X(01)00595-7.

Zhou, M.F., Kennedy, A.K., Sun, M., Malpas, J., and Lesher, C.M., 2002b, Neoproterozoic arc-related mafic intrusions along the northern margin of South China: Implications for the accretion of Rodinia: The Journal of Geology, v. 110, p. 611–618, doi:10.1086/341762.

Zhou, M.F., Yan, D.P., Wang, C.L., Qi, L., and Kennedy, A., 2006, Subduction-related origin of the 750 Ma Xuelongbao adakitic complex (Sichuan Province, China): Implications for the tectonic setting of the giant Neoproterozoic magmatic event in South China: Earth and Planetary Science Letters, v. 248, p. 286–300, doi:10.1016/j.epsl.2006.05.032.

Zhu, W., Zhang, Z., Shu, L., Lu, H., Su, J., and Wang, W., 2008, SHRIMP U-Pb zircon geochronology of Neoproterozoic Korla mafic dykes in the northern Tarim block, NW China: Implications for the long-lasting breakup process of Rodinia: Journal of the Geological Society of London, v. 165, no. 5, p. 887–890, doi:10.1144/0016-76492007-174.

Zuza, A.V., and Yin, A., 2014, Initial and boundary conditions for the evolution of the Central Asian orogenic system (CAOS): The Balkatach hypothesis: Geological Society of America Abstracts with Programs, v. 46, no. 6, p. 789.

Zuza, A.V., Reith, R., Yin, A., Dong, S.W., Liu, W.C., Zhang, Y.X., and Wu, C., 2013, Structural and tectonic framework of the Qilian Shan–Nan Shan thrust belt, northeastern Tibetan Plateau: Acta Geologica Sinica, v. 87, supplement, p. 1–3, doi:10.1111/1755-6724.12148_1 [English edition].

Zuza, A.V., Cheng, X., and Yin, A., 2016, Testing models of Tibetan Plateau formation with Cenozoic shortening estimates across the Qilian Shan–Nan Shan thrust belt: Geosphere, v. 12, no. 2, p. 501–532, doi:10.1130/GES01254.1.